Condition Assessment for Water Distribution Pipelines Using Inverse Transient Analysis and the Reconstructive Method of Characteristics

Chi Zhang

B.Eng., M.Eng.

Thesis submitted in fulfilment of the requirements for the degree of Doctor of Philosophy

The University of Adelaide

Faculty of Engineering, Computer and Mathematical Sciences

School of Civil, Environmental and Mining Engineering

Abstract

Modern civilisations rely on water distribution systems to deliver water resources to domestic and industrial consumers. During the lifespan of pipeline assets, they naturally deteriorate due to a combination factors such as ground movement, fatigue, high stresses, and external or internal corrosion. The gradual deterioration of pipelines may lead to the failure of pipelines which may have severe consequences in terms of water resource loss, disruption to industry, traffic and the wider community, repair costs and compensation claims. Developing an efficient and reliable pipeline condition assessment approach is essential to decision-making involving inspection, rehabilitation and replacement. Many existing methods can only investigate pipeline condition over a limited range, which makes them slow and expensive. Fluid transient-based methods can cover several kilometres of pipeline using a few seconds of transient-based test data, due to the fast wave propagation speed. In addition, a transient event can be generated and measured at existing access points along pipelines (for example, air valves or fire hydrants), so cutting the pipeline open and/or draining out the water from the pipeline is not required. Overall, fluid transient-based methods are cost-effective and non-invasive, which make them a promising tool for the future.

To achieve the goal of continuous condition assessment for water distribution pipelines, this research focuses on the Inverse Transient Analysis (ITA) method and the previously developed Reconstructive Method of Characteristics (RMOC). The research proposes a faster and improved ITA

approach by incorporating a new Head Based Method of Characteristics (HBMOC) and a flexible grid, which enhances the computational efficiency and avoids the need for incorporation of interpolation schemes such as those used in the traditional MOC approach. This efficient ITA approach is then developed into the multi-stage parameter-constraining inverse transient analysis (ITA_{MP}) by iteratively limiting the search-space, to overcome problem of lack of identifiability when inverse problems involve hundreds of decision variables. The previously developed RMOC for pipeline condition assessment requires a dead-end boundary and an access point immediately upstream of the dead-end boundary, which is difficult to achieve in the field. The RMOC is significantly generalised in this thesis by relaxing this requirement. The new generalised RMOC utilises two pressure transducers placed at any two interior points along a pipeline to achieve pipeline condition assessment. The number and location of pressure transducers required to achieve optimum identifiability are also investigated. It has been demonstrated by the generalised RMOC that if the pipeline condition between the two pressure transducers is unknown, pressure measurements by two transducers are not able to uniquely identify the wave speed distribution along a pipeline using transient-based methods. To improve identifiability, given that the first two sensors are N reaches apart (i.e. N pipe segments in the pipeline model), the third sensor should not be placed at nodes that are separated from any of the first two sensors by an integer multiple of N reaches. The generalised RMOC also provides insight into why general ITA methods struggle to find good solutions as it illustrates that an infinite number of plausible solutions are possible for the almost same pressure trace if the

wave speed values between transducers are allowed to vary and a third sensor is placed at an integer multiple location. The verification of ITA_{MP} and generalised RMOC by a field and a laboratory experiment, respectively, demonstrates that methods developed in this research can serve as a valuable screening tool for pipeline condition assessment in the real world.

This page is intentionally blank.

Statement of Originality

I certify that this work contains no material which has been accepted for the award of any other degree or diploma in my name, in any university or other tertiary institution and, to the best of my knowledge and belief, contains no material previously published or written by another person, except where due reference has been made in the text. In addition, I certify that no part of this work will, in the future, be used in a submission in my name, for any other degree or diploma in any university or other tertiary institution without the prior approval of the University of Adelaide and where applicable, any partner institution responsible for the joint-award of this degree.

I acknowledge that copyright of published works contained within this thesis resides with the copyright holder(s) of those works.

I also give permission for the digital version of my thesis to be made available on the web, via the University's digital research repository, the Library Search and also through web search engines, unless permission has been granted by the University to restrict access for a period of time.

Signed: ……Date: ……..

This page is intentionally blank.

Acknowledgments

I would like to express my gratitude and thanks to my supervisors, Prof. Martin Lambert, Prof. Angus Simpson and Dr. Aaron Zecchin. They have provided me with great support and effort in helping me to achieve my goals. Their skills, expertise and passion for research have inspired me along the journey. I feel honoured and privileged to undertake this research within this research group.

I would also like to thank Dr. Jinzhe Gong, who also played a role as a supervisor. He has always been very supportive and helpful throughout my candidature. He has given me numerous advice on technical problems, academic writing and also my personal life.

I thank all my fellow postgraduate students within the School for their friendship and sharing research experiences with me. I would also thank all the staff in the School of Civil, Environmental and Mining Engineering for their support and help over the years of my candidature. I thank Mr. Jianbo Long for all discussion during my doctoral candidacy.

I would like to thank my parents, Mr. Chunsheng Zhang and Ms. Guiyun Li, for their continuous support and encouragement. I also appreciate my girlfriend, Yafang Wang, for her invaluable companionship and love. The happy moments with my families have made my life here beautiful.

This page is intentionally blank.

Table of Contents

This page is intentionally blank.

List of Publications

The following peer-reviewed journal papers and conference papers are the outcomes of this research.

Journal papers

1) Zhang, C., Gong, J., Zecchin, A., Lambert, M., & Simpson, A. (2018). “Faster Inverse Transient Analysis with a Head-Based Method of Characteristics and a Flexible Computational Grid for Pipeline Condition Assessment.” Journal of Hydraulic Engineering, 144(4), 04018007.
2) Zhang, C., Zecchin, A. C., Lambert, M. F., Gong, J., & Simpson, A. R. (2018). "Multi-stage parameter-constraining inverse transient analysis for pipeline condition assessment." Journal of Hydroinformatics, 20(2), 281-300.
3) Zhang, C., Gong, J., Simpson, A. R, Zecchin, A. C. & Lambert, M. F. 2018 “Impedance estimation along pipelines by generalized reconstructive Method of Characteristics for pipeline condition assessment” Journal of Hydraulic Engineering, under review.
4) Zhang, C., Gong, J., Lambert, M. F., Simpson, A. R. & Zecchin, A. C. 2018 “Sensor placement strategy for pipeline condition assessment using inverse transient analysis” Water Resources Management, under review.

Conference paper

5) Zhang, C., Zecchin, A. C., Gong, J., Lambert, M. F., & Simpson, A. R. 2017 "Inverse transient analysis parameter estimation accuracy for systems subject to hydraulic noise and short damaged sections." the 37th IAHR World Congress, International Association for Hydro-Environment Engineering and Research (IAHR), Kuala Lumpur, Malaysia.

List of Tables

This page is intentionally blank.

List of Figures

Chapter 1

Introduction

1.1 Significance of anomaly detection and pipeline condition assessment in water distribution systems

Water distribution systems are key infrastructure for a modern civilisation. Water plays an essential role for the development and functioning of modern cities. The functions of water are diverse and cover not only domestic purposes and discharge of waste but also include ecological functions. Successful delivery of water resources to domestic and industry consumers requires reliable water distribution systems. However, as pipelines age, corrosion can occur both internally and externally on the pipe wall. As the pipe wall corrodes, the structural strength decreases until it reaches a point where the structural strength of the pipe fails to be able to withstand the pressure inside the pipe and to maintain pipe integrity. At that time cracking and blow out failure may occur. The consequences of pipeline failure can be severe in terms of water resources loss, disruption to industry, traffic and the wider community, repair costs and compensation claims.

The frequent occurrences of water main breaks have become a worldwide problem. In the first nine months of 2017, the state of South Australia (SA) in Australia has experienced 2528 water main breaks and leaks (9.4 per 100 km). In Australia, the median for water mains breaks is 12.8 per 100 km, in some regions served by the Grampians Wimmera Mallee Water Corporation (GWMWater) in the State of Victoria, this number is as high as 55.5 per 100 km (Bureau of Meteorology, 2016). In the USA, according to 2017 infrastructure report card, there are an estimated 240,000 water main breaks (12.6 per 100 km) per year, wasting over two trillion gallons of treated drinking water (ASCE, 2017).

To reduce the number of water main breaks, water authorities have allocated budgets for maintenance and replacement of pipelines on a regular basis. The scheduled maintenance and replacement is a proactive approach, so that the pipeline sections that are in poor condition and vulnerable to breaks can be repaired or replaced before the problem occurs. However, the difficulty is in identifying these pipe sections as they are usually buried underground and mostly inaccessible. In addition, the maintenance and replacement of water distribution systems are very expensive. The South Australia Water Corporation (SA water) in Adelaide, Australia initiated a four-year $137 million water main replacement program in 2016. In the USA, it is estimated that over the coming 40-year period, investments required for buried drinking water infrastructure will exceed $17 billion, about 54% of which accounts for pipeline replacement (AWWA, 2012).

The ability to pinpoint leaks in their early stage can prevent pipelines from bursts to avoid interruption to domestic and industry users. Scarce water

resources can be saved and the potential risks to public health can also be avoided if the small leaks in water distribution system are detected. The ability to assess pipeline condition assessment efficiently is essential for water authorities so that the number of pipelines break can be reduced and the budgets for pipeline inspection, rehabilitation or replacement can be spent wisely.

1.2 Limitations in traditional methods

Current leak detection methods and pipelines condition assessment are either invasive, expensive or limited to certain types of pipes. Closed-circuit television (CCTV) is a well-adopted technique for the leak detection in pipelines, and for pipeline condition assessment (the inspection of the pipeline internal surface) as well. CCTV inspection is mainly applied to sewers and storm water pipes. In a CCTV system, a camera is fitted on a robot or a wheeled platform that travels along the pipe recording the images in a videotape which will be inspected off-line by an operator. This method is slow and expensive. In addition, the existence of obstructions inside pipelines often makes deploying cameras difficult. The lack of visibility inside pipelines is another difficulty faced by CCTV inspection methods (Duran et al., 2002). Another common leak detection method is acoustic method by listening devices or leak noise correlator. However, these methods may provide false diagnosis when other acoustic signals (e.g. vibrations by traffic) contaminate the leak noise. The range of pipelines under investigation by acoustic methods is typically several hundred metres, which makes acoustic methods slow and expensive. (Fuchs and Riehle, 1991). Also, its application to plastic pipes is

problematic because of the lack of propagation of acoustic waves. (Hunaidi et al., 2000, Puust et al., 2010). Ground penetrating radar (GPR) method produces a continuous cross-sectional profile of subsurface features, which can be used for leak detection. Leaks are captured by detecting underground voids created by the leaking water or by detecting anomalies in the depth of the pipe as the radar propagation velocity changes due to soil saturation with leaking water (Hunaidi and Giamou, 1998). The main disadvantage comes from the fact that the profile provided by GPR might be distorted by high moisture contained in some certain types of soil (Hunaidi and Giamou, 1998) or anomalies like metal objects in the ground (Puust et al., 2010). Recently, more and more sensors have been installed permanently in water distribution systems to monitor pressure and flow in water distribution systems, which result in enormous amount of data. Machine learning, such as artificial neural network (ANN) (Mounce et al., 2009, Romano et al., 2012) and support vector machine (SVM) (Mounce et al., 2011) have been applied to measured data to identify potential leaks and bursts. In these methods, the algorithms define what should be normal behavior by learning historical data, and a reading far exceed the normal state will trigger an alarm. The main disadvantage of these methods is their inability to detect existing stable leaks (Mutikanga et al., 2012).

The most common method to assess pipeline condition by water authorities is examining the available historical information. Information regarding pipeline material, time of construction, soil condition, repair and maintenance history, surcharge loads, external groundwater and the chemical composition of the water is analyzed to develop a model to predict the remaining life of pipeline

assets (St. Clair and Sinha, 2012). However, this prediction strategy is based on the historical information, and not actual pipeline condition. Beside the CCTV methods that has been discussed, magnetic flux leakage (MFL) is widely used in gas pipelines inspection (Afzal and Udpa, 2002). MFL can locate damaged pipe walls by detecting a change of flux field resultant from the damaged areas. However, the application of MFL is limited to ferrous pipes only. In addition, MFL can only provide information around a specific point and also it requires access to the pipes' exterior, which is often difficult for buried pipelines (Liu and Kleiner, 2013). Guided wave ultrasonic method, which utilise low frequency ultrasonic guided waves to detect internal corrosion, has been commercialised (Lowe and Cawley, 2006). An ultrasonic wave is induced into the pipe system, and any change in the cross section causes a reflection, which can be analyzed to evaluate the position and characteristics of the source of the reflection. However, the test range of this method is limited to several tens of metres, which makes it slow to cover a long pipeline. Remote field eddy current method uses an exciting coil to create an electromagnetic field, which interacts with pipe walls. Detectors measure the strength of the remote field which is proportional to the thickness of the pipe wall (Mergelas and Kong, 2001). This technology does not require the sensors to be in close contact to the pipe wall. The disadvantage of this technology is in the fact that its application is limited to ferrous pipe and the pipe under inspection must be drained.

1.3 Fluid transient-based methods for anomaly detection

In the last two decades, fluid transient-based methods have been developed for anomaly detection (mainly for leaks, also for partial or extended blockages, and illegal branches) in pipelines. The configuration required by fluid transient-based methods is depicted in Fig. 1.1. A transient wave is generated by abruptly shutting the side discharge valve. The transient wave is then propagated along a pipeline. Due to the fast wave propagation speed (typically in the range of 800 to 1300 m/s in pressurized metallic water pipes), a few seconds of transient-based test data can cover several kilometres of pipeline, making the technique cost-effective.

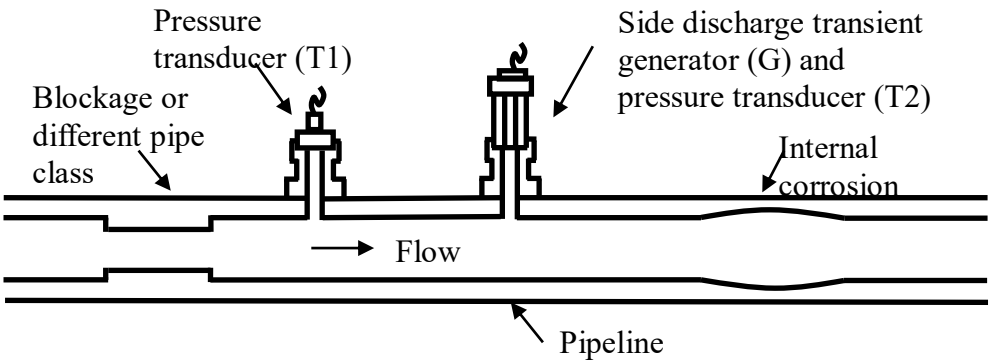

Figure 1.1 Configuration of fluid transient-based methods

When a transient pressure wave encounters an anomaly (e.g. a leak or a blockage), reflections are created. The reflections are recorded by one or multiple pressure transducers installed along the pipeline. Some pressure responses altered by the presence of anomalies are given in Fig. 1.2, which illustrates the effect of a leak, a partial blockage and an extended blockage on transient pressure responses. It can be seen that anomalies produce reflections

when a transient pressure wave encounters them. Anomalies like leaks or partial blockages may also induce extra damping in the transient pressure responses [Fig. 1.2 (a-b)]. The anomalies can be detected by analyzing the information contained in the pressure responses (e.g. the size and timing of reflection, the pattern of damping).

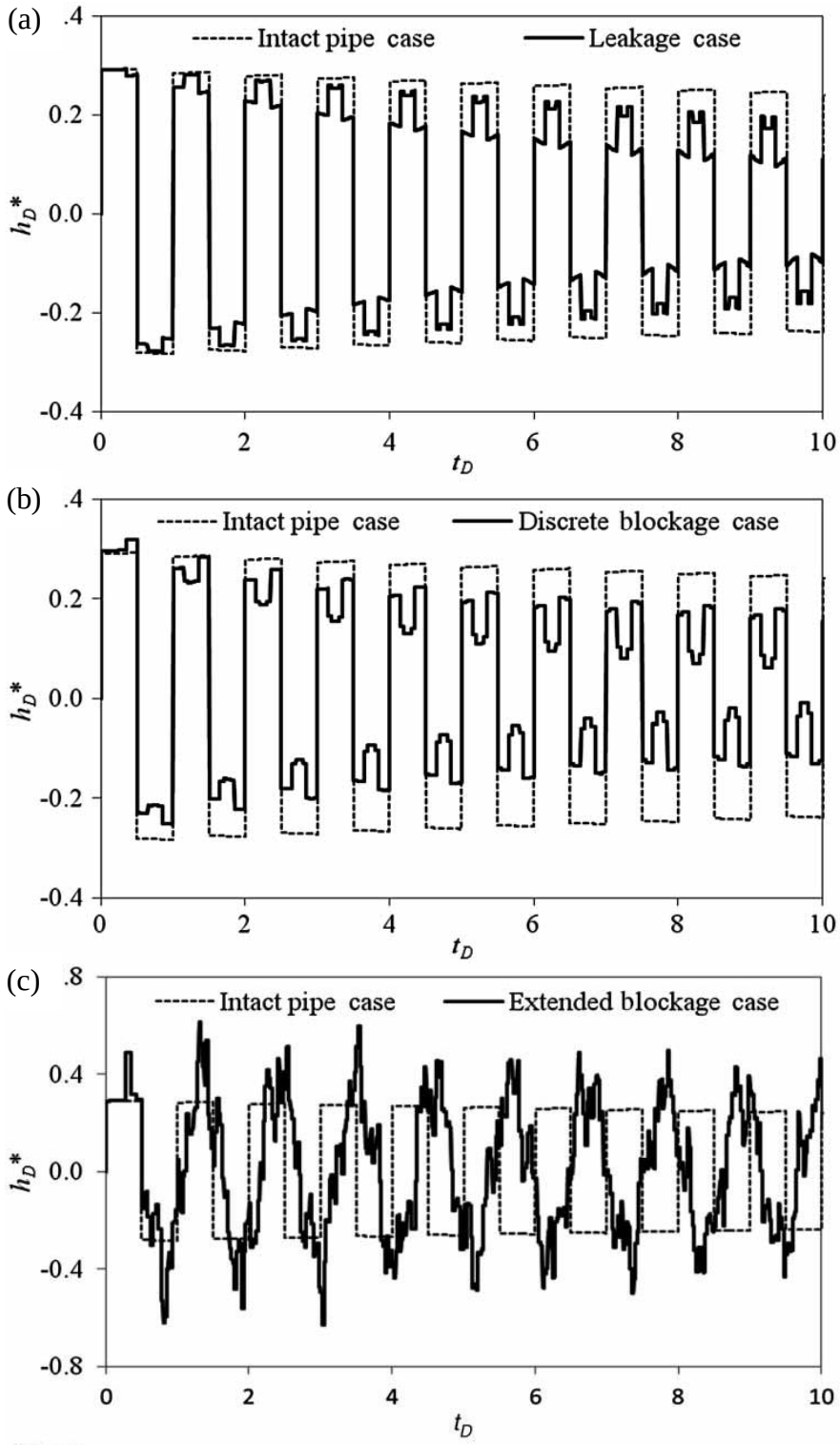

Figure 1.2. The effect of (a) leak, (b) partial blockage and (c) extended blockage on the transient pressure response (Lee et al., 2013)

Fluid transient-based methods can be categorised into three approaches: a) direct transient analysis, which analyses the time domain transient pressure response (e.g. signals in Fig. 1.2); b) frequency response function (FRF) based

methods, which calculate FRF based on the time domain transient pressure response, and then analyse FRF to pinpoint anomalies; c) inverse transient analysis, which calibrates parameters (e.g. the location and size of leak) to find a model which provide best match between its predicted pressure response and measured pressure response. The inverse transient analysis can be either in the time domain or the frequency domain. A detailed review of direct transient analysis, frequency response function (FRF) based method, and inverse transient analysis (ITA) is presented in the following sections.

1.3.1 Direct transient analysis

The existence of leaks, partial or extended blockages in pipelines will induce both reflections and extra damping in the transient response of pipelines. In time reflection methods, the size and arrival time of reflections are analyzed, and in transient damping methods, the pattern of damping in transient responses is analyzed, to enable detection of the existence of anomalies in pipelines.

Time reflection methods. Jönsson and Larson (1992) were one of the first to detect leaks by analyzing the size and arrival time of reflected pressure variations. The transient reflections method was formulated and also verified in a laboratory experiment (Brunone, 1999, Brunone and Ferrante, 2001). The ability of determining the timing of reflections (discontinuities in the measured pressure responses) was further enhanced by advanced single processing methods, including wavelet transform (Ferrante et al., 2007), cepstrum analysis (Taghvaei et al., 2006) and instantaneous frequency analysis (Ghazali et al., 2012).

Another pathway to increase the accuracy of the transient reflections method is through refinement of the system reflections using the impulse response function (IRF). The IRF is a function of the physical characteristics of a system only. The IRF converts all reflections to sharp pulses, so that the leaks can be located with a greater accuracy. Liou (1998) first extracted the impulse response of the system by using the cross-correlation method and applied the technique to a real-time pipeline leak detection. Lee et al. (2007) validated the impulse response method by an experiment and demonstrated the impact of signal bandwidth and background noise on the extracted IRF. The IRF is also applied in the partial blockages detection (Vítkovský et al., 2003).

Transient damping method. The research detecting anomalies by analyzing extra damping extracted from pressure responses is also available in the literature. Wang et al. (2002) detected leak occurrence by analyzing transient damping or the decay of a pressure signal and successfully applied the transient damping method in a laboratory experiment. The method was extended in Wang et al. (2005) for the purpose of partial blockage detection. The assumptions and applicability of transient damping method proposed by Wang et al. (2002) were examined by Nixon et al. (2006), where the authors claimed that at the moment the method can be applied to the simple Reservoir-Pipe-Valve system without other components (for example, junctions or branches).

Overall, the success of transient reflections method requires accurate detection of a small pressure signal of unknown shape, which may be masked by background noise if the leak is small. Also, it is extremely difficult to distinguish the reflections due to faults from the reflections due to unknown

components (i.e. junctions or branches) in a complex system. In addition, superposition of multiple reflections will make the pressure responses difficult to interpret. For the transient damping methods, the application is currently limited to simple reservoir-pipe-valve systems.

1.3.2 Frequency response function (FRF) based method

The FRF of a pipeline system is the Fourier transform of the IRF, thus FRF is also a function of the system's physical characteristics only. The FRF of an intact pipeline in a reservoir-pipeline-valve system consists of a series of uniformly-spaced and uniformly-sized harmonic peaks. The presence of anomalies (leaks, partial or extended blockages) reshapes the pattern of resonant frequencies by inducing an oscillatory pattern or shifting phases of the frequency peaks. Thus, the modified FRF pattern is used for detecting the existence of faults.

Mpesha et al. (2001) and Mpesha et al. (2002) proposed that the presence of a leak within pipeline system results in the formation of additional resonant peaks in the frequency response diagram. The location and magnitude of such leak-induced peaks are used to derive the position and magnitude of the leak. However, different opinions exist in the literature. Lee et al. (2005) analytically demonstrated that the presence of a leak induces a pattern such that the FRD no longer has equal-magnitude peaks. The analysis of the pattern can, therefore, yield information concerning the location and the size of the leak. The proposed leak detection method was verified by Lee et al. (2006) using a laboratory experiment conducted at the University of Adelaide. This leak-induced pattern based method has been extended to complex series pipe

systems by Duan et al. (2011). In order to facilitate the leak-induced pattern, multiple resonant frequency peaks are required, which requires a wide bandwidth in the transient input signal. Gong et al. (2012) utilized the relative size of the first three resonant responses to detect a leak, so that the bandwidth of the input signal only needs to be greater than five times the fundamental frequency.

FRF based methods have also been applied to detection of partial and extended blockages. The presence of a partial blockage induces an oscillation pattern on the odd frequencies (Mohapatra et al., 2006) and increases the amplitude of the even frequencies (Sattar et al., 2008). An experimental verification of partial blockages detection by the frequency response method was also found in Sattar et al. (2008). Duan et al. (2011) analytically proved that the presence of extended blockage will impose a frequency shift in the FRF, so that occurrences of the resonant peaks, in turn, can be used to calculate the size and location of the extended blockage. This has been verified by numerical analysis and a laboratory experiment (Duan et al., 2013). Meniconi et al. (2013) use FRF to determine the size of the blockage, and used a wavelet-based time reflection method to locate the blockage in laboratory experiments, and found the combination of these two methods improved the detection accuracy.

FRF based methods typically require higher bandwidth in the input signal, especially when the pipelines are short, and thus have a higher fundamental frequency. This poses a challenge for the transient generation in the field, since the step or pulse pressure wave generated by the valve closure is unlikely to fulfill the high bandwidth requirement. In addition, most of FRF

based methods have been developed for the single pipeline bounded by a reservoir and a valve. Finally, it is typically assumed that the pipeline has a uniform diameter and wave speed, which is unlikely to be the case in the field.

1.3.3 Inverse transient analysis (ITA)

ITA adjusts system parameters to minimize the difference between the measured responses and the simulated responses of the predicted model. A diagram of the ITA process is given in Fig. 1.3. Within the inverse parameter estimation process, the system parameters are updated within each iteration and are sent to the forward solver to generate the model predicted pressure response, which is then calibrated to the measured pressure response. The transient forward solver can be either in the time domain or the frequency domain. The predicted pressure response is compared to the measured pressure response to compute the objective function which indicates the "goodness of fit" of the model with the proposed parameter settings. The optimization algorithm then uses the objective function information to update the calibrated parameter estimates to provide candidates for improved estimates. The ITA then iterates this process until the termination criteria is reached.

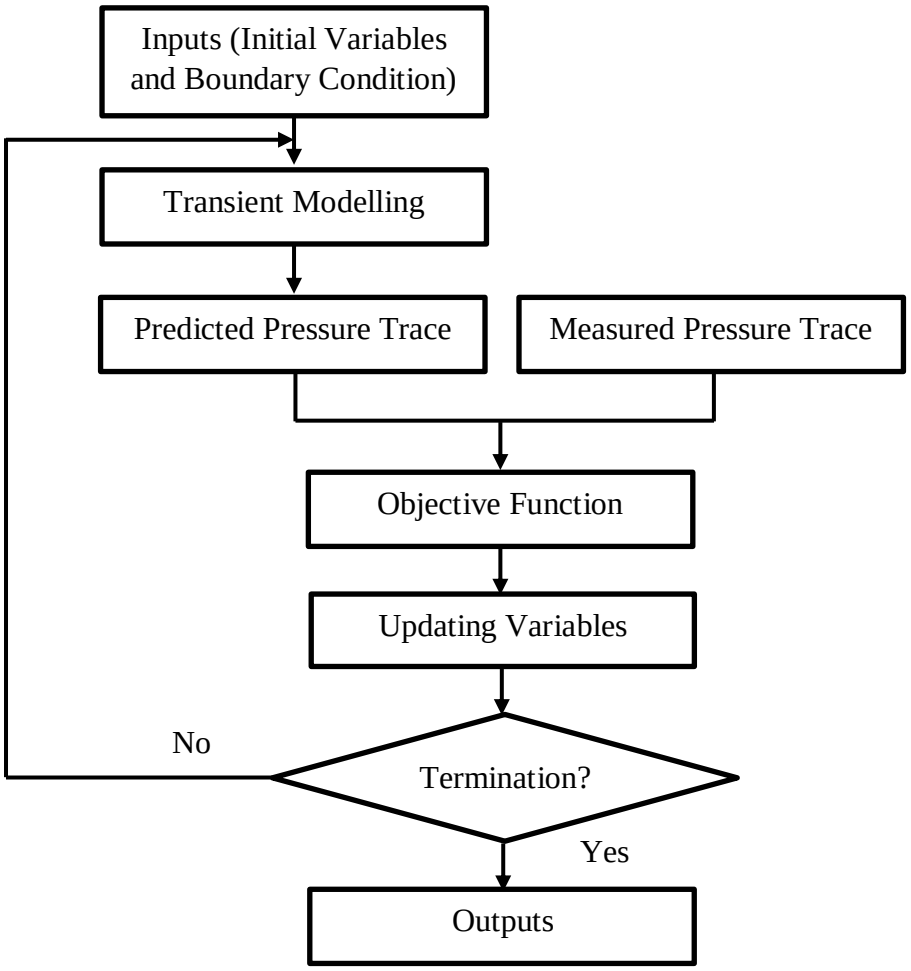

Figure 1.3 ITA algorithm flow chart

Inverse transient analysis (ITA) was first proposed by Liggett and Chen (1994) for the leakage detection and friction factor calibration. Since then ITA has been studied extensively for the anomalies detection in pipelines (Nash and Karney, 1999, Vitkovsky et al., 2001, Kapelan et al., 2004, Vítkovský et al., 2007, Kim, 2008, Covas and Ramos, 2010, Zecchin et al., 2013). To produce a predicted pressure response, modelling transient in systems can take place in the time domain and the frequency domain. The methods of characteristics (MOC) using a fixed grid is the most popular time domain transient simulator used in ITA (Wylie et al., 1993, Chaudhry, 2014). The MOC requires the Courant condition to be satisfied for each discretized reach.

A problem occurs when those reaches have different wave speeds. To overcome this problem, different interpolation methods, such as time line interpolation (Goldberg and Wylie, 1983), space line interpolation (Lai, 1988) and some high order interpolation schemes (Chen, 1995), have been developed. Through the interpolation process, numerical errors may be introduced to the computation of transient pressures (Ghidaoui and Karney, 1994, Ghidaoui et al., 1998). An alternative to interpolation methods is wave speed adjustment, in which wave speeds are altered so that the Courant condition is satisfied (Chen, 1995).

The success of ITA depends on the ability of the transient simulators to describe the pressure response. However, the MOC models cannot adequately represent the pressure dissipation and dispersion observed in real-world pipe systems (Zielke, 1968, McInnis and Karney, 1995, Vardy and Brown, 1995, Brunone et al., 2000, Vitkovsky, 2001, Covas et al., 2004, Stephens et al., 2011). In one laboratory case study conducted by Vitkovsky et al. (2001), which perhaps is the first verification of ITA method for leak detection, the authors pointed out that it was necessary to include unsteady friction in the modelling to account for the damping behavior when multiple periods transient is involved. Soares et al. (2011) used a creep function and viscoelasticity model to account for dispersion behavior in the PVC pipes. Covas and Ramos (2010) used both unsteady friction model and a viscoelastic model in cases studies, in which pipelines were made of polyethylene. The authors suggested that the ideal data duration for running ITA in a plastic pipe is one period of the pressure wave, as afterward other effects such as unsteady friction and pipe viscoelasticity dampen the transient event and dissipate the

leak reflections. Vítkovský et al. (2007) examined error sources in ITA and claimed that overall, the model error was likely to be the key factor that limited the application of ITA.

The frequency domain modelling method is also used in ITA, which results in the pressure responses in the frequency domain. To enable the objective function calculations, the frequency domain pressure responses can be converted back into the time domain, or the time domain measured pressure responses can be converted into the frequency domain. Kim (2007) developed the impedance matrix method, which is an extension of impulse response method developed by Suo and Wylie (1989). Then this method is incorporated into ITA for leakage, friction factor and wave speed calibration in a complex system (Kim, 2008). The impedance matrix method based ITA was further verified by an experiment conducted in a laboratory (Kim et al., 2014). Theoretically, the impedance matrix method can be applied to any complex system. However, the algorithm for constructing the address matrix is quite involved. Zecchin et al. (2009) developed a Laplace-domain admittance matrix that allows complete flexibility with regard to the topological structure of a network. A frequency domain ITA approach is formed by combining the Laplace-domain admittance matrix and maximum likelihood estimation (Zecchin et al., 2013). This ITA approach was further developed for the cases where unknown boundaries were involved (Zecchin et al., 2014), and it was also verified in a laboratory experiment for leak and branch detection (Capponi et al., 2017).

Optimisation algorithms are employed to adjust system parameters, so that the objective function values can be reduced. Gradient based methods, such as the

Levenberg-Marquardt (LM) method (Liggett and Chen, 1994), evolutionary algorithms, such as Genetic algorithm (GA) (Vítkovský et al., 2000), Shuffled Complex Evolution (SCE) (Vitkovsky et al., 2001, Stephens et al., 2013) or Particle Swarm Optimization (PSO) (Jung and Karney, 2008, Zecchin et al., 2013), or hybrid algorithms of both (Kapelan et al., 2003) have been used in ITA as the optimization algorithm.

It has been found that evolutionary algorithms performed better than the gradient-based methods (Vitkovsky et al., 2001). Kapelan et al. (2003) developed a hybrid GA algorithm by incorporating LM method when a new population is created by a GA. The hybrid algorithm maintains a similarly effective global search ability as that of a GA, and also enhances its local search ability, so that computational efficiency has been improved. Jung et al. (2006) compared five evolutionary algorithms [GA, PSO, SCE, Evolutionary Programming (EP) and Ant Colony Optimization (ACO)] with four benchmark functions (one of them is water distribution system calibration), and found that the SCE and PSO have stronger global convergence to escape from poor local optima for multimodal functions.

Identifiability problems for ITA applications have been observed in other work, and is a known problem for inverse problems more generally (Yeh, 1986). Within the study of Jung and Karney (2008), three different ITA scenarios were analyzed on an 11-pipe network, where each had a different number of measurement sites. The authors concluded that fewer measurement sites led to a better calibration error and faster convergence to the calibrated parameter values, but to a less accurate calibration result. Kapelan et al. (2004) pointed out that some poorly estimated parameters were due to an

inadequate quantity of observed information. That is, Kapelan et al. (2004) outlined that the parameter calibration problems could not be resolved by simply using an alternative search algorithm. The authors developed a framework for the effective incorporation of prior information into inverse transient analysis for pipe networks to improve the ill-posed nature of the inverse problem. The lack of identifiability is very likely to be associated with the complexity of the problem (i.e. the number of decision variables). The more decision variables involved in the calibration, the more complex the model is, and the harder it is to identify parameters. To promote the accuracy of calibration, several researchers developed different methods to reduce the complexity of the problem. Vítkovský et al. (2007) used a model parsimony approach, by starting with one potential leak location then gradually increasing the number of potential leak location. Both Covas and Ramos (2010) and Soares et al. (2011) adopted a strategy to minimize the number of leak candidates, starting with a set of leak candidates sparsely distributed throughout the system, and gradually reducing the set of candidates to those around the potential leak locations obtained in the earlier steps. Kim (2008) also adopted a similar multi-stage strategy to reduce complexity by starting the calibration with the initial search-space, which was the accumulated length of all the pipeline elements, and then restraining the search-space to a candidate pipeline element.

In contrast to extensively studied transducer placement for steady-state hydraulic model calibration (Bush and Uber, 1998, Lansey et al., 2001, Kapelan et al., 2005, Do et al., 2016), sensor placement design for transient hydraulic model calibration is very limited (Savic et al., 2009). Liggett and

Chen (1994) suggested that pressures should be measured at the most sensitive locations in networks. Vítkovský et al. (2003) treated the transient-state sensor placement design as an optimisation problem, in which GA was used to minimise or maximise three different indicators. It is likely that a good sensor placement design contains more information and makes identifying system parameters easier. However, the linkage between sensor placement design and identifiability of system has not been investigated.

1.4 Fluid transient-based methods for pipeline condition assessment

In almost all fluid transient-based methods for anomaly detection discussed above, it is common practice that some system parameters are assumed uniform or known while other parameters (usually the size and location of anomalies) are then determined. For example, in ITA for leak detection, it is typically assumed that internal diameter and wave speed of pipeline are uniform and known, and only leak locations and sizes are parameters to be calibrated.

In reality, the pipeline condition can be complex, the wall thickness (or wave speed, impedance) can vary from section to section. In these cases, assuming the whole pipeline is uniform in terms of wall thickness (or wave speed, impedance) makes anomaly detection problematic. Even in some frequency domain ITA applications (Kim, 2008, Zecchin et al., 2013) where leakage, friction factors and wave speeds in complex pipeline system are

simultaneously calibrated, the underlying assumption is still that each pipeline in the system is uniform (only one wave speed was allocated to each pipeline).

Research aiming to determine the wall thicknesses of all pipe sections is referred to as pipeline condition assessment. Currently, the research focused on this topic is limited.

Gong et al. (2016) developed a sub-sectional condition assessment technique and applied the technique in an asbestos cement pipeline in Australia. The arrival time of reflections enables calculation of wave speed of each section, which then can be used to determine average wall thickness of each pipe section. Lee et al. (2017) also determined the pipe wall conditions through wave speed measurement, but used a PIPE SONAR system (a new transient signal generation system) to minimize the interruption during transient tests. The limitation of the wave speed measurement strategy only account for the initial wave reflections. As a result, the resolution is several ten to hundred meters, which is relatively low.

Inverse transient analysis is capable of continuous pipeline condition assessment with a high resolution. The framework of ITA for pipeline condition assessment is same as ITA for leak detection as discussed in the previous section, except the decision variables are wave speeds or wall thicknesses of hundreds reaches after discretisation, instead of locations and sizes of leak.

Stephens et al. (2013) applied ITA in a 4-km mild steel pipe with cement mortar lining (MSCL) in South Australia, where the discretization using a 10 m spatial resolution resulted in 390 decision variables to calibrate. The pattern

of estimated wave speeds distribution, which was indicative of pipe condition, was compared with the intensive ultrasound wall thickness measurements, and general agreement was achieved. However, the authors also claimed that the accuracy and effectiveness of ITA were subjected to the high computational cost. Tuck and Lee (2013) applied ITA to estimate wall thickness variations in a 41.52 m stainless steel pipeline in the laboratory. However, no discretization was involved and the methodology is more like an extended blockage detection by inverse analysis.

Several issues remain for the further application of ITA for pipeline condition assessment in the field. One issue is identifiability under high dimensionality. High resolution in pipeline condition assessment results in high dimensionality in ITA. For example, to achieve a spatial resolution of 10 m, a 1000 m pipe is discretized into 100 sections, which results in 100 wall thicknesses to be determined. The identifiability of parameter estimation requires investigation under high dimensionality. Another issue is computational cost, which is also associated with the high dimensionality. The transient model has to be executed thousands to millions of times before a reasonable match between the predicted and measured pressure responses is achieved. Finally, how to select the number and location of pressure transducers also remains unknown.

In addition to ITA, Gong et al. (2015) applied a time-domain fluid transient analysis in a mild steel pipe with cement mortar lining in South Australia. This method originated from Gong et al. (2012), and directly maps the magnitude of wave reflections to the wall thicknesses. The field case study proved the method to be useful. However, only selected significant wave

reflections are analyzed, and the method fails to give continuous pipeline condition assessment (i.e. wall thickness information section by section along the pipelines).

To enable continuous pipeline condition assessment, Gong et al. (2014) first proposed reconstructive MOC (RMOC) to estimate impedance and wave speed distributions along a pipeline based on pressure measurements on a dead-end boundary. Unlike ITA that involves iterative optimization, reconstructive MOC is an analytical approach to calculate the pipeline impedance directly using pressure measurements, so it is much more computationally efficient than ITA. However, reconstructive MOC proposed by Gong et al. (2014) requires transient pressure generation and measurement immediately upstream of a dead-end boundary, which limited its applicability in the field where such a configuration is difficult to achieve.

1.5 Research aims

The overall goal of this research is to achieve continuous condition assessment for water distribution pipelines using Inverse Transient Analysis and Reconstructive Method of Characteristics. To achieve this goal, the following specific aims have been proposed and are investigated in this research:

Aim 1: To develop a transient simulation model to enhance computational efficiency and avoid interpolation errors. This transient simulation model will be linked to an evolutionary algorithm and form a faster version of ITA

Aim 2: To investigate issues of identifiability when inverse transient analysis has high dimensionality, and to develop a new strategy to overcome this problem. The new strategy will enhance identifiability of system parameters when ITA involves hundreds of decision variables.

Aim 3: To generalise the previously developed reconstructive MOC for continuous pipeline condition assessment. This will enable determination of wall thickness along the pipelines using transient pressure measurements at two transducers at close proximity.

Aim 4: To investigate the relevance of transducer placement (number and locations of transducers) to the identifiability of inverse transient problems. Proper selection of locations to install pressure transducers will enhance the accuracy of pipeline condition assessment.

Aim 5: To validate the new techniques developed within this research by laboratory and field experiments.

1.6 Organisation of thesis

This thesis has 6 chapters overall. The main body of this thesis (Chapters 2 to 5) is presented as a collection of the four journal publications arising from the undertaken research. Chapter 6 presents the conclusions from the research and discusses future possible work.

Chapter 2 presents a fast Inverse Transient Analysis (ITA) with a Head Based Method of Characteristics (HBMOC) and a flexible computational grid for condition assessment of long pressurized pipelines. HBMOC speeds up the transient modelling by decoupling head and flow computations. The use of a

flexible grid eliminates the need for interpolation, thus avoids interpolation errors and also increases modelling speed. The proposed ITA has been verified by conducting numerical case studies, and the comparison with the conventional ITA is also made. Aim 1 is achieved in Chapter 2.

Chapter 3 illustrates lack of identifiability when ITA approaches involve models using hundreds of discretized pipe reaches (therefore hundreds of model parameters) by analysis of a numerical example. In order to improve the parameter estimation accuracy of ITA applied to these high dimensional problems, Chapter 3 also develops a multi-stage parameter-constraining ITA (ITA_{MP}) approach for pipeline condition assessment. The proposed algorithm involves the staged constraining of the parameter search-space to focus the inverse analysis on pipeline sections that have a higher likelihood of being in an anomalous state. A field case study is investigated to verify the proposed method. Chapter 3 achieves Aim 2 by providing ITA_{MP} for pipeline condition assessment, and partially achieves Aim 5 by verifying ITA_{MP} in a 4-km pipeline in the field in South Australia.

Chapter 4 generalises the previously developed reconstructive Method of Characteristics (RMOC) method by relaxing the requirement of a dead-end boundary. Instead, the generalised RMOC as proposed requires two pressure transducers placed at any two interior points along a pipe to record pressure variations under a controlled transient event, based on which the parameters along the pipeline can be analytically determined through a smart use of MOC analysis backward in time. A laboratory experiment, where wall thickness and location of two sections with wall class changes, has been conducted to demonstrate the capability of the proposed method for continuous pipeline

condition assessment. Chapter 4 achieves Aim 3 by providing the generalised RMOC for pipeline condition assessment, and partially achieves Aim 5 by verifying the generalised RMOC in a laboratory experiment conducted at the University of Adelaide.

Chapter 5 investigates how the number and location of measurement stations affect the accuracy and robustness of the ITA-based pipeline wave speed estimation. An analytical analysis based on the generalised RMOC has been conducted to prove that two transducers to record pressure measurements are insufficient to identify the parameters along the pipe. When the number of transducers increases to three, the locations for three transducers are investigated by both a sensitivity analysis and multiple ITA case studies. Aim 4 is achieved in Chapter 5.

Chapter 6 summarises the major contributions of this research. Future possible work to advance the current research is also discussed.

This page is intentionally blank.

Chapter 2

Faster Inverse-Transient Analysis with a Head-Based Method of Characteristics and a Flexible Computational Grid for Pipeline Condition Assessment

(Journal Paper 1)

Zhang, C., Gong, J., Zecchin, A., Lambert, M., & Simpson, A.

School of Civil, Environmental and Mining Engineering, the University of Adelaide, Adelaide, SA 5005 Australia

Journal of Hydraulic Engineering, 144(4), 04018007.

This page is intentionally blank.

Statement of Authorship

Title of Paper	Faster Inverse-Transient Analysis with a Head-Based Method of Characteristics and a Flexible Computational Grid for Pipeline Condition Assessment
Publication Status	☑ Published ☐ Accepted for Publication ☐ Submitted for Publication ☐ Unpublished and Unsubmitted w ork w ritten in manuscript style
Publication Details	Zhang, C., Gong, J., Zecchin, A., Lambert, M., & Simpson, A. (2018). Faster Inverse Transient Analysis with a Head-Based Method of Characteristics and a Flexible Computational Grid for Pipeline Condition Assessment. Journal of Hydraulic Engineering, 144(4), 04018007.

Principal Author

Name of Principal Author (Candidate)	Chi Zhang
Contribution to the Paper	Conception and design of the project Analysis and interpretation of research data Draft the paper
Overall percentage (%)	75%
Certification:	This paper reports on original research I conducted during the period of my Higher Degree by Research candidature and is not subject to any obligations or contractual agreements with a third party that would constrain its inclusion in this thesis. I am the primary author of this paper.
Signature	Date 02/03/2018

Co-Author Contributions

By signing the Statement of Authorship, each author certifies that:

i. the candidate's stated contribution to the publication is accurate (as detailed above);
ii. permission is granted for the candidate in include the publication in the thesis; and
iii. the sum of all co-author contributions is equal to 100% less the candidate's stated contribution.

Name of Co-Author	Jinzhe Gong
Contribution to the Paper	Conception and design of the project Analysis and interpretation of research data Critically revising the paper so as to contribute to the interpretation
Signature	Date 02/03/2018

Name of Co-Author	Aaron Zecchin
Contribution to the Paper	Conception and design of the project Analysis and interpretation of research data Critically revising the paper so as to contribute to the interpretation
Signature	Date 2/3/2018

Name of Co-Author	Martin Lambert		
Contribution to the Paper	Conception and design of the project Analysis and interpretation of research data Critically revising the paper so as to contribute to the interpretation		
Signature		Date	2/3/17

Name of Co-Author	Angus Simpson		
Contribution to the Paper	Conception and design of the project Analysis and interpretation of research data Critically revising the paper so as to contribute to the interpretation		
Signature		Date	2 Mar 2018

Please cut and paste additional co-author panels here as required.

Abstract

Targeted and proactive pipeline condition assessment is critical for cost-effective maintenance of aging water transmission and distribution systems. The current research proposes a fast Inverse Transient Analysis (ITA) with a Head Based Method of Characteristics (HBMOC) and a flexible computational grid for condition assessment of long pressurized pipelines. Compared with conventional ITA, the key innovations of the proposed method include (i) the development and use of an innovative forward modelling scheme HBMOC to enhance computational efficiency, and (ii) the use of a flexible characteristics grid to avoid the need for interpolation and hence enhance the accuracy by satisfying the Courant condition in all iterations of forward modelling. To examine and verify the proposed method, numerical simulations are conducted in a pipeline with multiple sections of deterioration (simulated by changes in the wavespeed). Both the conventional ITA and proposed ITA are applied to the numerical pipe model and the wavespeeds estimated by different ITA approaches are compared. It is concluded that the proposed ITA is more accurate and four times more computationally efficient than the conventional ITA. The impact of neglecting of friction in the proposed approach is shown to be insignificant given that the proposed ITA was aimed to condition assessment of transmission mains and only transient pressures that covers the pipe section of interest is analysed.

This page is intentionally blank.

2.1 Introduction

Water transmission and distribution systems are extensive in scale and the majority are buried underground. The aging of the system leads to a degraded pipeline condition, which can negatively impact the water system supply through a reduction in hydraulic transmission ability, lowering of water quality and may result in pipe rupture. An environment of aging water transmission and distribution system assets around the developed world compels the evolution of accurate, labour and time saving condition assessment methods. Cost-effective detection of deteriorated sections in critical pipelines would enable water authorities to reduce their exposure to the risk of pipeline failure and increase their ability to maintain a reliable water supply service.

Over the past two decades, many fluid transient-based techniques have been proposed for pipeline fault detection and condition assessment, including leak detection (Brunone and Ferrante, 2001, Wang et al., 2002, Lee et al., 2006, Duan et al., 2011, Gong et al., 2013, Meniconi et al., 2013, Capponi et al., 2017), blockage detection (Wang et al., 2005, Duan et al., 2013, Meniconi et al., 2013) and wall condition assessment (Stephens et al., 2008, Stephens et al., 2013, Gong et al., 2014, Gong et al., 2015, Gong et al., 2016), and generalised parameter estimation (Zecchin et al., 2013, Zecchin et al., 2014). Among the transient-based techniques, the Inverse Transient Analysis (ITA) has the potential to achieve cost-effective and spatially continuous condition assessment for long pipelines (Stephens et al., 2013). ITA was first proposed by Liggett and Chen (1994) for leak detection and friction factor calibration in

pipe networks. The ITA technique has been further developed mainly for the purpose of leak detection in pipelines (Vitkovsky et al., 2001, Vítkovský et al., 2003, Covas and Ramos, 2010). For pipeline condition assessment using the ITA technique, the frequency domain ITA attacks attention (Zecchin et al., 2013, Zecchin et al., 2014, Kim, 2016). However, compared with time domain methods, frequency domain methods have limitation associated with detection of multiple faults. Among the research on time domain ITA, Stephens et al. (2008), (2013) determined the location and magnitude of lost lining and internal corrosion of a cement mortar lined steel pipeline in the field; Tuck and Lee (2013) estimated wall thickness variations in a laboratory pipeline. Despite the ability of time domain ITA to describe transient response in detail, several issues hinder the application of conventional ITA techniques.

A key issue is the computational efficiency. Substantial and potentially prohibitive computational effort is required for current ITA methods due to the extensive iterative forward modelling process. The MOC-based transient model simulator, which is used to calculate the predicted transient pressures, typically needs to be executed tens of thousands, to millions, of times throughout the iterative optimisation process. Depending on the problem, it may take a very long time to have wavespeeds estimated by an ITA approach on a pipe in the scale of thousands of meters. Stephens et al. (2013) commented that a better optimized solution may be found if greater computational capacity was available.

Another key issue is the accuracy of the transient modelling. A fixed characteristic grid, in which calculations are undertaken at uniformly spaced points along the pipes axial extent, is widely adopted in the implementation of

the MOC (Ghidaoui et al., 2005). The fixed grid MOC will encounter problems in the ITA approach, where the wavespeeds vary from reach to reach within the computational grid and also iteration to iteration within the inverse optimisation procedure. Since the reach length and time step are both constant in the fixed-grid strategy, the Courant condition (Wylie et al., 1993, Chaudhry, 2014) is not guaranteed to be satisfied for all reaches. Consequently, interpolation methods (Goldberg and Wylie, 1983) are required. Through the interpolation process, numerical error may be introduced to the computation of transient pressures. Energy expressions developed by Ghidaoui et al. (1998) demonstrated that both time-line and space-line interpolation attenuate the total energy in the system, causing dissipation and dispersion of the propagating wave fronts. It is difficult to quantify or bound the energy dissipation during the inverse analysis, since the wavespeeds vary continuously on an interval. Ghidaoui and Karney (1994) pointed out that the only way of achieving accurate, general solutions for hyperbolic equations is to keep the time step small and the Courant number as close to one as possible. Jung and Karney (2008) repeated the process of discretization until the smallest Courant number exceeded 0.75 and then used a linear timeline interpolation in ITA. Strategies like this, in turn, will quadratically increase the number of computational points (and as a result, the number of parameters requiring estimation), which can significantly increase the complexity and computational cost, and sometimes make the inverse problem unmanageable. A compromise has to be made with the hope of limiting the interpolation error with a manageable number of decision variables (Stephens et al., 2013).

Considering these two issues (substantial computational demand and interpolation error in the transient modelling (Stephens et al., 2013)) that hinder the application of ITA, the research presented in this paper focuses on the development of a more computationally efficient and accurate ITA technique to assess pipeline condition. A novel head-based MOC (HBMOC) with a flexible grid approach for more efficient forward modelling and for avoiding interpolation, and thus the interpolation error, is proposed. The inverse calibration of pipeline parameters (the wavespeed in each reach) is then achieved by linking the new forward modelling approach to an objective function and an optimization algorithm. To validate the proposed new ITA method, numerical simulations are conducted on a single pipeline with multiple sections of deterioration (pipe sections with various wavespeeds). The numerical results confirm that the proposed new ITA technique can detect and locate the deteriorated pipe sections more accurately than the conventional ITA approach, and uses less than a quarter of the computational time which is required by the conventional ITA approach.

2.2 Background: Conventional ITA methods applied to transmission mains

This section reviews the testing configuration for transient-based pipeline condition assessment in the field (Stephens et al., 2013, Gong et al., 2015) and the conventional ITA approach for pipeline condition assessment.

2.2.1 ITA transmission line test configuration

A typical configuration used for transient-based pipeline condition assessment in the field is given in Fig. 2.1(a), where a transient generator and multiple pressure transducers are employed. Different transient generators (Stephens et al., 2004, Brunone et al., 2008, Taghvaei et al., 2010) have been used previously to induce a pressure head rise by an abrupt change of discharge after steady state is achieved. The transient generator assumed for the research in this paper is a side discharge valve that is restricted with a nozzle to generate a pressure head rise in the pipe of 2 to 15 m. An incident transient pressure wave is generated by an abrupt closure of the side discharge valve after opening and releasing a flow until steady state is achieved. The generated transient pressure wave will propagate in both the upstream and downstream directions along the pipe under test. Reflections occur when a transient wave encounters physical changes associated with deterioration, such as wall thickness variations. The reflections propagating along the pipe can be measured by the multiple transducers mounted on the pipe.

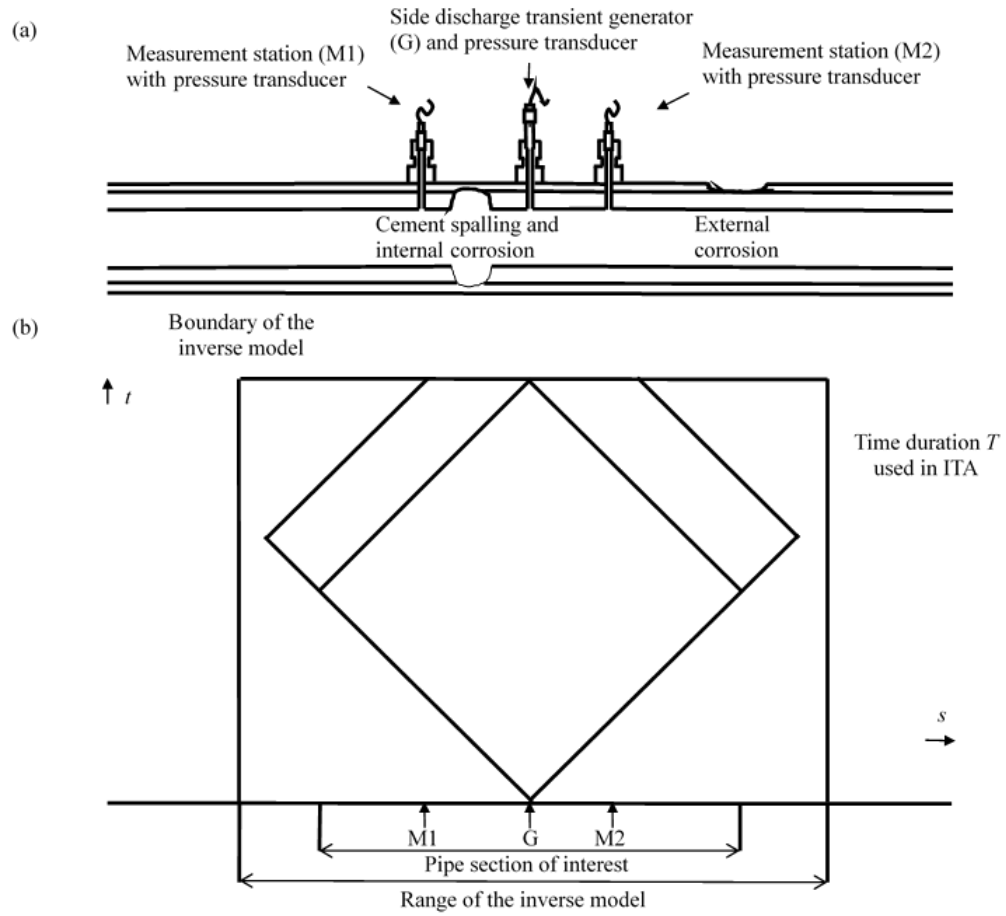

Figure 2.1 (a) A typical field experiment configuration (Gong et al., 2015) and (b) the range of the inverse model and the zone of quiet boundary

In the context of this paper, pipeline condition assessment refers to detection of a pipe class change, a pipe section which is made up of a different material and pipe deterioration (such as the spalling of cement mortar lining, internal or external corrosion), which all introduce a change in wavespeed. The wavespeed of the transient is determined by Eq. (2.1)

$$a = \sqrt{\frac{K/\rho}{1 + (K/E)(D/e)c_1}} \tag{2.1}$$

in which a = wavespeed of the transient; K = bulk modulus of the fluid; ρ = density of the fluid; E = Young's modulus of the pipe wall material; D =

internal diameter of the pipeline; e = pipe wall thickness; and c_1 = constraint factor, depending on the structural restraint condition of the pipeline (Wylie et al., 1993).

According to Eq. (2.1), spalling of cement mortar lining, external and internal corrosion result in a reduced wall thickness and internal corrosion also may result in a larger internal diameter, thereby yielding a smaller wave speed. Similarly, a greater wavespeed is expected for a thicker wall, such as a higher class of pipe. Pipes of different class or pipes made up of segments of different materials also result in different wavespeeds. Due to the occurrence of pressure wave reflections resulting from sections with a different wavespeed, the measured transient pressure response will be affected (i.e. transient pressure responses measured at multiple stations are a function of the wavespeeds along the pipe). For example, if a mild steel pipe (diameter of 600 mm, wall thickness of 5 mm, wavespeed of 1007 m/s) is excited by a 7 m transient, the 1 mm wall thickness reduction results in a decrease of 50 m/s in wavespeed and a 0.43 m pressure reflection. Consequently, the calibration of wavespeeds can be used for pipeline condition assessment.

2.2.2 Building of the inverse model

This paper is aimed at pipeline condition assessment of transmission mains whose scale is usually large. As a result, the initial pressure rise and drop of the generated transient has a duration of several or several tens of seconds. Instead of investigating the whole transmission main, it is proposed that an inverse model be built such that only the pressure traces that cover the pipe section of interest are used to match in the ITA to limit the number of decision

variables. The illustration of building an inverse model can be found in Fig. 2.1(b). The time duration of the measured transient response used in ITA (T) is determined according to the pipeline range of interest and the location of measurement stations by making sure that initial reflections of the pipeline in the range of interest are captured by multiple measurement stations. The range of the inverse model has to accommodate all the reaches which contribute to the time duration T of measured transient responses at all measurement stations. Numerical boundary conditions are placed at the upstream and downstream of the inverse model to provide equivalent steady state conditions (Stephens et al., 2013). By such a placement, the reflections from the numerical boundaries will be beyond the time duration of T and as a result will have no influence on the ITA.

2.2.3 ITA algorithm

Given a data set of the transient pressures are recorded by pressure transducers mounted on the generator and measurement stations, the ITA can be employed to estimate the sub-sectional wavespeed distribution along the pipeline length, and by implication, the pipeline's condition is also identified. A flow chart describing the general process of ITA algorithm is shown in Fig. 2.2.

This figure is identical to Figure 1.3. Please refer to Figure 1.3 in Chapter 1.

Figure 2.2 ITA algorithm flow chart (note that the term "Variables" refers to the wavespeed parameters used in the forward model in this paper)

Before the iterative inverse process is undertaken, the generic form of the forward model is set-up (i.e. pipeline of interest and numerical boundaries), and the parameter bounds (i.e. minimum and maximum plausible wavespeeds)

are identified (first box in Fig. 2.2). Within the inverse parameter estimation process, the wavespeed parameters are updated within each iteration and are sent to the forward solver to generate the calibrated model's predicted pressure trace. The predicted pressure trace is compared to the measured pressure trace to compute the objective function which indicates the "goodness of fit" of the model with the proposed parameter settings. The optimisation algorithm then uses the objective function information to update the calibrated parameter estimates to provide candidates for improved estimates. The ITA then iterates this process until the termination criteria is met.

2.3 The proposed new ITA technique

To solve the challenges faced by conventional ITA, a head-based MOC (HBMOC) approach that is implemented on a flexible grid is developed to replace the conventional fixed grid MOC in the transient model simulation (transient modelling stage in Fig. 2.2). HBMOC accelerates the transient modelling by decoupling head and flow computations. The use of flexible grid eliminates the need of interpolation, thus avoids interpolation error and also increases modelling speed. These proposals are demonstrated to significantly enhance the computational efficiency and accuracy in ITA.

2.3.1 Head-based Method of Characteristics (HBMOC)

The proposed head-based MOC approach only involves the computation of the transient pressure head over time, therefore saving computational cost when compared with conventional MOC that calculates the head and flow

simultaneously. The absence of the transient flow information does not impede the implementation of ITA since it is usual that only the transient pressure responses are measured in field pipelines and compared with the predicted pressure responses in the optimization process. Instead of using the two classic compatibility equations and a triangular sub-grid in each calculation as used in the conventional MOC, the HBMOC uses four simplified compatibility equations and a diamond sub-grid for each step. For the arbitrary diamond grid shown in Fig. 2.3(b) (extracted from the entire computational grid in Fig. 2.3(a)), the compatibility equations valid along four characteristic lines are simplified by removing the friction term (see justification later on in the paper) as:

$$C_1^+: H(x,t) - H(x-\Delta x_1, t-\Delta t) + B_1[Q_u(x,t) - Q_d(x-\Delta x_1, t-\Delta t)] = 0 \tag{2.2}$$

$$C_1^-: H(x,t) - H(x+\Delta x_2, t-\Delta t) - B_2[Q_d(x,t) - Q_u(x+\Delta x_2, t-\Delta t)] = 0 \tag{2.3}$$

$$C_2^-: H(x-\Delta x_1, t-\Delta t) - H(x, t-2\Delta t) - B_1[Q_d(x-\Delta x_1, t-\Delta t) - Q_u(x, t-2\Delta t)] = 0 \tag{2.4}$$

$$C_2^+: H(x+\Delta x_2, t-\Delta t) - H(x, t-2\Delta t) + B_2[Q_u(x+\Delta x_2, t-\Delta t) - Q_d(x, t-2\Delta t)] = 0 \tag{2.5}$$

in which H is the piezometric head, Q_u, Q_d are the upstream and downstream discharges, the impedance B is defined as $B_i = a_i/gA_i$, where a = wavespeed of the transient; g = gravitational acceleration; A = cross-sectional area.

All the nodes can be simulated as a leak (with a discharge associated with the head and a leak coefficient) or a generator (with a discharge associated with

the closure of the valve). At any time *t*, the continuity equation must be satisfied at all the nodes:

$$Q_l(x,t) = Q_u(x,t) - Q_d(x,t) \tag{2.6}$$

where Q_l is the discharge from the generator or a leak.

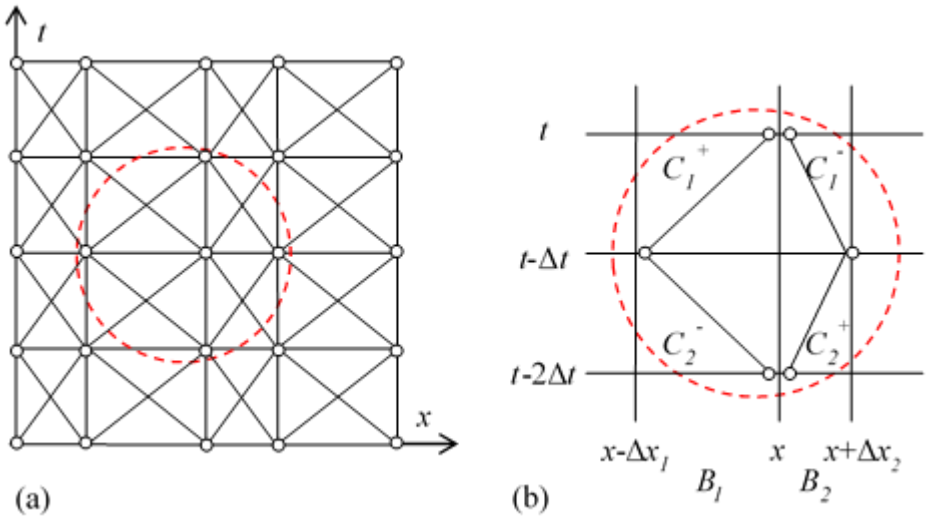

Figure 2.3 (a) A typical flexible characteristic grid and (b) its diamond sub-grid for HBMOC simulation (the flexible grid will be discussed in the following section)

To facilitate structured calculation, Eq. (2.2-2.6) can be assembled into a matrix form to yield:

$$\mathbf{AH} + \mathbf{BQ} = \mathbf{C} \tag{2.7}$$

where vectors (**H**, **Q**, **C**) and matrices (**A**, **B**) are defined as:

$$\mathbf{H} = [H(x,t) \quad H(x-\Delta x, t-\Delta t) \quad H(x+\Delta x, t-\Delta t) \quad H(x,t-2\Delta t)]^T$$

$$\mathbf{Q} = [Q(x,t) \quad Q(x-\Delta x, t-\Delta t) \quad Q(x+\Delta x, t-\Delta t) \quad Q(x,t-2\Delta t)]^T$$

$$\mathbf{C} = [0 \quad -B_2 Q_l(x,t) \quad 0 \quad -B_2 Q_l(x,t-2\Delta t)]^T$$

$$\mathbf{A} = \begin{bmatrix} 1 & -1 & 0 & 0 \\ 1 & 0 & -1 & 0 \\ 0 & 1 & 0 & -1 \\ 0 & 0 & 1 & -1 \end{bmatrix}$$

$$\mathbf{B} = \begin{bmatrix} B_1 & -B_1 & 0 & 0 \\ -B_2 & 0 & B_2 & 0 \\ 0 & -B_1 & 0 & B_1 \\ 0 & 0 & B_2 & -B_2 \end{bmatrix}$$

Where $[\cdot]^T$ denotes the transpose of the vector of $[\cdot]$. It can be shown that **B** is a reduced rank matrix with rank = 3, where the left null space of **B** is spanned by the row vector

$$\mathbf{b}_{null} = \begin{bmatrix} B_2 & B_1 & -B_2 & -B_1 \end{bmatrix}$$

which satisfies

$$\mathbf{b}_{\text{null}}\mathbf{B} = [0\ 0\ 0\ 0]$$

$$\mathbf{b}_{null}\mathbf{A} = \begin{bmatrix} B_1 + B_2 & -2B_2 & -2B_1 & B_1 + B_2 \end{bmatrix}$$

Multiplying Eq. (2.7) through by $\mathbf{b}_{\text{null}}$ to eliminate the **Q** term yields $\mathbf{b}_{\text{null}}\mathbf{AH} = \mathbf{C}$ which can be expanded and rearranged as

$$\begin{aligned} H(x,t) = {} & \frac{2B_2}{B_1 + B_2} H(x - \Delta x_1, t - \Delta t) \\ & + \frac{2B_1}{B_1 + B_2} H(x + \Delta x_2, t - \Delta t) - H(x, t - 2\Delta t) \\ & + \frac{B_1 B_2}{B_1 + B_2} [Q_l(x, t - 2\Delta t) - Q_l(x, t)] \end{aligned} \quad (2.8)$$

Eq. (2.8) indicates that the pressure at node (x, t) can be determined by the pressure at nodes $(x-\Delta x_1, t-\Delta t)$, $(x+\Delta x_2, t-\Delta t)$, $(x, t-2\Delta t)$, together with the impedance B_1, B_2 and the discharge variation at node x from $t-2\Delta t$ to t.

If a transient generator was placed at node *x*, which is the case of the present study, the discharge variation can be interpolated based on the steady-state valve discharge and the valve closure time or back calculated from the measured magnitude of the wave front. For example, if generator is fully closed at *t* and it is closed within one time step, $Q_l(x_1,t)$ is zero and $Q_l(x_1,t-2\Delta t)$ is the steady state valve discharge. When the impedance is uniform along the pipe and the pipe is frictionless, Eq. (2.8) is equivalent to the Joukowsky equation.

After the valve at generator is fully closed and no leak exists along the pipe (which is the case of the present study, all nodes have zero discharge after a transient is generated), Eq. (2.8) can be simplified to be:

$$H(x,t) = \frac{2B_2}{B_1+B_2} H(x-\Delta x_1, t-\Delta t) + \frac{2B_1}{B_1+B_2} H(x+\Delta x_2, t-\Delta t) - H(x,t-2\Delta t) \tag{2.9}$$

After the initial steady-state of pressure is determined (as is typically measured by the pressure transducers under sufficiently quiescent conditions), Eq. (2.9) can be used in a time marching process to form the HBMOC. A similar equation for isolating flow can be derived in a similar way using **A** and rank (**A**) = 3 if required, which would create a flow-based MOC approach.

The decoupling of pressure and flow is achieved by combining four compatibility equations and neglecting friction, thereby reducing the computational requirements of the HBMOC in comparison to the conventional MOC. Computational efficiency is a very important property of

a forward model for the purpose of ITA. As can be seen in Eq. (2.9), for each time step and interior node, pressure can be computed by one equation. In the conventional MOC, as both pressure and flow are coupled with each other, pressure and flow have to be calculated separately by two equations. Note that the floating point operation (FPO) count of the computations and the memory required in the proposed method is significantly reduced by isolating pressure and eliminating interpolation. Consequently, the transient model simulation can be accelerated. The impact of neglecting the effect of friction will be investigated in the numerical case studies to follow.

The proposed method can also be applied to leak detection by using Eq. (2. 8) (when the node *x* represents a leak). Substituting the orifice equation into Eq. (2. 8) converts it to a quadratic equation expressed only in terms of head, which enables head calculation in the absence of flow. As a result, in addition to pipeline condition assessment, the proposed method is also capable of leak detection, although this aspect is not considered in this paper.

2.3.2 Flexible grid

A flexible characteristic grid is used in the implementation of HBMOC, eliminating the need for interpolation associated with the use of a fixed characteristic grid and accelerating modelling process. Tuck and Lee (2013) mentioned a constant time step discretisation in which the space step can be altered, but no further details were discussed. Gong et al. (2014) used an implicit and flexible grid in the reconstructive MOC method, however, it was used for calculating the transient head and flow back in time along

characteristic lines and not for the purpose of ITA as proposed in the current research.

Within the flexible grid for ITA, the length of each reach Δx_i is flexible and updated in each forward simulation iteration, while the time step Δt and number of reaches N are fixed throughout the inverse analysis. During an iterative inverse optimization process, estimated wavespeeds (slopes of characteristic lines) are changing in each iteration. In each iteration, the length of each reach Δx_i can be determined by holding $\Delta x_i = a_i \Delta t$ according to the varying wavespeed. This novel flexible grid approach eliminates the need for interpolation.

When a fixed grid is used, the discretization of pipe between measurement sites is based on known distance between sites and a constant reach length Δx. However, when a flexible grid is used, the discretization is based on the arrival time of the transient at each site and the constant time step Δt. For example, considering the typical configuration in field tests (Fig. 2.1), and assuming that the transient is generated at time $t = T_G$ and arrives at the measurement stations Mi at time $t = T_{Mi}$, the number of reaches between Mi and G, is determined as

$$N_{Mi-G} = \frac{T_{Mi} - T_G}{\Delta t} \tag{2.10}$$

After the time duration (T) of the measured transient response to be used in ITA is determined, the number of reaches from a boundary of inverse model to the nearest measurement sites M_i (e.g. from the model upstream boundary to M1) can be determined by Eq. (2.11):

$$N_{B-Mi} = \left\lceil \frac{T - T_{Mi}}{2\Delta t} \right\rceil \tag{2.11}$$

where $\lceil \cdot \rceil$ denotes the round up or ceiling function. Eq. (2.11) makes sure that all the reaches that contributes to the transient response used in ITA (time duration of *T*) are accommodated in the inverse model.

2.3.3 Objective function and optimization algorithm

The objective function used in the proposed ITA approach is defined by Eq. (2.12):

$$OF(\mathbf{a}) = \frac{1}{N_{MS} N_{TS}} \sum_{i=1}^{N_{MS}} \sum_{j=1}^{N_{TS}} \left| H_{i,j}^{m} - H_{i,j}(\mathbf{a}) \right| \tag{2.12}$$

where N_{MS} = number of measurement stations (including the generator station if the transient is recorded there); N_{TS} = number of time steps; $H_{i,j}^{m}$ = measured pressure response; $H_{i,j}$ = predicted pressure response from the calibrated model; $\boldsymbol{a} = [a_1, \ldots, a_N]^T$ is the vector of unknown wavespeeds, where a_k = wavespeed of *k*th reach. The absolute difference objective function provides an intuitive explanation of the error, namely it is the mismatch of piezometric head per data point.

Either gradient based methods, such as the Levenberg-Marquardt (LM) method (Liggett and Chen, 1994), or evolutionary algorithms, such as Genetic algorithm (GA) (Vítkovský et al., 2000), Shuffled Complex Evolution (SCE) (Vitkovsky et al., 2001, Stephens et al., 2013) or Particle Swarm Optimization (PSO) (Jung and Karney, 2008, Zecchin et al., 2013), or a hybrid algorithm (Kapelan et al., 2003) can be used in ITA as the optimization algorithm. In the

proposed ITA method, Particle Swarm Optimization (PSO) is adopted as the optimization algorithm, as this was found to be a reliable and parametrically insensitive real-valued optimisation algorithm (Eberhart and Kennedy, 1995), with successful parameter estimation applications for transient-state pipeline networks (Zecchin et al., 2013).

2.4 Numerical simulations

In order to verify the effectiveness and evaluate the performance of the proposed ITA, numerical simulations were conducted in a pipeline with multiple sections of deterioration. A typical reservoir-pipe-valve system was used as the "true" model to generate transient pressure traces at the specific measurement locations by conventional MOC modelling. These transient pressure traces were used as the measured pressure responses for the ITA process. Both the conventional and proposed ITA approaches were applied to the simulated measured pressure traces to estimate the wavespeeds and to detect the deterioration along the pipeline. The results are analysed and compared in the following sections. The effect of neglecting friction has also been investigated.

2.4.1 Preliminaries

2.4.1.1 System configuration

The configuration of the numerical pipeline system used to verify the proposed ITA method is given in Fig. 2.4. A typical reservoir-pipe-valve system was used where the 1320 m long pipe has a uniform diameter of D = 600 mm. The central 1000 m pipe was considered the section of interest for

the ITA. The wavespeed of the intact undamaged pipe sections was 1000 m/s. Four sections of deterioration distributed along the pipe were considered, where their lengths and wavespeeds, which are designed to avoid any discretization error in the initial MOC modelling, are as given in Fig. 2.4. The transient generator, G, was modelled as a side-discharge valve with a steady-state flow rate of $Q_v = 0.04$ m^3/s. The incident wave was generated by abruptly shutting the valve. The initial steady-state discharge in the pipeline was $Q_0 = 0.2$ m^3/s (the velocity $V = 0.71$ m/s).

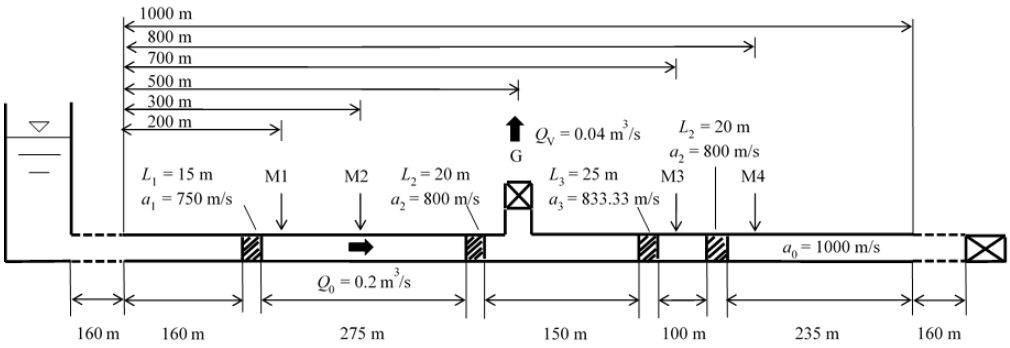

Figure 2.4 Numerical experiment pipeline configuration

2.4.1.2 Numerically simulated pressure traces

Conventional MOC modelling with a sampling frequency of 2000 Hz, was conducted on the pipeline system described in Fig. 2.4. The transient wave was generated after the closure of a side-discharge valve at time $t = 0.2$ s. The time duration (T in Eq. (2.11) of the transient response used in ITA was set to be 1.22 s. This 1.22 s long pressure response does not contain any reflections from the reservoir and valve boundary. Conventional MOC modelling was performed twice on this pipeline configuration, with Darcy-Weisbach friction factors of 0 (frictionless case) and 0.02 (a roughness height of 0.52 mm)

respectively. This frictionless and friction data sets have provided the two case studies that are considered in the results below.

2.4.1.3 Control parameters in two ITA approaches

The setting of the ITA parameters, including the number of decision variables, iterations and the range of search space, are discussed in this section.

For the conventional ITA implementation, a fixed grid MOC and a linear time line interpolation (Goldberg and Wylie, 1983) scheme were adopted. A discretisation of 5 m for a 1320 m pipeline resulted in 264 reaches in total. For the proposed ITA implementation, considering the time duration of numerically simulated pressure trace (T = 1.22 s), a time step Δt (0.005 s, 10 times the sampling interval) and an arrival time of transient pressure (which can be read from the numerically simulated pressure traces), the number of reaches can be calculated by Eqs. (2.10) to (2.11), totalling 268 reaches overall.

The number of decision variables was set equal to the number of reaches, therefore being 264 and 268 for the conventional and proposed ITA, respectively. The number of particles for the PSO algorithm is usually greater than or equal to the number of decision variables, and within this study this was set to 300. Restricting the number of iterations and the range of search space can reduce the inverse problem to a manageable level. The number of iterations was set to 5,000 after preliminary trials. This resulted in 1,500,000 evaluations in total, which was sufficient to consistently exhibit convergence. The feasible search space for each wavespeed parameter was restricted to

between 650 m/s and 1050 m/s. In a field experiment, the search space can be determined by prior information about the pipeline.

2.4.2 Results

Both the conventional ITA and the proposed ITA, as previously described, were applied to estimate the wavespeeds and detect sections of deterioration along the pipeline. Two case studies were undertaken. Both the conventional and proposed ITA approaches were executed 10 times. The estimated wavespeeds in the 10 runs were averaged as the results to be compared. A sensitivity analysis was carried out to further investigate the impact of neglecting friction. All programs were run in the environment of a personal computer (Windows 7, Intel(R) Core(TM) i5-3470s CPU @ 2.90Hz 8.00 GB RAM).

2.4.2.1 Case study 1 – frictionless pipeline

Fig. 2.5 shows the average wavespeeds estimated by the two different ITA approaches. Wavespeeds estimated by the proposed ITA contain less erratic spatial variation and are closer to the theoretical wavespeeds in comparison to those estimated by the conventional ITA, which possesses significant variations in the wavespeed estimates. The variations, especially those that exist at points where the pipe condition changes, are consistent with the fact that the Courant number is much less than 1 at those points. This indicates that variations in the wavespeed estimation are likely attributed to the presence of interpolation. Fig. 2.6 shows the envelope of wavespeeds from 10 executions for different random number seeds by the two different ITA approaches. In general, the envelope of wavespeeds estimated by the proposed ITA is

narrower than those estimated by the conventional ITA, which indicates that wavespeeds calibrated by the proposed ITA were more consistent between different executions, implying that for the case considered, the proposed ITA is more robust at finding consistently good wavespeed estimates.

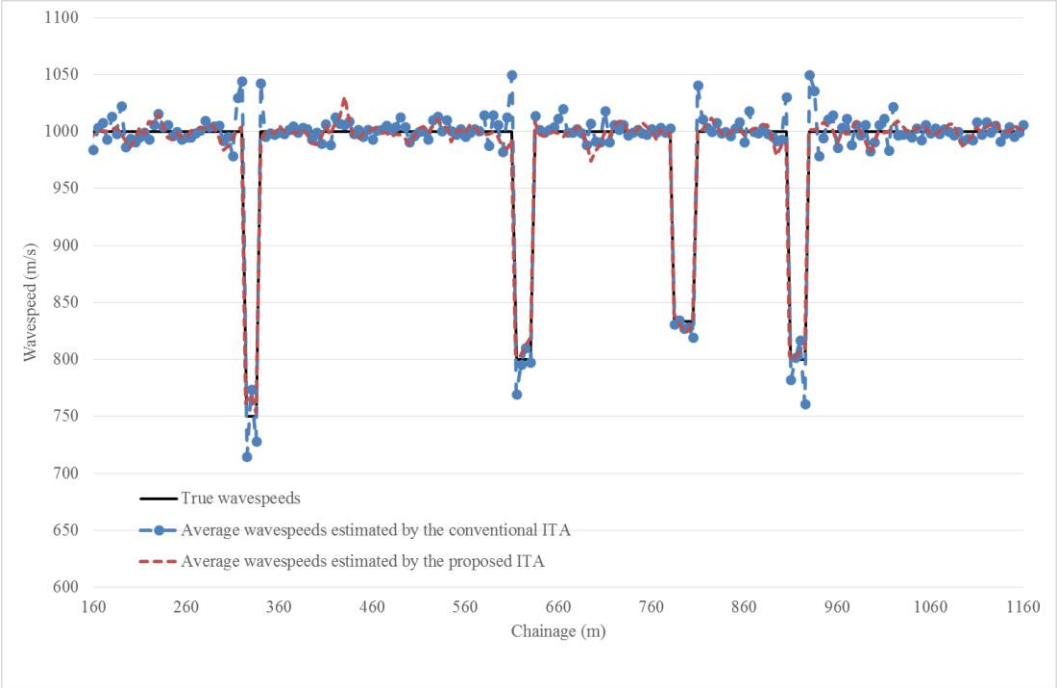

Figure 2.5 Comparison of the estimated and true wavespeeds by different ITA approaches

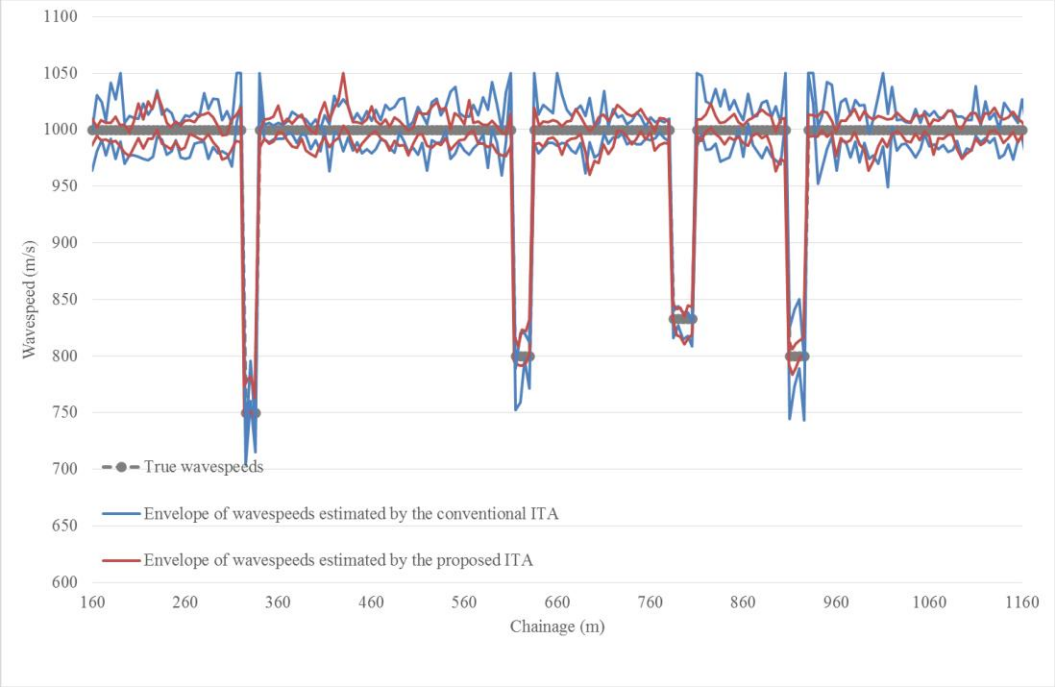

Figure 2.6 Comparison of the envelopes of wavespeeds estimated by different ITA approaches for 10 different PSO runs

For the deteriorated sections, it can be seen from Fig. 2.5 that they were accurately estimated by the proposed ITA. For the conventional ITA, even though the sections of deterioration were identified, the average wavespeeds exhibit variations around the actual wavespeeds. Table 1 shows the minimum and maximum wavespeed estimates and average and relative error of four deteriorated sections by two ITA approaches respectively in Case Study 1. It can be seen from Table 1 that all estimated average and relative errors of the proposed ITA are less than those of the conventional ITA, indicating that the proposed ITA estimated wavespeeds of deteriorated sections more accurately.

Table 2.1 Summary statistics of wavespeed estimates of the four deteriorated sections for Case Study 1 (without friction) by the conventional and proposed ITA approaches

		Section 1	Section 2	Section 3	Section 4
True model	Wavespeed (m/s)	750.0	800.0	833.3	800.0
Conventional ITA	Min estimate (m/s)	714.9	769.3	819.0	760.6
	Max estimate (m/s)	773.6	810.0	834.7	817.0
	Average error (m/s)	26.9	12.0	5.9	19.1
	Average relative error	3.59%	1.50%	0.71%	2.39%
Proposed ITA	Min estimate (m/s)	753.0	800.5	823.0	799.1
	Max estimate (m/s)	768.8	819.8	840.0	807.7
	Average error (m/s)	***12.0***	***9.1***	***5.2***	***4.5***
	Average relative error	***1.60%***	***1.14%***	***0.62%***	***0.57%***

Note: A certain deteriorated section is covered by multiple reaches. The minimum and maximum calibrated wavespeed were selected in this table. The average error is calculated by averaging individual errors. The smallest error for each section is italicised and bolded.

[a]Average relative error = average error / theoretical value * 100%.

The estimated results can also be assessed by a comparison of numerically simulated and predicted pressure traces. Fig. 2.7 provides the pressure traces of the numerically simulated and the predicted pressure reflections at M3 after the transient was generated. It can be observed that there is almost an indiscernible difference between the numerically simulated and the predicted pressure traces obtained by the wavespeeds estimated by the proposed ITA approach. The predicted pressure trace obtained with the wavespeeds estimated by the conventional ITA is distorted by a numerical dispersion, which was assumed to be introduced by the process of interpolation.

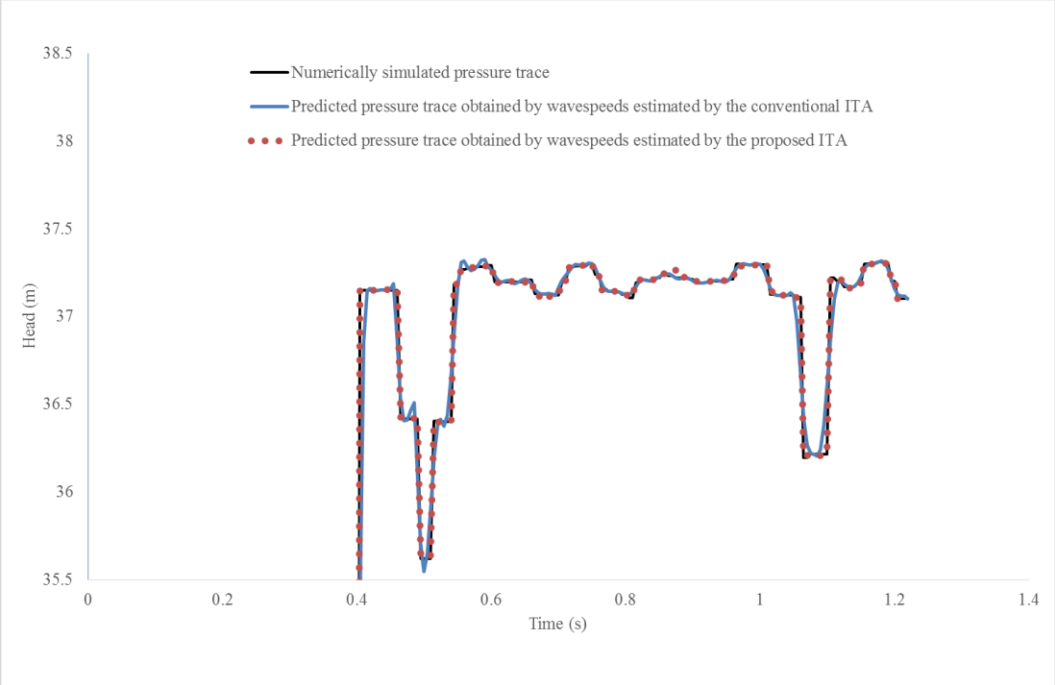

Figure 2.7 Comparison of the numerically simulated pressure trace (with a friction factor f = 0.00) and the predicted pressure trace obtained with wavespeeds estimated by different ITA approaches at M3

The introduction of a flexible grid may lead to a mismatch between the actual model and the calibrated model. To examine this mismatch, the estimated distance from the 4 measurement stations (M1, M2, M3 and M4) to the generator (G) were calculated to be 300.08 m, 199.98 m, 199.80 m and 299.80 m, respectively, after the model was calibrated. Compared with the actual distance of 300 m, 200 m, 200 m and 300 m, the errors are insignificant. All the numerical experiments that were carried out proved this mismatch to be insignificant. However, it is recommended to check this mismatch when the flexible grid is adopted. A penalty term in the objective function can be used if necessary.

The computational wall clock time required for the conventional and proposed ITAs was 5h 56min and 1h 24min respectively (Note: the time quoted was the simulation time required for 10 executions). The proposed ITA used only 24% of the computational time required by the conventional ITA, which is a result of the accelerated transient model simulator HBMOC and the flexible grid approach. Case Study 1 provide results that show that the proposed ITA is a significantly more computationally efficient and accurate alternative to the conventional ITA.

2.4.2.2 Case study 2 – pipeline with friction

As previously discussed, the steady friction term in the compatibility equations is neglected in the derivation of the HBMOC. The purpose of Case Study 2 is to assess the impact that the inclusion of steady-friction in the measured pressure responses has on the accuracy of the proposed ITA to estimate the pipe wavespeeds. The conventional and proposed ITAs for estimating wavespeeds, as in Case Study 1, were performed using the 'measured pressures' resulting from the MOC modelling with a Darcy-Weisbach friction factor of 0.02.

All the final objective function values of the 10 ITA runs in Case Study 1 and 2 are given in Fig. 2.8. Objective function values of the proposed ITA are significantly less in comparison to those of the conventional ITA, indicating that predicted pressure traces obtained by the proposed ITA match numerically simulated pressure traces better, which has been confirmed in Fig. 2.7. For the conventional ITA, objective function values of two case studies are comparable, because friction was included in its forward model. For the proposed ITA, objective function values of Case Study 2 is slightly greater

than those of Case Study 1, which can be explained by the fact that friction was excluded in its forward model.

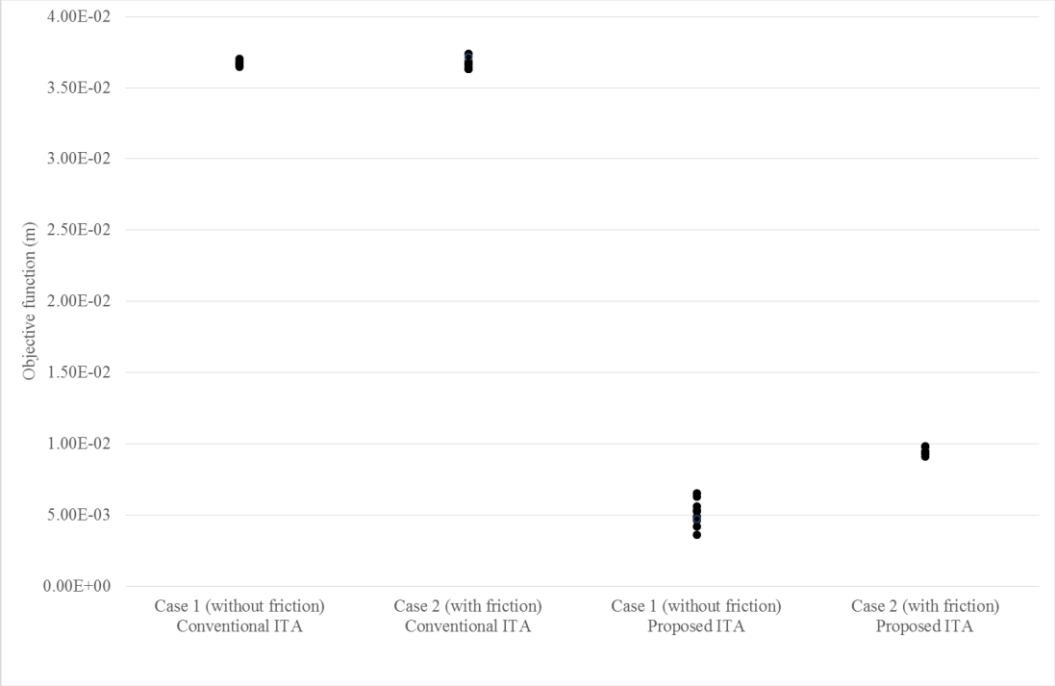

Figure 2.8 Objective function values of all 10 runs of ITA by two ITA approaches for two case studies.

The average wavespeeds estimated by the two ITA approaches are given in Fig. 2.9. The average wavespeeds estimated by the conventional ITA still exhibited significant variations, which is considered to be attributed to numerical errors in the interpolation methods. Compared with conventional ITA, the proposed ITA estimated wavespeeds more accurately, despite the fact that it neglects the effect of friction (which existed in the numerically simulated pressure trace).

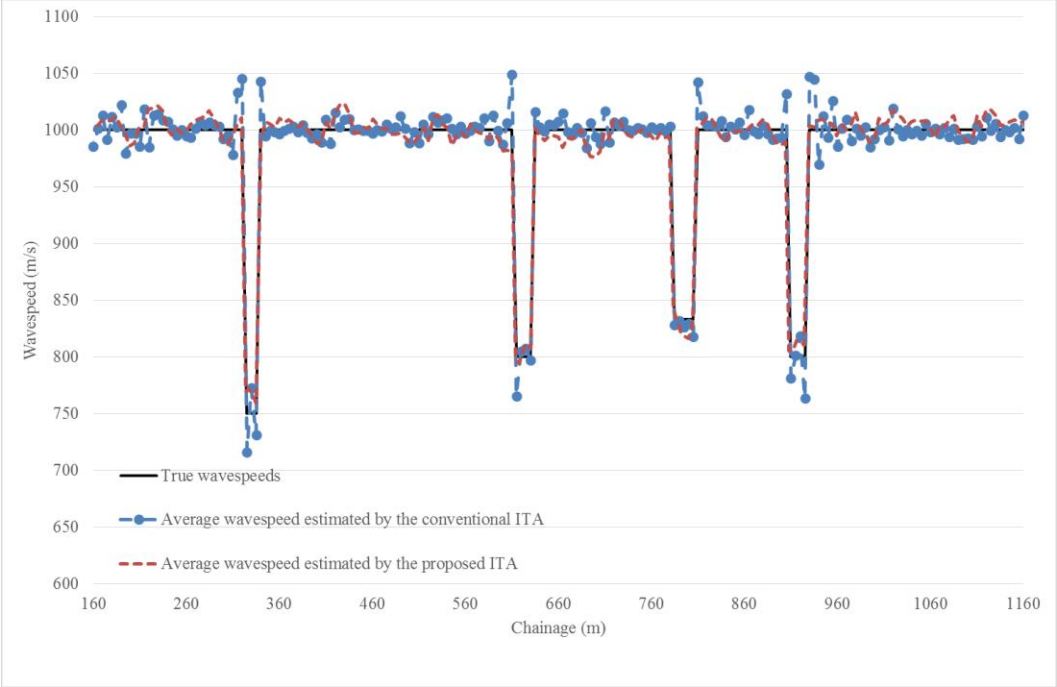

Figure 2.9 Comparison of the estimated and true wavespeeds by different ITA approaches

Table 2 shows the minimum and maximum wavespeed estimates and average and relative error of four deteriorated sections by two ITA approaches respectively in Case Study 2. The proposed ITA typically yielded improved estimates of the wavespeeds for all sections, in all cases (in the one occurrences where the conventional method yielded a better estimate). Compared with the relative errors in Case Study 1, the relative errors are slightly greater due to the additional complexity of the effects of friction.

In Case Study 2, the proposed ITA which excluded the friction term was applied to the numerically generated "measured pressure response" which included friction loss. Results have confirmed that neglecting the effects of friction does not compromise the accuracy of the wavespeed calibration, in

terms of the fit between predicted and measured pressures and estimation of wavespeeds, as illustrated by Figure 2.9 and Table 2.

Table 2.2 Summary statistics of wavespeed estimates of the four deteriorated sections for Case Study 2 (with friction) by the conventional and proposed ITA approaches

		Section 1	Section 2	Section 3	Section 4
True model	Wavespeed (m/s)	750.0	800.0	833.3	800.0
Conventional ITA	Min estimate (m/s)	716.4	765.7	817.6	763.9
	Max estimate (m/s)	772.8	807.8	831.9	818.5
	Average error (m/s)	25.1	12.6	***6.6***	18.7
	Average relative error	3.35%	1.58%	***0.79%***	2.34%
Proposed ITA	Min estimate (m/s)	759.2	794.3	816.7	805.4
	Max estimate (m/s)	772.1	811.7	842.0	814.8
	Average error (m/s)	***17.1***	***7.0***	9.6	***9.9***
	Average relative error	***2.28%***	***0.87%***	1.15%	***1.24%***

Note: A certain deteriorated section is covered by multiple reaches. The minimum and maximum calibrated wavespeed were selected in this table. The average error is calculated by averaging individual errors. The smallest error for each section is italicised and bolded.

[a]Average relative error = average error / theoretical value * 100%.

To further investigate the impact of neglecting friction, three other cases were also conducted on the same model configuration (Fig. 2.4) as a sensitivity analysis of the effect of friction. However, different velocities *V* from the reservoir to the side discharge valve at the generator (resulting in different Reynolds numbers and slight different friction factors, which can be found in

Table 3) were used to represent various levels of pipe friction. The effect of friction is greatest when velocity in the pipeline is maximum corresponding to 2.83 m/s. It is confirmed by these cases that neglecting friction does not compromise the detection of deteriorated sections. Even in the extreme case (velocity V = 2.83 m/s, Reynolds number Re = 1,490,476, friction factor f = 0.0193, where the effect of friction is maximized), the deteriorated sections were still successfully detected. These results are not discussed in detail for brevity.

Table 2.3 Velocities, Reynolds numbers and friction factors in the sensitivity analysis

	E1	E2	E3	E4
Velocity (m/s)	0.71	1.41	2.12	2.83
Reynolds number	372,619	745,238	1,117,857	1,490,476
Friction factor	0.02	0.0196	0.0194	0.0193

2.5 Discussion

The ITA approach proposed in this paper does not include friction in the transient modelling. Effects of steady or unsteady friction (Pezzinga, 2000, Adamkowski and Lewandowski, 2006, Prashanth Reddy et al., 2011) is essential in the numerical modelling of pressure and flow over a longer period, than is being considered in this research. A study by Duan et al. (2011) also indicated that the contribution of unsteady fiction effect is less important in practical pipe systems than in laboratory experiments. The proposed approach is aimed at the analysis of the pressure response (that covers the pipe section of interest after transient is generated) from field transmission mains

whose flow is relatively low. In the scenarios considered by this research, the impact of friction is minor.

Friction has also been omitted in other transient based leak detection methods proposed by Ferrante et al. (2009), which coupled wavelets analysis and a Lagrangian model. Meniconi et al. (2015) applied this frictionless method in the Milan pipe system to detect anomalies. Stephens et al. (2013) claimed that the effect of varying the pipeline roughness from relatively smooth to rough (increasing steady-state friction factor) introduced relatively minor changes in the predicted responses when the authors applied ITA for determining the internal wall condition in the field. Stephens et al. (2013) found that the inclusion of unsteady friction also resulted in a relative minor change to the predicted transient response, so it was excluded in the ITA process to reduce computational time.

The HBMOC approach is implemented on a flexible grid, which allows elimination of interpolation error in the forward process. In the scenarios considered by this paper where only the pressure responses that covers the pipe section of interest is analysed, interpolation error usually outweighs the error of neglecting friction. In the cases where friction cannot be ignored, a conventional MOC that is implemented on a flexible grid would be a suitable alternative.

Results from Case Study 2, which were designed to assess the capability of the proposed ITA under the condition where the friction was included in the "measured pressures", confirm that exclusion of friction effect in ITA does not compromise the accuracy of model calibration, given the scenarios

considered by this paper where only pressure responses which covers pipe section of interest was analysed.

2.6 Conclusions

An efficient and accurate ITA technique for pipeline condition assessment has been developed in this research. A head-based MOC approach has been developed and a flexible characteristic grid has been introduced, which together have been demonstrated to provide a more accurate and computationally efficient forward modelling approach in the ITA process. In the proposed method, the forward model was linked to the Particle Swarm Optimization algorithm to form an Inverse Transient Analysis approach. A sum of the absolute error minimization criterion was applied to guide the optimization of the wavespeed variation. The capability of using the proposed method for leak detection is also discussed briefly.

The numerical experiments conducted confirm that the wavespeeds along a single pipeline can be estimated accurately by the proposed ITA, while the wavespeeds estimated by the conventional ITA were distorted by numerical dispersion introduced by interpolation. The computational time required for the proposed ITA was significantly reduced (to a quarter that of the conventional ITA). The impact of neglecting friction has also been discussed. Results of Case Study 2, in which the proposed ITA was applied to the measured pressure traces including friction loss, confirms that exclusion of friction effect does not compromise the accuracy of model calibration, given the scenarios considered by this paper where only pressure responses which covers pipe section of interest was analysed. The sensitivity analysis also

confirms that even in the extreme case where the effect of friction is maximized, deteriorated sections were still successfully detected by the proposed ITA.

The proposed ITA, which incorporated Head Based Method of Characteristics and a flexible computational grid, improved computational efficiency and accuracy, making ITA a significant step forward towards cost-effective continuous assessment of transmission mains in the field.

Chapter 3

Multi-stage parameter-constraining inverse transient analysis for pipeline condition assessment

(Journal Paper 2)

Zhang, C., Zecchin, A. C., Lambert, M. F., Gong, J., & Simpson, A. R.

School of Civil, Environmental and Mining Engineering, the University of Adelaide, Adelaide, SA 5005 Australia

Journal of Hydroinformatics, 20(2), 281-300.

This page is intentionally blank.

Statement of Authorship

Title of Paper	Multi-stage parameter-constraining inverse transient analysis for pipeline condition assessment
Publication Status	☐ Published ☑ Accepted for Publication ☐ Submitted for Publication ☐ Unpublished and Unsubmitted w ork w ritten in manuscript style
Publication Details	Zhang, C., Zecchin, A. C., Lambert, M. F., Gong, J., & Simpson, A. R. (2018). Multi-stage parameter-constraining inverse transient analysis for pipeline condition assessment. Journal of Hydroinformatics, jh2018154.

Principal Author

Name of Principal Author (Candidate)	Chi Zhang
Contribution to the Paper	Conception and design of the project Analysis and interpretation of research data Draft the paper
Overall percentage (%)	75%
Certification:	This paper reports on original research I conducted during the period of my Higher Degree by Research candidature and is not subject to any obligations or contractual agreements with a third party that would constrain its inclusion in this thesis. I am the primary author of this paper.
Signature	Date 02 / 03 / 2018

Co-Author Contributions

By signing the Statement of Authorship, each author certifies that:

i. the candidate's stated contribution to the publication is accurate (as detailed above);

ii. permission is granted for the candidate in include the publication in the thesis; and

iii. the sum of all co-author contributions is equal to 100% less the candidate's stated contribution.

Name of Co-Author	Aaron Zecchin
Contribution to the Paper	Conception and design of the project Analysis and interpretation of research data Critically revising the paper so as to contribute to the interpretation
Signature	Date 2 / 3 / 2018

Name of Co-Author	Martin Lambert
Contribution to the Paper	Conception and design of the project Analysis and interpretation of research data Critically revising the paper so as to contribute to the interpretation
Signature	Date 2/3/18

Name of Co-Author	Jinzhe Gong		
Contribution to the Paper	Conception and design of the project Analysis and interpretation of research data Critically revising the paper so as to contribute to the interpretation		
Signature		Date	01/03/2018

Name of Co-Author	Angus Simpson		
Contribution to the Paper	Conception and design of the project Analysis and interpretation of research data Critically revising the paper so as to contribute to the interpretation		
Signature		Date	2 Mar 2018

Please cut and paste additional co-author panels here as required.

Abstract

Fault detection for water distribution systems is of critical importance for water authorities to maintain pipeline assets effectively. This paper develops an improved Inverse Transient Analysis (ITA) method for the condition assessment of water transmission pipelines. For long transmission pipelines ITA approaches involve models using hundreds of discretized pipe reaches (therefore hundreds of model parameters). As such these methods struggle to accurately and uniquely determine the many parameter values, despite achieving a very good fit between the model predictions and measured pressure responses. In order to improve the parameter estimation accuracy of ITA applied to these high dimensional problems, a multi-stage parameter-constraining ITA approach for pipeline condition assessment is proposed. The proposed algorithm involves the staged constraining of the parameter search-space to focus the inverse analysis on pipeline sections that have a higher likelihood of being in an anomalous state. The proposed method is verified by numerical simulations, where the results confirm that the parameters estimated by the proposed method are more accurate than the conventional ITA. The proposed method is also verified by a field case study. Results show that anomalies detected by the proposed methods are generally consistent with anomalies detected by ultrasonic measurement of pipe wall thickness.

This page is intentionally blank.

3.1 Introduction

Model calibration is the process of determining the model parameters to obtain a model representation of the system of interest that satisfies a certain criterion, i.e. a goodness of fit metric between the system measurements and the simulated model (Savic *et al.* 2009). Inverse Transient Analysis (ITA) (Liggett & Chen 1994), one of the popular transient-based methods (Meniconi *et al.* 2013; Gong *et al.* 2014; Massari *et al.* 2014; Capponi *et al.* 2017; Duan 2017), is a process of pipe system parameter estimation using measured transient pressure data and a hydraulic transient model. The inverse analysis is achieved by adjusting pipeline system parameters (such as leak locations and sizes, friction factors, water demands or hydraulic transient wave speeds) so that the calibrated model's predicted response matches the measured response (typically the temporal measurements of pressure). In the case of hydraulic transient wave speeds, the calibrated parameter is closely related to the pipeline condition (Stephens *et al.* 2013), as the wave speed is related to the wall thickness and internal diameter of the pipe, which change as the pipe wall corrodes. As such, a well calibrated model provides valuable information about the pipeline condition, which serves as guidance for water authorities to assess infrastructure condition, and maintain assets strategically.

Despite the fact that ITA has been widely studied, the scale of the problems that have been considered (i.e. the number of system parameters) is relatively small. ITA was first proposed by Liggett & Chen (1994) for leakage and friction factor calibration. Within their numerical study, 15 parameters, including 11 friction factors and four leak sizes, were calibrated for a small

11-pipe network. Jung & Karney (2008) considered a numerical case study, where the wave speed, diameter and friction factor of 11 pipes, four possible leakages and one water demand were calibrated simultaneously (38 parameters overall), on the same network as Liggett & Chen (1994). The average error of the parameter estimates was, in general, greater than 30% and the authors claimed the error associated with estimated wave speeds tends to compromise the calibration of other parameters. Shamloo & Haghighi (2010) also conducted ITA on the same network to detect potential leaks. The absolute errors of the 17 parameter estimates (six leak sizes and 11 friction factors) were all below 5% by optimizing the transient generation and the choice of measurement site.

Concerning the laboratory verification of ITA, Vitkovsky *et al*. (2001, 2007) calibrated the leak size for a laboratory system consisting of a 37.2 m long copper pipe with an internal diameter of 22.1 mm. A total of 15 leak candidate locations were considered where the measured pressure trace contained multiple periods of the transient wave in the pipe system. Covas & Ramos (2010) applied ITA to a 272 m high-density polyethylene pipe with an internal diameter of 50.6 mm and a 1.3 km polyethylene pipe with an internal diameter of 70 mm. Multiple models were considered, where the number of calibrated parameters was less than 30 for each model. Soares *et al*. (2011) applied ITA to a system composed of looped PVC pipes with a total length of 203.20 m. The potential leak locations in the inverse model was 7. It is worth pointing out that both Covas & Ramos (2010) and Soares *et al*. (2011) adopted a strategy to minimize the number of leak candidates, starting with a set of leak candidates sparsely distributed throughout the system, and gradually reducing

the set of candidates to those around the potential leak locations obtained in the earlier steps.

ITA in the frequency domain has also attracted attention. Kim (2008) developed an address-oriented impedance matrix method for the generic calibration of several parameters, such as the location and quantity of leakage, the friction factor, and the wave speed simultaneously. The method was numerically verified by a 12-pipe network. Kim (2008) also adopted a similar multi-stage strategy to Covas & Ramos (2010), starting the calibration with the initial search-space, which was the accumulated length of all of the pipeline elements, and then restraining the search-space to a candidate pipeline element. Zecchin *et al*. (2013) developed a frequency-domain maximum likelihood estimation method to identify parameters of fluid line networks, in which different types of parameters including wave speed, diameter, and length of pipe were calibrated simultaneously. The proposed method was applied on an 11-pipe network using turbulent steady friction and turbulent unsteady friction pipe models, which resulted in parameter estimation problems of dimension 33 and 55, respectively. Compared with time domain ITA, there are fewer laboratory or field verification works for frequency domain applications of ITA. Laboratory verification of the frequency domain ITA is found in the research by Kim *et al*. (2014), where location and discharge of a single leak, together with other parameters, such as wave speed were calibrated. Capponi *et al*. (2017) also successfully located and sized one leak, one blockage and one branch with high accuracy in a controlled laboratory environment.

As outlined above, the complexity of the inverse problem (i.e. the dimensionality of the parameter estimation space) is limited in most previous research. An exception is the work by Stephens *et al*. (2013), where ITA was applied to a mild steel cement-lined transmission mains in rural South Australia. In this work, the wave speeds of 390 reaches, along a 6 km section of pipe were calibrated to infer internal pipe wall condition. The pattern of estimated wave speeds by ITA were generally consistent with ultrasonic measurements taken along the pipe, although this was not always the case. However, within this application, Stephens *et al*. (2013) claimed that it was almost certain that the optimal solution was not found, due to a limitation on the number of objective function evaluations used by the optimizer (given the high computational cost of overall millions evaluations) and model error. Additionally, the authors also believed that, given the high dimensionality of the problem, it was very likely that non-unique solutions existed, meaning that there were very many local optimum solutions with similar objective function values. However, this issue was not explored in detail in their work.

Non-uniqueness of solutions for ITA applications has been observed in other work, and is a known problem for inverse problems more generally (Yeh 1986). Within the study by Jung & Karney (2008), three different ITA scenarios were analyzed on an 11-pipe network, where each had a different number of measurement sites. The authors concluded that fewer measurement sites led to a better calibration error and faster convergence to the calibrated parameter values, but to a less accurate calibration result. Kapelan *et al*. (2004) pointed out that some poorly estimated parameters were due to an inadequate quantity of observed information. That is, Kapelan *et al*. (2004)

outlined that the parameter calibration problems could not be resolved by simply using an alternative search algorithm. To improve the ill-posed natural of the inverse problem, a framework for the effective incorporation of prior information into inverse transient analysis for pipe networks was developed. However, these two approaches to enhance the identifiability are not always feasible in field tests, where access points to install pressure transducers are limited, and prior information is not always available. Instead of increasing the number of measurement sites or incorporating prior knowledge of a system, another strategy to enhance parameter identifiability of ITA is to reduce the complexity of the inverse problem by limiting the number of decisions (Kim 2008; Covas & Ramos 2010) or limiting the range of the search-space.

The interval for a parameter's search-space is typically the minimum and maximum feasible values of the parameter to be calibrated, and they are typically the same for every reach. However, in the case of wave speed calibration in ITA, typically sections of pipe in a normal state (e.g. sections in a generally good condition) have wave speed values within a small band about a nominal value, and it is only anomalous sections (e.g. sections with severe deterioration) that possess significant uncertainty and variability in the wave speed values that they can take. Therefore, if the search-space can be properly adjusted for each reach to account for the reduced uncertainty for normal sections of pipe, better parameter estimates can be expected within the limited search-space.

To enhance parameter identifiability of ITA on a complex transmission main, a multi-stage parameter-constraining ITA is proposed in this paper. This paper

is organized as follows: to highlight lack of identifiability achieved by the conventional ITA on a complex transmission mains system, a numerical example with a highly variable pipe wall condition is considered (represented by hundreds of reaches each with different wave speeds). It is confirmed within this example that the conventional ITA is not able to uniquely identify the correct wave speed values, despite achieving parameter estimations that provide a very good fit of the predicted and measured pressure responses. To tackle this problem, a multi-stage parameter-constraining ITA is proposed. The proposed algorithm works by iteratively generating sets of parameter estimates and coincidentally modifying the search-space interval for the subsequent estimates. Based on a statistical analysis of the set of estimates, each reach is classified as normal (parameter values close to the nominal values) or anomalous (parameter values significantly different from the nominal values). Different search-space intervals are allocated to each reach based on the outcome of the classification. Parameter estimation within the properly narrowed search-space will lead to concentration of parameter estimates and elimination of outliers, thus identifiability of parameters by ITA is enhanced. This algorithm is followed by a numerical verification and discussion about the sensitivity to the relevant parameters. Finally, the method is verified by a field case study.

3.2 Background: lack of identifiability within ITA application

The problem of lack of identifiability for applications involving the conventional ITA method are explored within this section with a numerical

example application on a Reservoir-Pipeline-Valve (RPV) system. Within this section, the numerical example illustrates that when applying the conventional ITA to a relatively complex (yet realistic) inverse problem, the identifiability of the wave speed parameters is relatively poor. This is evidenced by the fact that independent inverse runs (using a stochastic or evolutionary optimization approach with different random number sequences) yielded a large variability in the optimal parameter estimates, despite the high similarity in the estimates associated calibration error. The data of the system is described in the next sub-section, followed by a discussion, where it is demonstrated that the conventional ITA suffers from the problem of lack of identifiability.

3.2.1 Numerical example

A typical RPV system (Figure 3.1) is used to simulate a transmission main throughout this paper. The wave speed distribution along the pipe is depicted in Figure 3.2. Wave speeds of 115 normal reaches are in the range of 950–1000 m/s. A total of 13 reaches (nine sections in Figure 3.2), whose wave speeds are either less than 950 m/s or greater than 1000 m/s, are used to represent different wall thickness pipe sections due to different pipe classes or wall condition. A transient wave is generated by instantaneously shutting the side discharge valve at node G when t = 0.2 s. The pressure responses at locations M1, M2 and G are obtained by numerical simulation using the MOC in which the time step $\Delta t = 0.01$ s. The length of each reach was determined by $\Delta x_i = a_i \Delta t$ to satisfy Courant Condition. This avoids interpolation errors in the forward model when synthetically generating the "measured" pressure

traces. Only a duration of 1.2 s after the transient generation is considered in the ITA to avoid reflections from the boundaries of the RPV system.

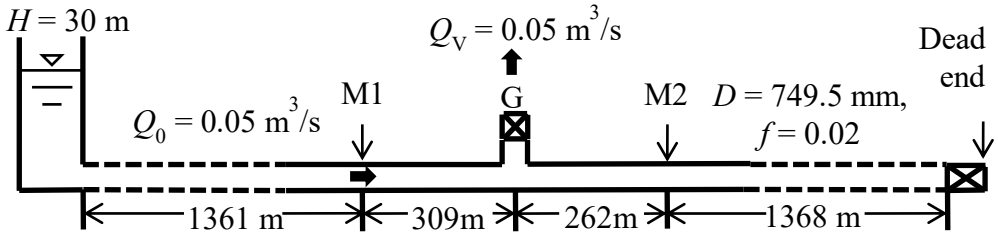

Figure 3.1 Numerical experiment pipeline configuration.

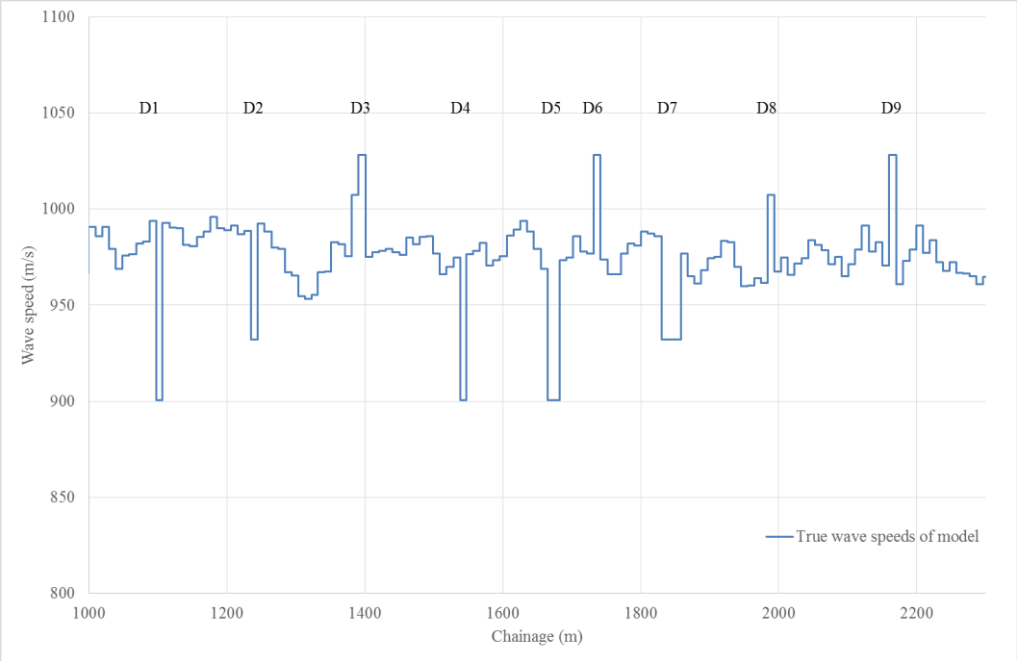

Figure 3.2 True wave speeds of the numerical model.

The conventional ITA used in this paper is the efficient version proposed by Zhang *et al*. (2017), in which the Head Based Method of Characteristics (HBMOC) is employed as the transient simulator. Particle Swarm Optimization (PSO) (Poli *et al.* 2007) was employed as the optimization algorithm – to account for the stochastic nature of PSO, the ITA is run multiple times (with different starting random number seeds) to provide a statistical characterization of the algorithms performance. The objective

function is defined as the squared difference between the measured responses and the predicted responses by the calibrated model summed over all measurement stations to form a maximum likelihood estimation. A time step of 0.01 s was used in the ITA. Considering the 1.2 s pressure trace used in ITA and the location of measurement sites, an inverse model with 128 reaches is required, to accommodate all reaches contributing to the 1.2 s pressure trace. As such, the number of decision variables is 128, and for PSO, the number of particles is 150 with 10,000 iterations (resulting in 1,500,000 evaluations overall), which were selected so as to allow for convergence of the algorithm's search. The search-space was set to be [800 m/s, 1050 m/s], and the decision variables were treated as continuous within this range by the PSO.

3.2.2 Example results and discussion

Figure 3.3 presents a series of boxplots for the wave speeds estimated in each reach by ten independent runs. It can be seen that the interquartile range (IQR) of the wave speeds for each reach are generally large, which means that the wave speed estimates of the independent runs are spread diversely throughout the wide search-space (i.e. starting from different random number seeds, the PSO ended up with significantly different solutions). This high variability amongst the parameter estimates limits a clear interpretation of the results, and the ability to use these estimates for the detection of the anomalous sections.

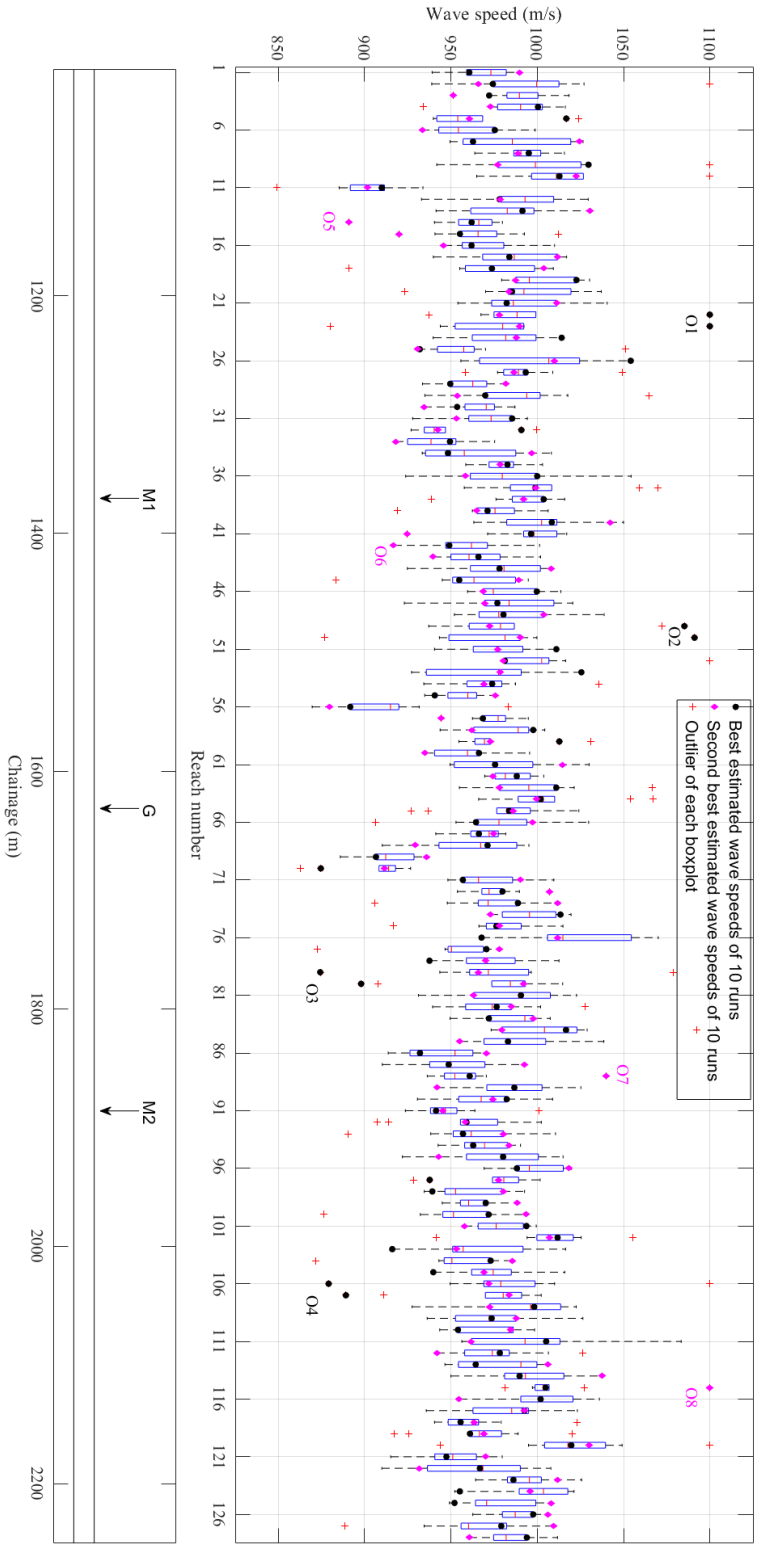

Figure 3.3 Boxplot of wave speeds estimated by ten independent runs, and the top two best estimated wave speed sets (ranked in terms of objective function). O1-O8 are the distinct outliers existing in the top two best estimated wave speeds.

To understand why the conventional ITA parameter estimates in Figure 3.3 yield such high variance, the envelopes of ten predicted pressure traces and the match between measured pressure trace and predicted pressure trace obtained by the best solution from the ten runs (ranked in terms of objective function) are given in Figure 3.4. Despite the existence of outliers in the estimates (O1–O4 in Figure 3.3), the best wave speed estimates solution still provides an excellent match between its predicted pressure traces and the measured pressure trace. The closely wrapped envelopes of predicted pressure traces indicate that reasonable match was achieved by every set of wave speed estimates. The fact that such an excellent model fit can be achieved for such vastly different parameter estimates means that the objective function is not sufficiently informative to allow for the discrimination between different parameter sets. These findings support the observations from Kapelan *et al*. (2004) concerning estimation issues arising from data information limitations for certain ITA applications.

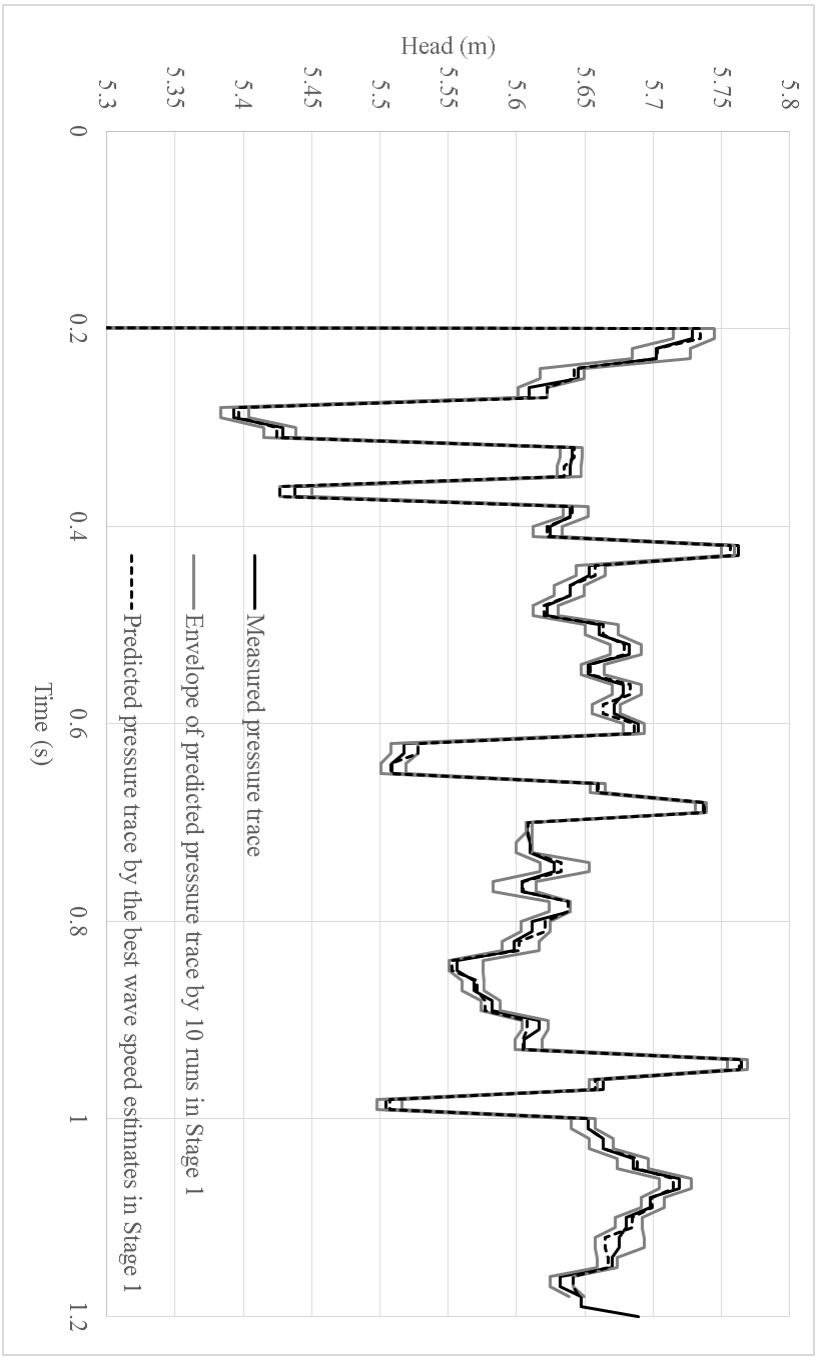

Figure 3.4 Measured pressure trace, predicted pressure trace obtained by the best solution from the ten runs (ranked in terms of objective function) and the envelopes of ten predicted pressure traces.

3.3 Proposed method: multi-stage parameter-constraining ITA (ITA_{MP})

3.3.1 Overview

In the previous example, it has been illustrated that, for the conventional ITA, independent parameter estimates are widely spread throughout the search-space. Despite the reasonable match between the modelled and measured pressure traces, distinct outliers exist in the estimates, suggesting that multiple local optimum exist in the relatively large search-space. This limitation of the conventional ITA to correctly identify parameter estimates for large-scale problems has motivated the iterative parameter-constraining approach of the proposed method.

The motivating for the proposed method is outlined in the following. Transmission mains are typically installed with a similar design and are deteriorated in a similar way, unless the cumulative effect of soil or groundwater corrosion and external loaded forces increase degradation in some sections. Besides these severely deteriorated sections, undocumented class changes with different wave speeds and pipe sections replaced by plastic pipe section with lower wave speeds are also anomalous sections in transmission mains. Compared with the majority sections which are in similar conditions, these anomalous sections are localized to a limited number of short discrete sections along the pipeline. The wave speed parameter values for the normal sections are confined to within a small interval about a nominal value, as there is much less uncertainty about the values that the normal

sections can take. In contrast, the anomalous sections contain wave speed values lie within a much broader interval, as there is significant uncertainty about the values that the anomalous sections can take. Therefore, it is expected that the effectiveness and accuracy of the ITA parameter estimation process would be increased if adaptive search-space parameter intervals were used to allow for a narrowing of the interval for sections that were recognized as normal, and maintaining a broader interval for sections that were identified as anomalous. Based on this idea, a multi-stage parameter-constraining ITA (ITA_{MP}) method is proposed. In this approach, the search-space is iteratively limited, guiding the solutions closer to the true parameter values.

3.3.2 The ITAMP algorithm

The flowchart of the ITA_{MP} algorithm is given in Figure 3.5. The algorithm comprises multiple iterative stages, and each stage involves the sub-stage of new solution generation, reach classification, search-space updating for the next stage and the termination criteria check. Details of the four sub-stages are presented in the following sub-sections.

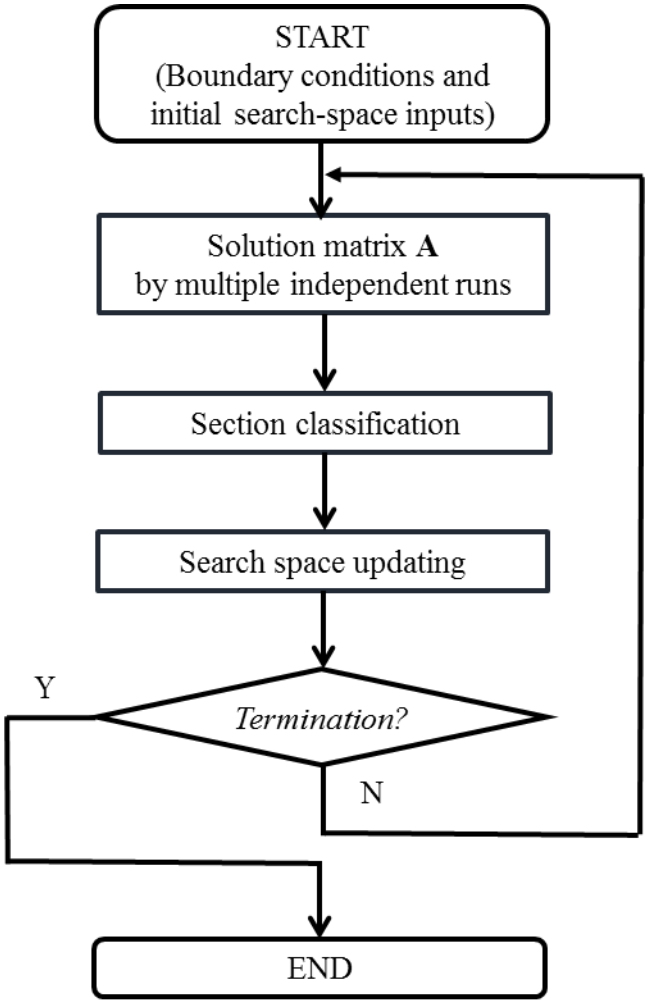

Figure 3.5 The flow chart of multi-stage parameter-constraining ITA algorithm.

3.3.2.1 Sub-stage 1: New solution matrix generation

The objective function used in the proposed ITA approach is defined by Equation (3.1):

$$\mathrm{OF}(\boldsymbol{a}) = \frac{1}{N_{MS}N_{TS}} \sum_{i=1}^{N_{MS}} \sum_{j=1}^{N_{TS}} (H_{i,j}^{m} - H_{i,j}(\boldsymbol{a}))^2 \qquad (3.1)$$

where N_{MS} = number of measurement stations (including the generator station if the transient pressure variation is also recorded there); N_{TS} = number of time steps; $H_{i,j}^{m}$ = measured pressure response at *i*th measurement station and *j*th time step; $H_{i,j}$ = predicted pressure response at *i*th measurement station and *j*th

time step from the calibrated model; $\boldsymbol{a} = [a_1, \ldots, a_N]^T$ is the vector of unknown wavespeeds, where a_k = wave speed of *k*th reach, where the search for the wave speeds is typically bounded as $a_k \in [a_{min,n}, a_{max,n}]$. The search-space in Stage 1 $[a_{min,1}, a_{max,1}]$ is determined by the maximum and minimum feasible parameter values. The search-space in Stage *n* $[a_{min,n}, a_{max,n}]$ is determined in the Stage *n*–1 and it is explained in the following section "search-space updating for the next stage".

All the solutions from *M* different independent ITA runs are saved in a solution matrix $\mathbf{A_n}$, which is defined as:

$$\mathbf{A_n} = \begin{bmatrix} \boldsymbol{a}_{1,n}^T \\ \vdots \\ \boldsymbol{a}_{M,n}^T \end{bmatrix} = \begin{bmatrix} a_{1,1,n} & \cdots & a_{1,N,n} \\ \vdots & \ddots & \vdots \\ a_{M,1,n} & \cdots & a_{M,N,n} \end{bmatrix}$$

where $a_{i,j,n}$ = *i*th wave speed estimation of the *j*th reach; *N* = number of reaches; *M* = number of independent ITA runs; *n* = stage number.

3.3.2.2 Sub-stage 2: Section classification

The solution matrix $\mathbf{A_n}$ provides a data set of wave speed estimates for each reach. A fundamental assumption of the proposed process is that the previous applications of ITA have been effective in their optimization strategy, and that the majority of estimates are, at least, within the neighborhood of the global optimum wave speed solution $\boldsymbol{a}^*$. Given this assumption, the classification of whether a reach is considered *normal* or *anomalous* is based on analyzing the data set for each reach to determine if the estimates are significantly different from the nominal properties of the entire set of wave speed estimates. That is, given the set of wave speed estimates $\boldsymbol{a}_{k,n}$ for reach *k*, $\{a_{1,k,n}, \ldots, a_{M,k,n}\}$, the

classification process aims to determine the likelihood that the statistical properties of this set are consistent with the statistical properties of the wave speed estimates for a normal section of pipe as characterized by the data set $\mathbf{A}_{/k,n}$ (the data set comprised of all elements of $\boldsymbol{A}_n$ excluding column *k*, represented as the subscript $/k$). If the statistical properties of the *k*th reach are consistent with the properties of a normal section of pipe, then the reach is classified as *normal*, if not, then it is classified as *anomalous*.

Given the fact that the properties of the estimates of a normal section of pipe are unknown a priori, the data set $\boldsymbol{A}_{/k,n}$ comprised of the wave speed estimates for the rest of the pipeline are used to characterize a normal section. This approach to the characterization of the estimates for a normal section is justified on the basis that a fraction of reaches will be in an anomalous state (sections with severely deteriorated conditions, undocumented or replaced pipe sections with different material), and the majority reaches will be in the normal state (generally good condition or similarly deteriorated condition). This means that within this larger data set (all elements of $\mathbf{A}_{/k,n}$) the influence of estimates for the anomalous sections on the statistics of this set will be small compared to the influence of the normal sections. This is particularly the case when order statistics are used to characterize the set, as these are insensitive to outliers in a data set.

An appropriate statistical test to undertake the comparison of the *k*th reach data set $\boldsymbol{a}_{k,n}$ with $\mathbf{A}_{/k,n}$ is the Mann–Whitney U test (Hollander *et al.* 2013). This test provides a non-parametric approach to compare two data sets to determine the likelihood that a random sample of one data set will be less than

(or greater than) a random sample of the other data set. The null hypothesis of this test is that both sets are distributed about the same median value, meaning that it is equally likely that a sample from one data set will be less than (or greater than) a sample from the other. A rejection of the null hypothesis means that it is more likely that both sets are not distributed about the same median value. In the classification context of this paper, a reach is classified as *normal* if the null hypothesis holds, and is classified as *anomalous* if the null hypothesis is rejected. The acceptance or rejection of the null hypothesis is dependent on the comparison of the *p*-value for *k*th reach, $p_{k,n}$, returned by Mann–Whitney U and the specified significance level α_n. The null hypothesis is accepted if $p_{k,n} \geq \alpha_n$, and is rejected if $p_{k,n} < \alpha_n$.

The significance level α_n is a fundamental parameter of the proposed method. A physical interpretation of the significance level can be considered as follows: under the assumption that *m* % of the pipe reaches will be classified as *anomalous*, the associated significance level is given by:

$$\alpha_n = m - \text{th percentile of } \mathbf{P_n}. \tag{3.2}$$

where $\mathbf{P_n} = \{p_{1,n}, \dots, p_{M,n}\}$. The advantage of considering *m* as the user specified parameter is its interpretation as providing an upper bound on the percentage of the pipe that is assumed to be in an anomalous state. It is therefore recommended that *m* should be set greater than the assumed percentage of anomalous sections of the pipeline under investigation. The appropriate choice of *m* will be investigated in the section on numerical verification. The outcome of this stage are the two sets: $C_{0,n}$ = the set of

reaches that are classified as normal; and $C_{A,0}$ = the set of reaches classified as anomalous.

3.3.2.3 Sub-stage 3: Search-space updating for the next stage

Different search-space intervals are allocated for different reaches in the next stage, depending on the set $C_{0,n}$ or $C_{A,n}$ that the reach belongs to. The detection of an anomalous section is the focus of the parameter estimation, as a result, a reach classified as *anomalous* ($a_{k,n}, k \in C_{A,n}$) will retain the original wide wave speed search interval $[a_{min,1}, a_{max,1}]$ so that the estimation strategy is still able to search within the full search-space.

A reach which is classified as *normal* ($a_{k,n}, k \in C_{0,n}$) will be allocated a narrower wave speed search interval $[a_{,min,n+1}, a_{max,,n+1}]$ in the next stage. The new search-space bounds $a_{min,n+1}, a_{max,n+1,}$ for a reach classified as normal are determined by percentile values of $A_{n,0}$:

$$a_{min,n+1} = p - \text{th percentile of } A_{0,n} \tag{3.3}$$

$$a_{max,n+1} = q - \text{th percentile of } A_{0,n} \tag{3.4}$$

where $q > p$; $A_{0,n} = \{a_{i,j,n} : i \in C_{0,n}, j = 1, \dots, M\}$.

$A_{0,n}$ is the collection of multiple estimates for all reaches which are classified as normal, so the statistics of $A_{0,n}$ can be used to represent the parametric range that the wave speed values of the normal reaches are within. Considering the likely existence of outliers in the estimates in $A_{0,n}$, p and q percentile of $A_{0,n}$ are used to determine the new search-space bounds. Compared with the original search-space $[a_{min,1}, a_{max,1}]$, the new search-

space $[a_{min,n+1,}, a_{max,n+1,}]$ is a narrower interval. The choice of percentile rank *p* and *q* will be discussed in the section on numerical verification.

3.3.2.4 Sub-stage 4: Termination criteria

The algorithm is terminated from iterating in Stage 2 when the *M* multiple solutions generated within the updated search-space at Stage *n* all have a larger objective function than the previous best objective function from iteration Stage *n*–1. The algorithm aims to minimize the objective function, so if it fails to decrease the objective function, thus fails to improve the match between the calibrated models and the measured data, there is sufficient reason to believe that a failure of finding a better solution is attributed to an improper updated search-space, so the algorithm is terminated.

3.4 Numerical study

A numerical experiment was conducted to verify the proposed ITA_{MP}. The numerical model is the same as in Figure 3.1. The number of reaches is *N* = 128; and the number of independent ITA runs for different starting random number seeds is *M* = 10, where PSO was used as the optimization algorithm.

Nine cases were considered given different values of *m*, *p* and *q* (see Table 1). Case 3 (*m* = 15, *p* = 5 and *q* = 95) is discussed in detail in the section "Results and discussions". The other cases are discussed in the section "Choice of *m*, *p* and *q* values".

Table 3.1 m, p and q values for nine different cases that were investigated

	Case 1	**Case 2**	**Case 3**	**Case 4**	**Case 5[a]**	**Case 6**	**Case 7**	**Case 8**	**Case 9**
m	5	10	15	20	15	15	15	15	15
p	5	5	5	5	0	1	2	10	15
q	95	95	95	95	100	99	98	90	85

[a]In Case 5, the search-space bound $a_{n,min}$ and $a_{n,max}$ are determined by the minimum and maximum of $A_{n,0}$. For simplicity, the minimum and maximum of $A_{n,0}$ are noted as 0th or 100th percentile of $A_{n,0}$, which technically do not exist.

3.4.1 Detailed results for Case 3

For Case 3, the objective functions of all independent ITA runs are given in Figure 3.6. From this figure it is seen that the ITA_{MP} terminated after Stage 3, making the total number of independent ITA runs equal to 30. The ten ITA runs in Stage 1 ended up with a diverse set of solutions due to the random nature of the optimization algorithm and the relatively large search-space, which is consistent with the diverse wave speed estimates in Figure 3.3. A significant reduction in the objective function value can be seen in Stage 2, after the first search-space update. Solutions in Stage 2 show more consistency in their objective function values within narrowed search space.

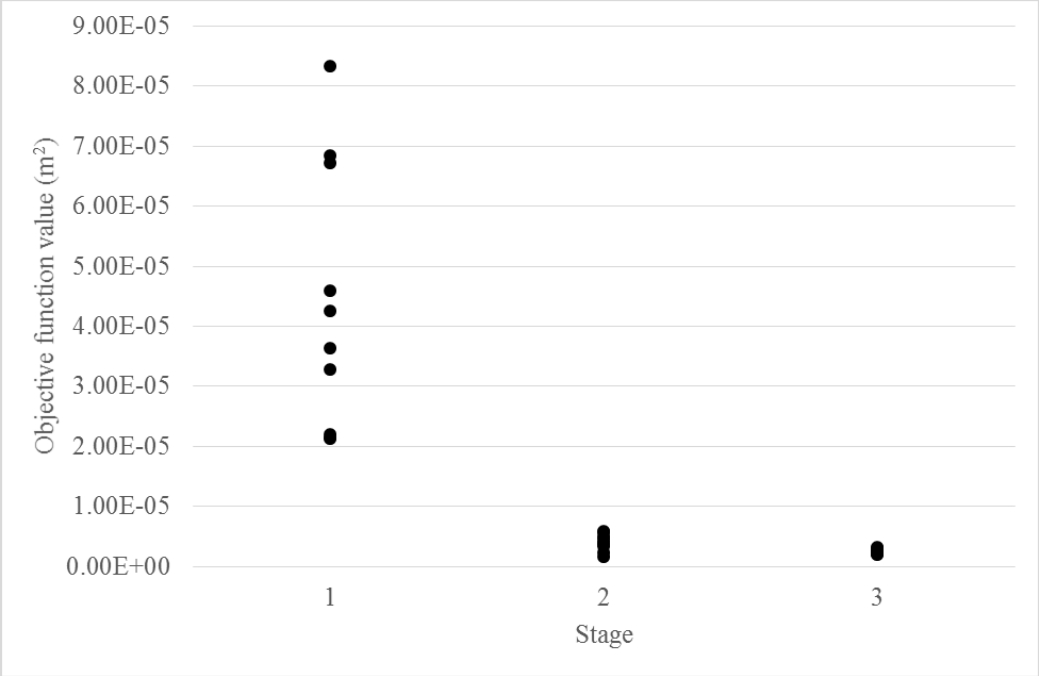

Figure 3.6 Objective function of each independent run in all stages (ten runs at each stage).

Figure 3.7 presents the boxplot of the wave speed estimates in Stage 2. Compared with the wave speed estimates in Stage 1 in Figure 3.3 (the result of Stage 1 is the results of the conventional ITA, since the conventional ITA is terminated after multiple independent runs is Stage 1), the IQR of wave speed of each reach become significantly less. For the proposed approach, the wave speed estimates become increasingly concentrated around the true wave speeds of the model, making the interpretation of the results and detection of anomalous sections easier.

Figure 3.7 Boxplots of wave speed estimates in Stage 2.

From Figure 3.7, it also can be seen that the outliers existing in the Stage 1 estimates (for example, O1–O8 in Figure 3.3) were not present in the estimates of Stage 2. Elimination of the outliers was due to the section classification, and consequent search-space updating, in ITA_{MP}. Interestingly, these outliers from the single run in Stage 1 were identified as normal sections in Stage 2, because the estimates of the other independent runs yielded statistics consistent with the normal value. As a result, in the next stage, the search-space was properly narrowed, and a better solution was found.

The enhanced identifiability of wave speed estimates also resulted in an improvement in the match of the measured and predicted pressure traces, for which the traces at the generator location are given in Figure 3.8. All independent wave speed estimates in Stage 2 provided an almost indistinguishable match between measured and predicted pressure traces, indicated by shrunk envelopes of predicted pressure traces in Stage 2, compared with those in Stage 1 in Figure 3.8.

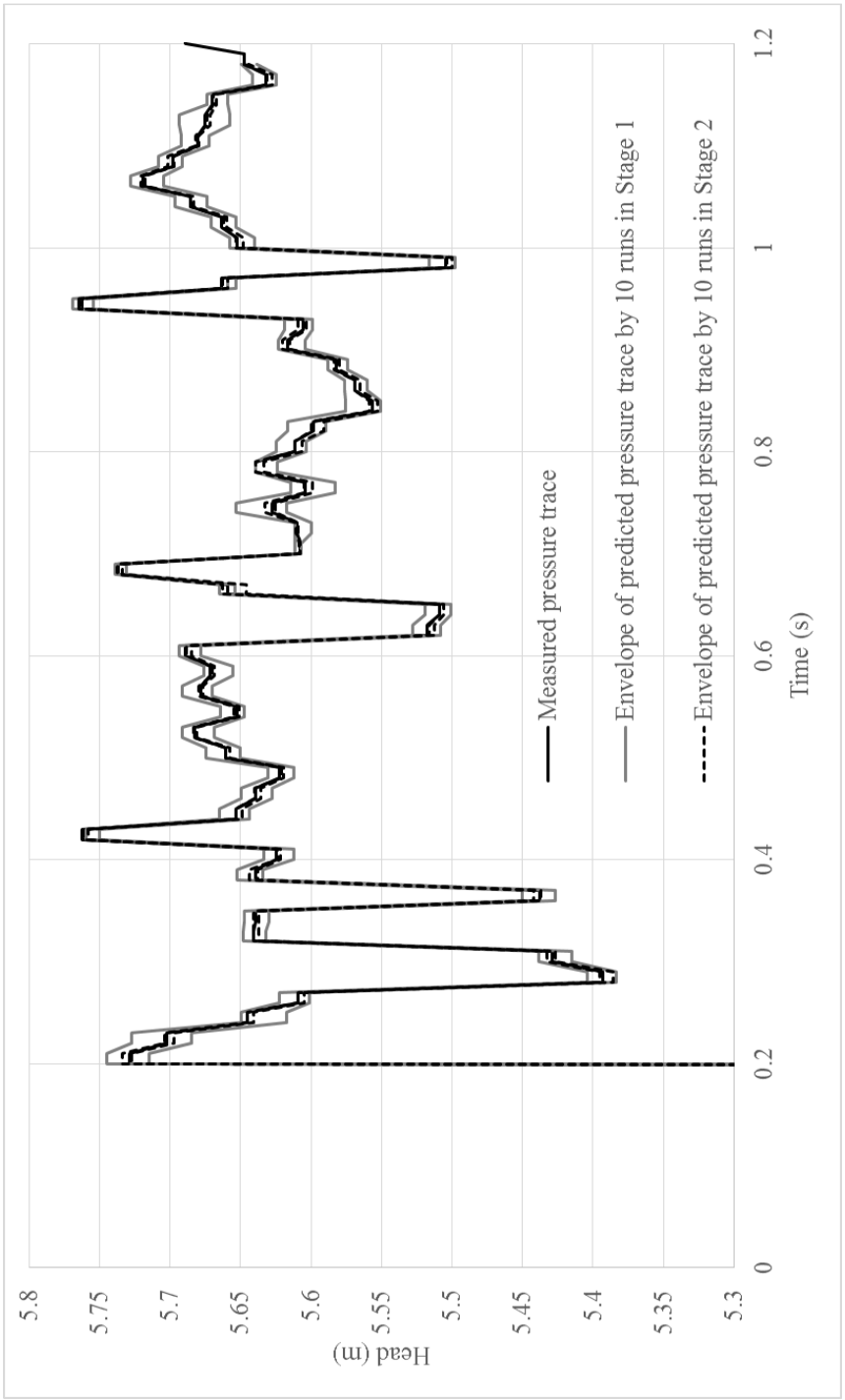

Figure 3.8 Comparison of the envelopes of ten predicted pressure traces in Stage 1 and Stage 2.

3.4.2 Sensitivity to the percentile rank parameters m, p and q

The sensitivity of the ITA_{MP} results to the percentile rank parameters *m*, *p* and *q* is discussed in this section. Three parameters *m*, *p* and *q* are percentile ranks in Equations (3.2)–(3.4) to determine the significance level in the Mann–Whitney U test and search-space bounds for next stage ITA runs in Stage 2.

As explained in the section "numerical experiment", among 128 reaches of the inverse model, 13 reaches (or a total of nine sections) are anomalous, meaning that the proportion of anomalous reaches is 10.2%. It has been explained that the percentile rank *m* represents the proportion of reaches which will be identified as anomalous reaches within ITA_{MP}. Case 1 ($m = 5$, $p = 5$, $q = 95$) is used as an example to illustrate the impact of a smaller *m* on the results. In Case 1, the ITA_{MP} algorithm terminated after Stage 2. Figure 3.9 represents the single best wave speeds of Stage 2.

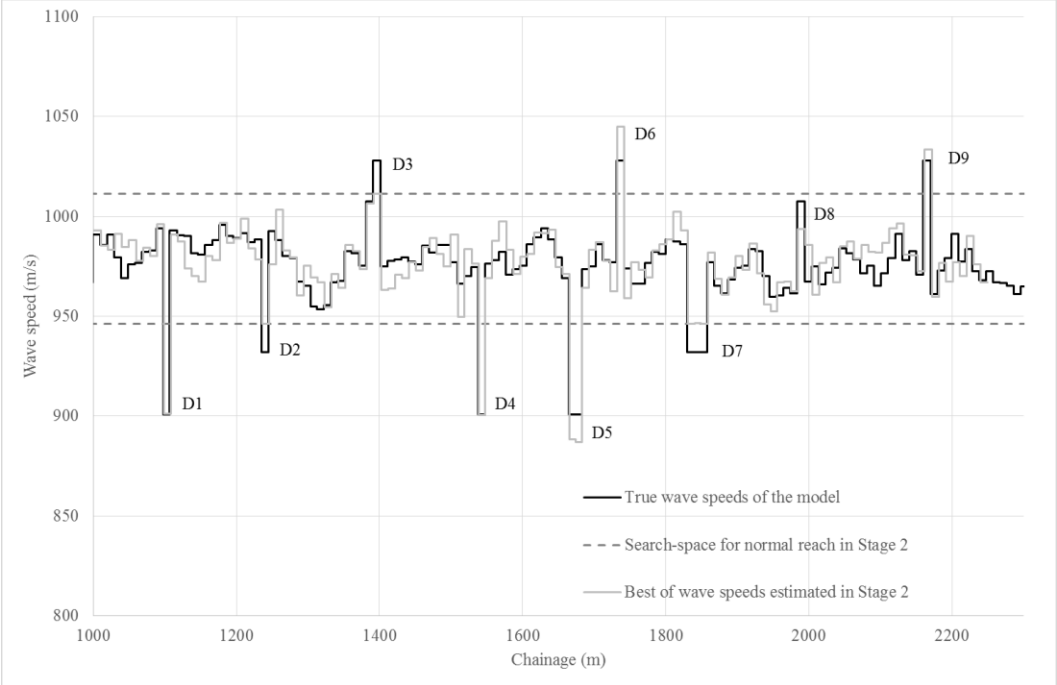

Figure 3.9 True wave speeds of the model, the best estimated wave speeds of Stage 2 and current search-space for normal reaches.

It can be seen in Figure 3.9 that the anomalous sections D1, D4, D5, D6 and D9 were successfully identified. However, anomalous sections D2, D3, D7, which are closer to the normal wave speeds (compared with those of D1, D4, D5, D6 and D9), were identified as normal sections because a smaller *m* was used and only 5% of reaches were allowed to be identified as anomalous reaches. The wave speeds of these three sections reach their maximum or minimum values (the boundaries of the search-space for normal sections).

With regard to the Cases 2 to 4 where the *m*% values are all greater than 10.2% (the true proportion of anomalous reaches), the boxplots of estimates in Cases 2 - 4 combined (that is 30 estimates for each reach) are given in Figure 3.10. Comparison between the boxplots in Case 3 alone (Figure. 3.7) and Cases 2 - 4 combined demonstrates that as long as *m*% is greater than the

proportion of anomalous sections, the choice of the percentile rank *m* has little sensitivity to the wave speed calibration. In conclusion, it is recommended that *m* is set to be greater than the assumed proportion of anomalous sections. In field applications, *m* can be chosen based on the prior information, if available, or by a trial and error strategy.

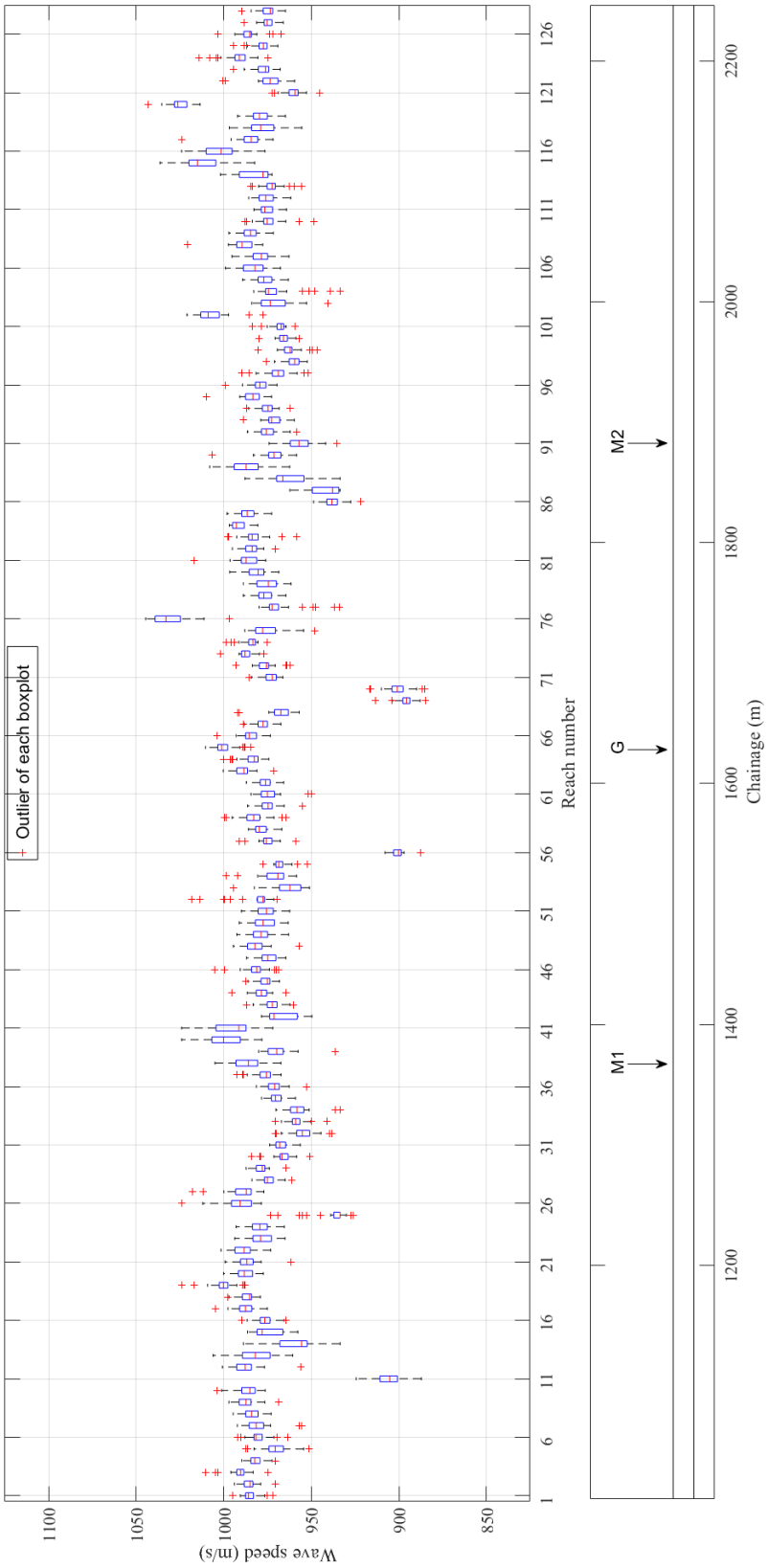

Figure 3.10 Boxplots of wave speed estimates in Cases 2–4.

A comparison of Cases 5 - 9 with Case 3 is made to explore the impact of variations in the percentile rank parameters p and q. Figure 3.11 shows the search-space interval for normal sections of different stages for the different cases. In Case 5 (p = 0, q = 100), the search-space bound $a_{n,min}$ and $a_{n,max}$ for the normal sections are determined as the minimum and maximum of normal section matrix $A_{n,0}$. These Case 5 bounds are almost the same as the original search-space, and as a result, ITA_{MP} terminated after Stage 2 as no further improvement was achievable. This proves that limiting the search-space is the driving force behind the improvement of the wave speed estimation in ITA_{MP}.

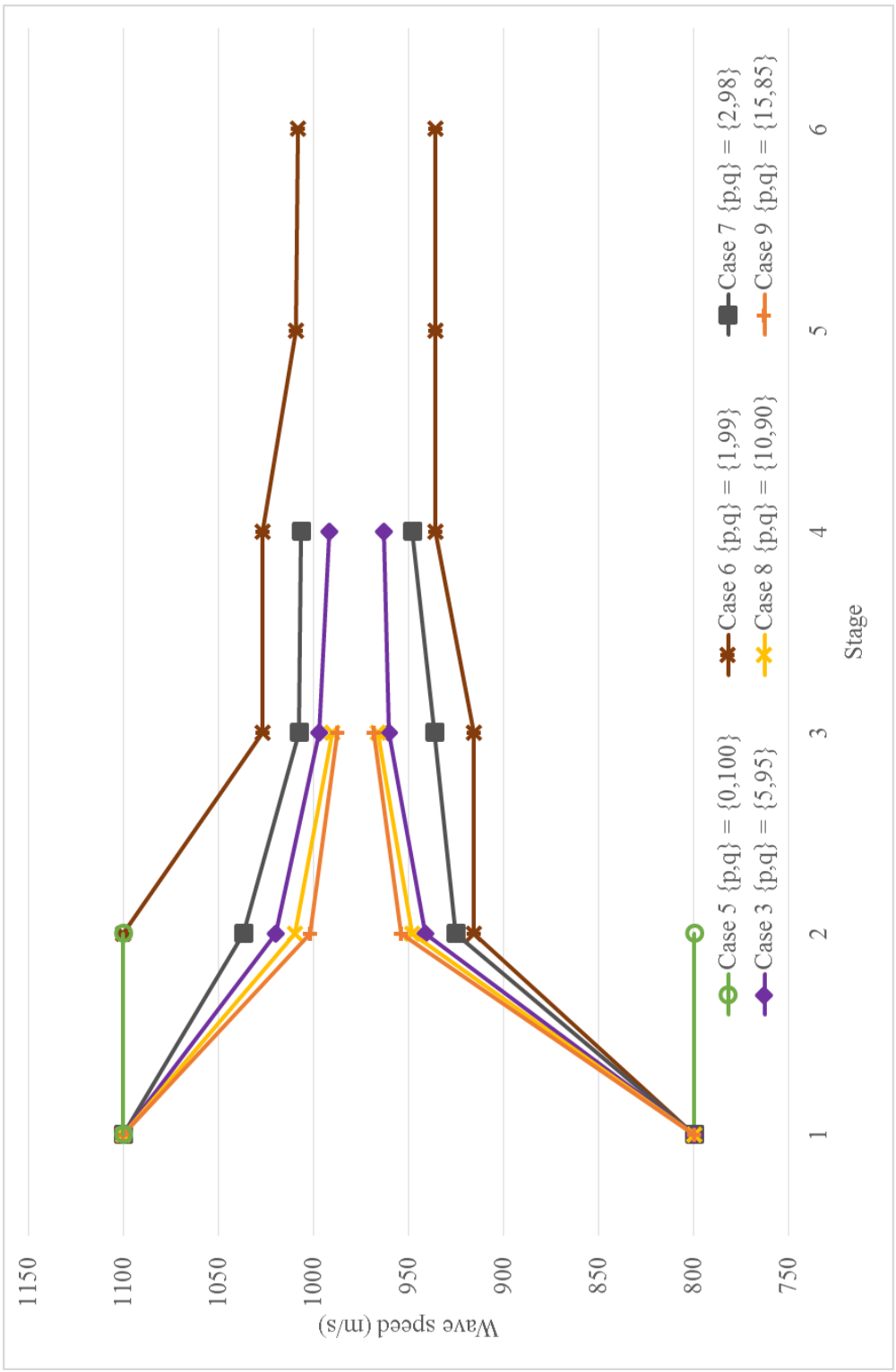

Figure 3.11 Search-space for identified normal section when different percentile ranks p and q were used.

As the percentile rank *p* becomes greater and *q* becomes smaller, the updated search-space becomes narrower, and ITA_{MP} was observed to terminate earlier. This is because for the increasingly narrow search-space, more normal reaches have wave speed values that violate the search-space bounds, yielding a reduced calibration performance. This side effect of ITA_{MP} is that some normal reaches are not allowed to take their true values, if their wave speeds are out of the narrowed search-space range. However, from the perspective of the detection of anomalous sections, this side effect can be considered unimportant as the accurate calibration of the normal sections does not affect the anomalous section detection. Overall, the results from Cases 5–9 demonstrate that the estimated wave speeds, especially those of anomalous sections, are not sensitive to different values for the percentile ranks *p* and *q*.

3.5 Field case study

3.5.1 Preliminaries

A field case study on the Morgan–Whyalla transmission pipeline (MTP) in South Australia was conducted to verify the multi-stage parameter-constraining ITA (the reader is referred to Stephens *et al*. (2013) and Gong *et al*. (2015) for more details on the field case study). The pipeline is made of mild steel with cement mortar lining (MSCL), is in good condition with intact cement mortar lining has an internal diameter of 727.5 mm. The configuration of the pipeline under investigation (from chainage 14,900 to 18,900 m) is given in Figure 3.12. For the series of field experiments, the transient waves were generated by shutting scour valve SC24 abruptly. Three transducers

were installed at air valves AVFP43 and AVFP44, and scour valve SC24 to record the transient pressure response.

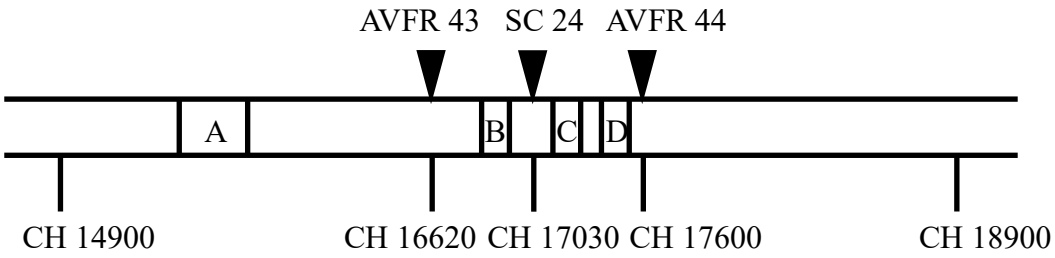

Figure 3.12 Configuration of the section of MTP (Note that CH refers to chainage, and sections A, B, C and D are four known thicker-walled sections).

The measured pressure traces at AVFR43, SC24 and AVFR44, in which the underlying long-period pressure oscillations were removed by a low-pass filter, are given in Figures 3.16–18 (where they are compared with predicted pressure trace of the calibrated model). A time step of 0.0135 s and a duration of 4.4 s of the measured pressure traces were used in ITA_{MP} to cover the 4-km pipe section of interest. This setup of the inverse problem resulted in the number of reaches in the inverse model being $N = 383$. The number of independent ITA runs of different random number seeds in each sub-stage was set to be $M = 10$. In each independent ITA run, for the adopted optimization algorithm PSO, the number of particles and the number of maximum iterations were set to be 400 and 3000, respectively. The percentile ranks were chosen as $m = 20$, $p = 5$ and $q = 95$.

3.5.2 Results

Objective function values of all independent ITA runs are given in Figure 3.13. Similar to Figure 3.6 (the objective function of the numerical study), a

significant reduction is found when the search-space was updated for the first time. The ten objective function values became concentrated gradually up to Stage 4, when multiple ITA runs failed to find a better solution within the third updated search-space.

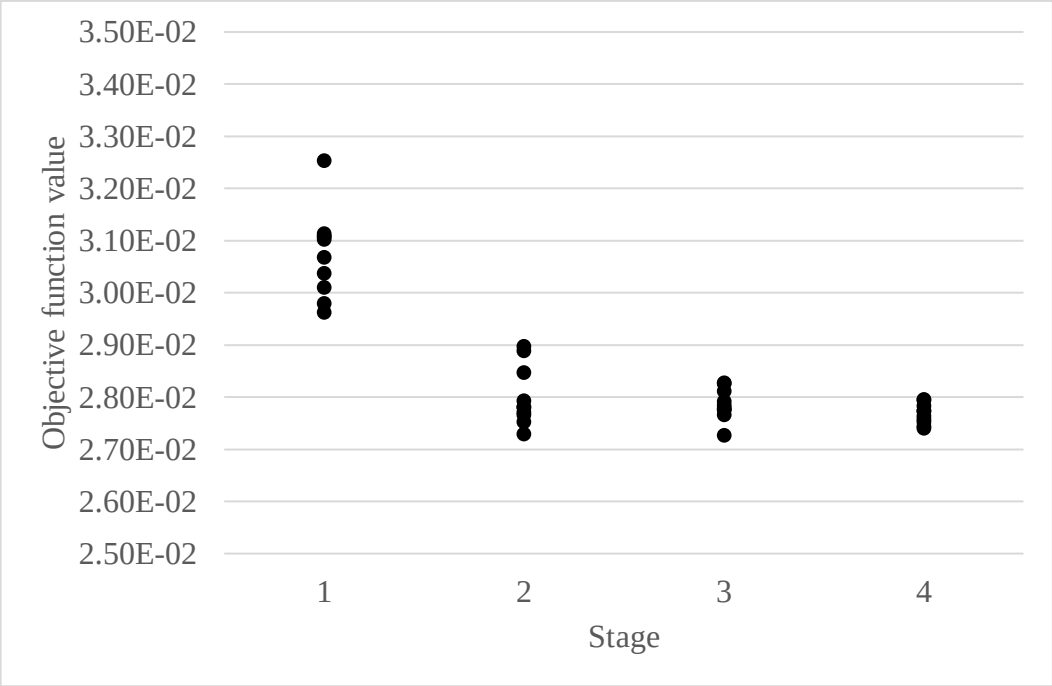

Figure 3.13 Objective function of each independent run in all stages.

Figure 3.14(a,b) represents boxplots of the wave speed estimates in Stage 1 and Stage 3. Extensive ultrasonic wall thickness measurements were manually undertaken using an ultrasonic thickness measurement instrument at 5 m intervals along the MTP between chainages 14,900 and 18,900 m (Stephens *et al.* 2013). Measurements were taken at eight points around the circumference of the pipe at each location. All ultrasonic wall thickness measurements are given in Figure 3.14(c).

Four known thicker-walled sections of pipeline A, B, C and D, confirmed by the ultrasonic measurements, are captured by wave speed estimates in both

Stage 1 and Stage 3. Other unknown anomalous sections (for example, section F) are also identified by ultrasonic measurements and wave speed estimates in both Stage 1 and 3. However, the IQR of Stage 3 is significantly less than that of Stage 1. Less variation in wave speed estimates enable less false positives identification and more accurate abnomal section detection. Section E, which is depicted in Figure 3.15, is used to demonstrate benefits the ITA_{MP} brings.

According to the ultrasonic measurements, a small fraction of the section from chainage 16,159.2 to 16,329.2 m (*Xc* in Figure 3.15(c)) is very likely to be in the anomalous state. It is identified by ITA results in both Stage 1 and Stage 2, they are *Xa* in Figure 3.15(a) and *Xb* in Figure 3.15(b), respectively. However, several sections in the dashed box in Figure 3.15(a) are likely to be interpreted as the anomalous sections, although they should not be. After ITA_{MP} is applied, wave speed estimates of those sections are close to their nominal values, thus they are identified as normal sections, which is consistent with ultrasonic measurments. The true anomalous section *Xb* is highlighted as a result. To summarise, ITA_{MP} provided a clear interpretation of the parameter estimates, and improved the ability to use these estimates for the detection of the anomalous sections.

However, a few true anomalous sections (for example, section G in Figure 3.14) were missed by ITA_{MP}. This is likely due to the coarse spatial resolution (roughly 12 m, the 4 km pipe section was discretized into more than 300 reaches) used in the ITA_{MP}. The ultrasonic measurement is taken at 5 m intervals, so the length of several anomalous sections was less than the spatial resolution used in ITA_{MP}. As a result, those anomalous sections were missed by ITA_{MP}.

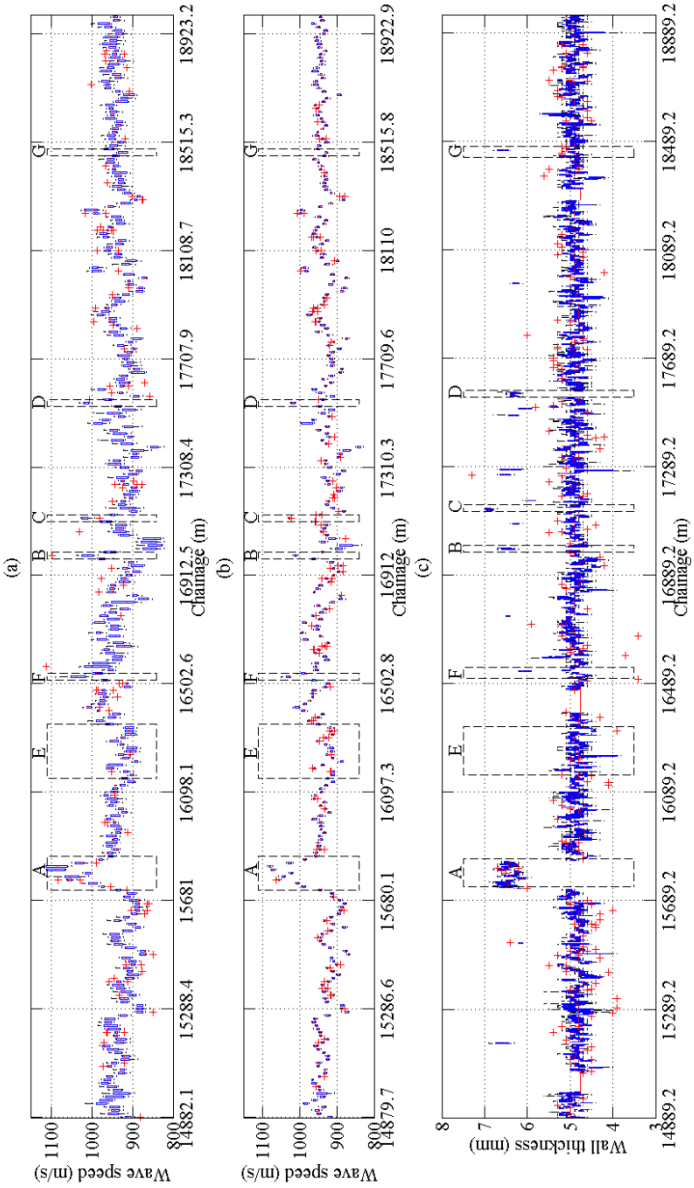

Figure 3.14 (a) Boxplots of wave speed estimates in Stage 1; (b) boxplots of wave speed estimates in Stage 3; (c) boxplots of wall thickness ultrasonic measurements.

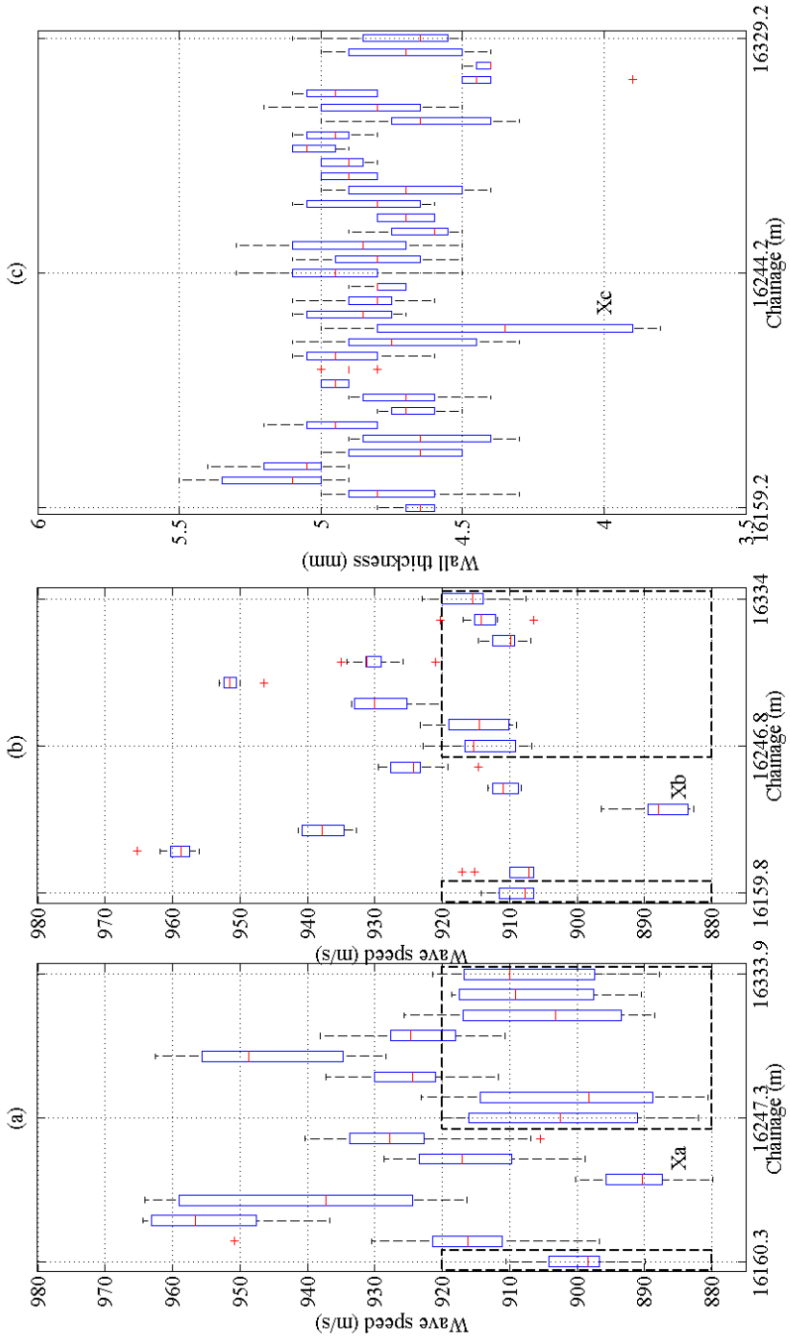

Figure 3.15 Enlarged plot of section E in Figure 3.14.

The comparison between the measured pressure trace and the predicted pressure trace obtained by the best estimated wave speeds (ranked in terms of objective function value) in Stage 3 is also examined. Figures 3.16–18 show the comparison between the measured pressure trace and the predicted pressure trace obtained by the best estimated wave speeds from Stage 3. The high frequency pressure fluctuations at SC24 are due to high frequency pressure oscillations, and resultant cavitation, within the pipework of the generator. The inverse model is not able to describe this phenomenon, so they did not appear in the predicted pressure traces in Figure 3.17. The pressures at ACFP43 and ACFP44 also exhibit significant oscillations in the first 0.5 s period after the transient has arrived. The oscillations were likely due to the oscillations generated at SC24, so the pressures of the first 0.5 s have been excluded from the objective function calculations. It can be seen that a reasonable match between the measured and predicted pressure trace is achieved for the time period 0.5 s after the wave front.

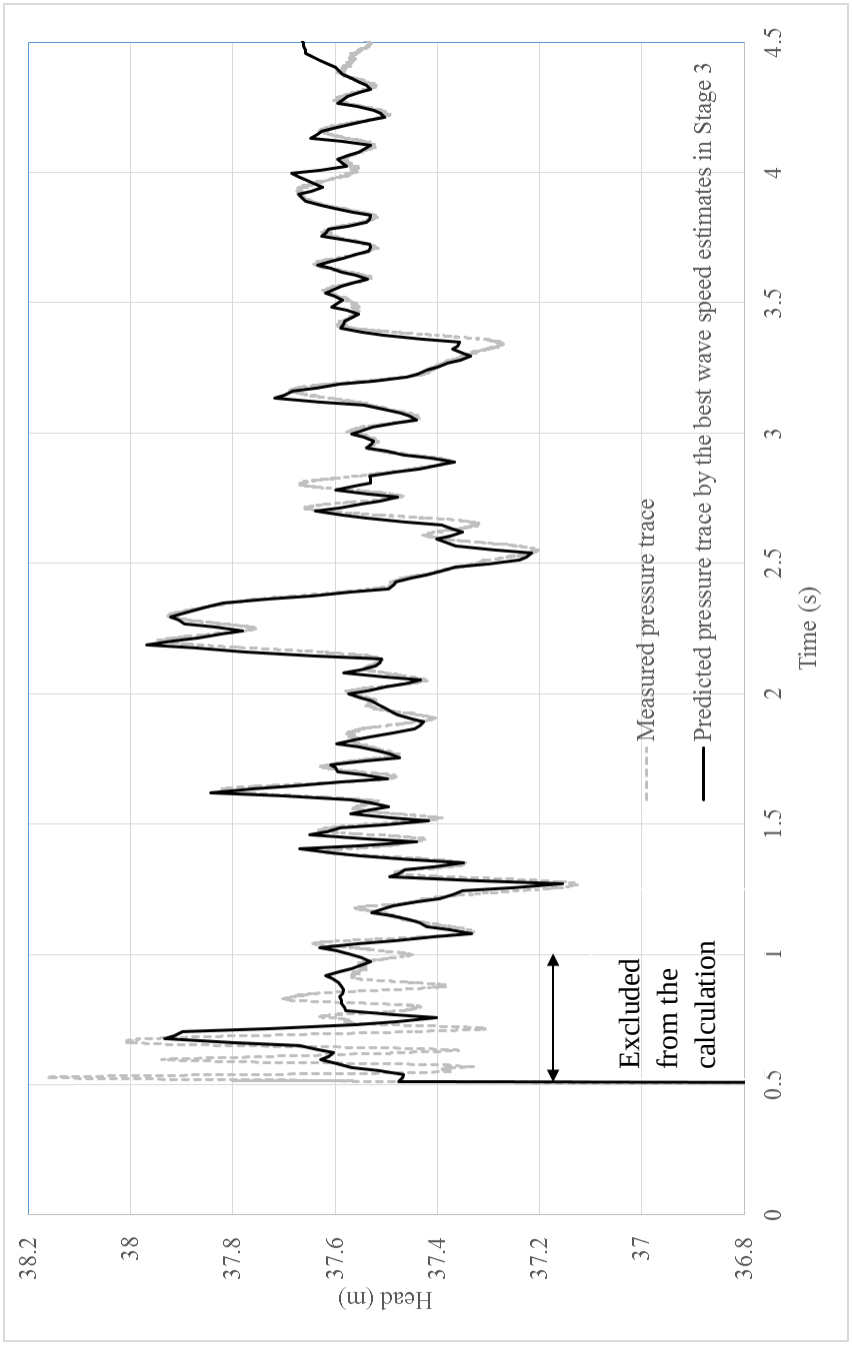

Figure 3.16 Comparison of the measured pressure trace and the predicted pressure trace obtained by best estimated wave speeds of Stage 3 at ACFP43.

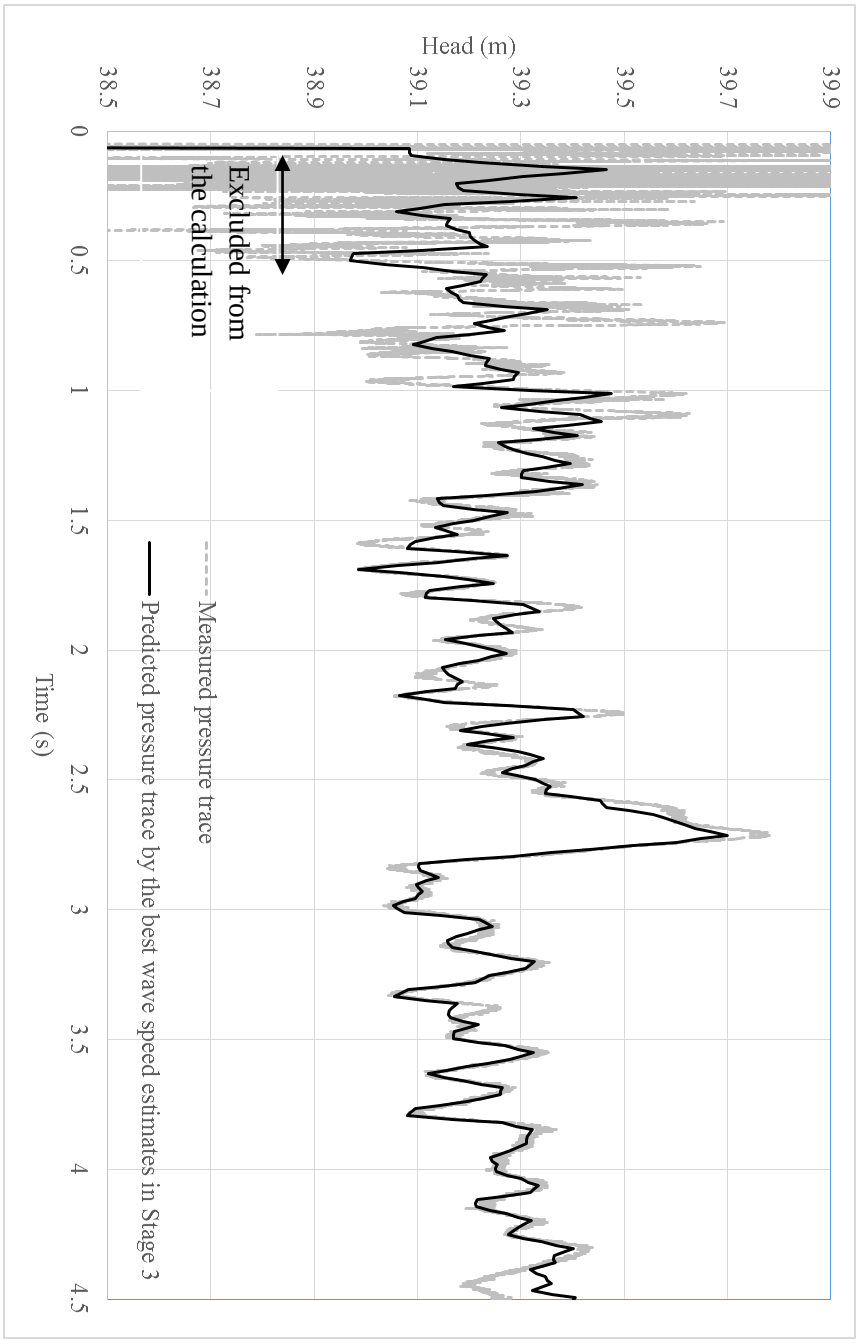

Figure 3.17 Comparison of the measured pressure trace and the predicted pressure trace obtained by best estimated wave speeds of Stage 3 at SC24.

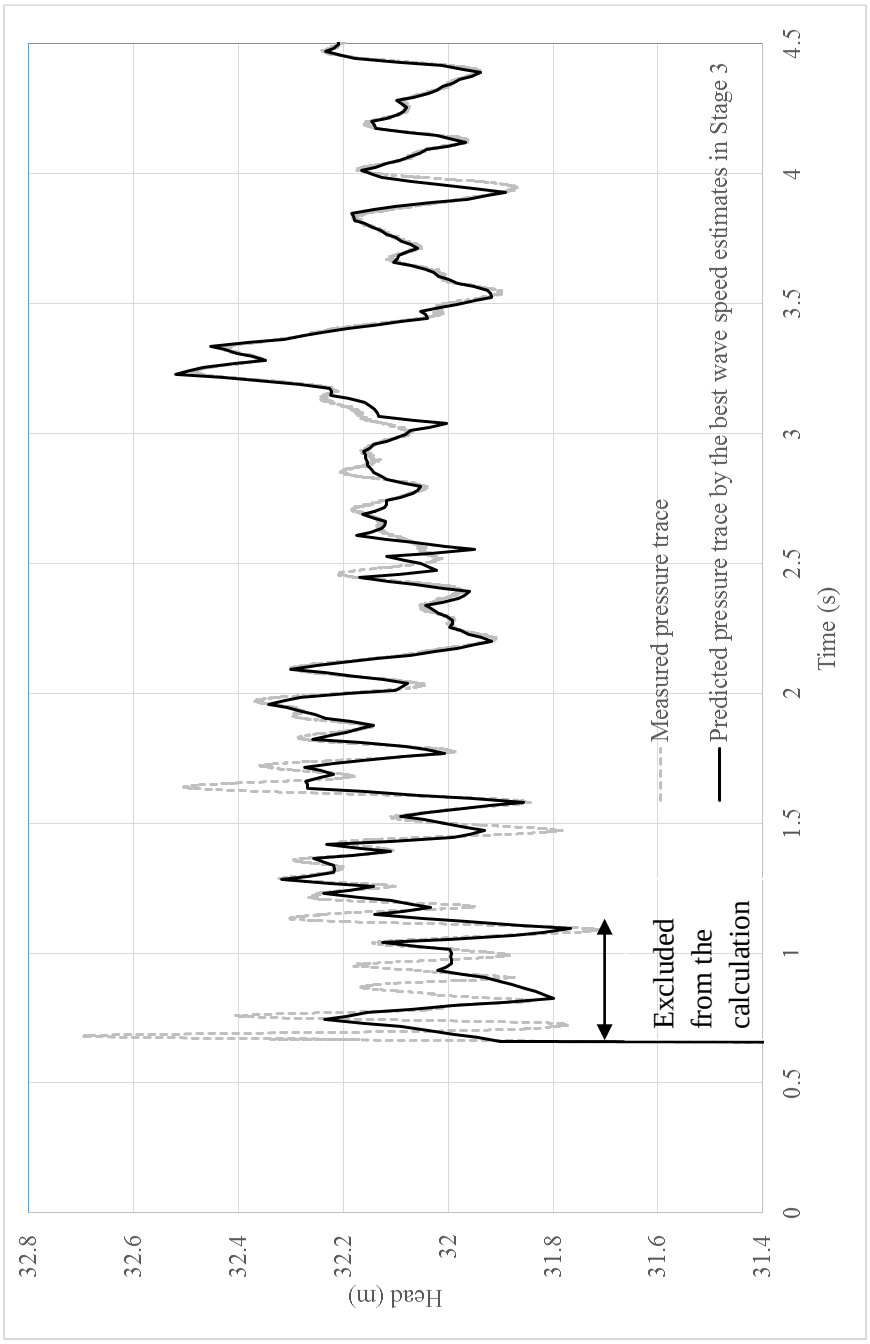

Figure 3.18 Comparison of the measured pressure trace and the predicted pressure trace obtained by best estimated wave speeds of Stage 3 at ACFP44.

Overall, given the difficulty of the field problem that ITA_{MP} attempted, the anomalous sections identified by Stage 3 are generally consistent with the sections identified by ultrasonic measurements. The identifiability is improved compared with the conventional ITA (Stage 1 in the ITA_{MP}), which is indicated by less variation in the wave speed estimates and a decreased objective function (meaning a better match between the predicted and measured pressure traces).

3.6 Conclusions

Parameter identifiability is a problem commonly encountered in large-scale ITA applications for determining pipeline condition. To tackle this problem, multi-stage parameter-constraining ITA (ITA_{MP}), a new method for pipeline condition assessment, has been developed and is presented in this paper. ITA_{MP} iteratively generates sets of parameter estimates and modifies the search-space interval for the generation of subsequent estimates based on identifying a reach as either in a normal or anomalous state. The parameter estimates for the normal reaches become increasingly concentrated and outliers in the parameter estimates are eliminated, thus identifiability of parameter values is enhanced.

This method has been verified by a numerical study in this paper. The results show that the wave speeds estimated by the conventional ITA (equivalent to Stage 1 of ITA_{MP}) possess a number of anomalous wave speed estimates, despite the methods seemingly being a reasonable match to the numerical data. After Stage 2, the estimated wave speeds are much closer to the true wave speeds, and a large proportion of anomalous estimates are eliminated.

A field case study on a section of the Morgan transmission pipeline in South Australia has been conducted to verify the capability of ITA_{MP} to assess pipeline condition assessment by identifying anomalous sections. Wave speed estimates by ITA_{MP} has less variance and higher identifiability than the conventional ITA. The results show a reasonable consistency between anomalous sections detection by ITA_{MP} and available ultrasonic measurements, demonstrating that ITA_{MP} can be used as a tool for pipeline condition assessment in the field.

This page is intentionally blank.

Chapter 4

Impedance estimation along pipelines by generalized reconstructive Method of Characteristics for pipeline condition assessment

(Journal Paper 3)

Zhang, C., Gong, J., Simpson, A. R, Zecchin, A. C. & Lambert, M. F.

School of Civil, Environmental and Mining Engineering, the University of Adelaide, Adelaide, SA 5005 Australia

Journal of Hydraulic Engineering, (submitted).

This page is intentionally blank.

Statement of Authorship

Title of Paper	Impedance estimation along pipelines by generalized reconstructive Method of Characteristics for pipeline condition assessment
Publication Status	☐ Published ☐ Accepted for Publication ☑ Submitted for Publication ☐ Unpublished and Unsubmitted work written in manuscript style
Publication Details	Zhang, C., Gong, J., Simpson, A. R, Zecchin, A. C. & Lambert, M. F. 2018 "Impedance estimation along pipelines by generalized reconstructive Method of Characteristics for pipeline condition assessment" Journal of Hydraulic Engineering, under review.

Principal Author

Name of Principal Author (Candidate)	Chi Zhang
Contribution to the Paper	Conception and design of the project Analysis and interpretation of research data Draft the paper
Overall percentage (%)	75%
Certification:	This paper reports on original research I conducted during the period of my Higher Degree by Research candidature and is not subject to any obligations or contractual agreements with a third party that would constrain its inclusion in this thesis. I am the primary author of this paper.
Signature	Date 02/03/2018

Co-Author Contributions

By signing the Statement of Authorship, each author certifies that:

i. the candidate's stated contribution to the publication is accurate (as detailed above);
ii. permission is granted for the candidate in include the publication in the thesis; and
iii. the sum of all co-author contributions is equal to 100% less the candidate's stated contribution.

Name of Co-Author	Jinzhe Gong
Contribution to the Paper	Conception and design of the project Analysis and interpretation of research data Critically revising the paper so as to contribute to the interpretation
Signature	Date 02/03/2018

Name of Co-Author	Angus Simpson
Contribution to the Paper	Conception and design of the project Analysis and interpretation of research data Critically revising the paper so as to contribute to the interpretation
Signature	Date 2 Mar 2018

Name of Co-Author	Aaron Zecchin		
Contribution to the Paper	Conception and design of the project Analysis and interpretation of research data Critically revising the paper so as to contribute to the interpretation		
Signature		Date	2/3/2018

Name of Co-Author	Martin Lambert		
Contribution to the Paper	Conception and design of the project Analysis and interpretation of research data Critically revising the paper so as to contribute to the interpretation		
Signature		Date	2/3/18

Please cut and paste additional co-author panels here as required.

Abstract

Reliable and efficient pipeline condition assessment in water transmission mains is required to locate deteriorated sections, such that water authorities can rehabilitate or replace vulnerable sections to prevent pipe failure. In this paper, a novel method is developed to estimate the pipeline impedance and pipeline wall thickness through hydraulic transient testing. The previously developed reconstructive Method of Characteristics (RMOC) algorithm is generalized in the current research by relaxing the requirement of a dead-end boundary. Instead, the generalized RMOC as proposed requires two adjacent pressure transducers placed at any interior locations along a pipe to record head variations under a controlled transient event. The parameters along the pipeline can be analytically determined though a smart use of MOC analysis backwards in time. The configuration required by the proposed method makes it applicable in the real world. The proposed approach is firstly verified by a numerical experiment, where three sections with different wall thicknesses (representing deteriorated sections) are successfully identified. The new technique is then verified by a laboratory experiment, where wall thickness and location of two sections with wall class changes are identified.

This page is intentionally blank.

4.1 Introduction

Ferrous pipes have been used to transport potable water for centuries (Mcneiill and Edwards, 2001). The loss of protective lining and subsequent internal wall corrosion or tuberculation is a great concern, since they result in pipe condition deterioration and water quality deterioration (Volk et al., 2000). The tuberculation is formed by iron oxide from dissolved iron and can be accumulated to form extended blockages, which reduce hydraulic transmissibility and increase pumping cost (Stephens, 2008). The detection of distributed deterioration, including the loss of protective lining, internal or external wall corrosion, and extended blockages, is of importance for water utilities to cost-effectively maintain, rehabilitate and replace their pipe assets.

The non-intrusive and cost-effective nature of transient-based methods has made them promising for pipeline anomaly detection and pipeline condition assessment (Colombo et al., 2009). In addition to intensive study of transient-based detection methods for discrete anomalies such as leaks (Brunone, 1999, Kapelan et al., 2003, Lee et al., 2006, Vítkovský et al., 2007, Covas and Ramos, 2010, Gong et al., 2012) and partial blockages (Wang et al., 2005, Sattar et al., 2008), studies on distributed deterioration such as extended blockages and extended wall corrosion have also attracted attention in recent years.

Among transient-based methods, the system frequency response (SFR) methods may be used to not only detect leaks (Jönsson and Larson, 1992, Mpesha et al., 2001, Lee et al., 2005, Gong et al., 2012), but also detect blockages. Duan et al. (2011) analytically proved that the presence of

extended blockage will impose frequency shift in SFR, so that occurrences of the resonant peaks, in turn, can be used to calculate the size and location of the extended blockage. This has been verified by numerical analysis and a laboratory experiment (Duan et al., 2013). Meniconi et al. (2013) coupled the SFR-based frequency-domain method with the wavelet method for the purpose of blockage detection, and found that detection accuracy and calculation efficiency were improved. However, the SFR-based method can only detect a limited number of defects which are localized to some discrete sections along the pipeline.

Inverse transient analysis (ITA), a calibration method to minimize the difference between the measured data and the predicted numerical model by adjusting model parameters, has the potential to achieve continuous pipeline condition assessment with a high spatial resolution. Stephens et al. (2013) applied ITA for a mild steel cement mortar lined (MSCL) pipe in South Australia for cement mortar lining spalling and internal wall corrosion detection. The ITA results were consistent with ultrasonic wall thickness measurements in identifying major wall thickness changes. However, the authors acknowledged that the ITA could have benefited from a greater computational budget (i.e. longer optimization runtimes), but practical constraints could potentially lead to infeasibly large runtimes. In order to enhance the computational efficiency of ITA, Zhang et al. (2018a) developed a new ITA approach in which a head-based MOC and a flexible characteristic grid were used. The computation cost of the new ITA approach was found to be about a quarter of the traditional ITA approach. This ITA approach was further improved by a multiple-state parameter-constraining approach to

enhance the parameter identifiability in Zhang et al. (2018b), and was verified for a 4-km pipeline in the field. Research on frequency-domain ITA (Zecchin et al., 2013, Zecchin et al., 2014, Rubio Scola et al., 2016), which has potential for blockage detection and pipeline condition assessment, was limited to numerical studies only.

Gong et al. (2012) developed a method to detect extended sections with wall thickness changes by analyzing the size and timing of the major wave reflections following a transient pressure excitation. This direct-wave-analysis method was applied to field case studies on a MSCL pipe (Gong et al., 2015) and an asbestos cement pipe (Gong et al., 2016). To enable continuous pipeline condition assessment, Gong et al. (2014) first proposed the reconstructive MOC (RMOC) method to estimate impedance and wave speed distributions along a pipeline based on head measurements on a dead-end boundary. Unlike ITA that involves iterative optimization, the RMOC method is an analytical approach to directly calculate the pipeline impedance by tracing back characteristic lines from the head measurements recorded by transducers, so it is much more computationally efficient than ITA approaches. However, the RMOC method proposed by Gong et al. (2014) required a dead-end boundary and access points immediately upstream of the dead-end boundary to connect a side discharge valve and a transducer for transient pressure generation and measurement. Such a configuration is often difficult to achieve in the field and thus limits the applicability of the method.

To overcome this problem, the RMOC is generalized in this paper, where the requirement of the dead-end boundary is relaxed. Instead of one pressure transducer immediately upstream of the dead-end boundary, two adjacent

pressure transducers are used, and they can be placed adjacent to one another anywhere along the pipeline. The relaxation of a dead-end boundary and flexible placement of two sensors makes the generalized RMOC more applicable.

The paper is organized as follows. The configuration in field tests that is required for the newly generalized algorithm is presented and the problem is defined. This is followed by an illustration of the generalized RMOC algorithm. Then the algorithm is verified by a numerical case study, where three pipe sections with different wall thicknesses are detected with high accuracy. Next the algorithm is verified by a laboratory experiment, where two pipe sections with different wall thicknesses exist on both sides of the transient generator and compound reflections are received by two pressure adjacent transducers. Finally, conclusions are given.

4.2 Problem formulation

The configuration in field applications of pipe condition assessment required by the generalized RMOC approach is depicted in Fig. 4.1(a). Two adjacent pressure transducers (T1 and T2) together with a side discharge valve transient generator (G) are installed at two adjacent interior locations along the pipeline for the transient measurements and generation. In applications to real water pipeline systems, they can be connected to a pipeline via available access points, such as fire hydrants and air valves. For the transducers, which only require small fittings, they can also be connected by hot tapping if needed. Recently developed in-pipe fiber optic sensor array by Gong et al.

(2018) makes it possible to insert two adjacent transducers into a pipeline through a single access point. Such a connection does not increase labour cost in field tests, since only one measurement site is required, like the previous RMOC using one transducer before a dead-end boundary.

The configuration is discretized in the *x*-*t* plane as shown in Fig. 4.1(b). The steady state base flow in the pipeline $\boldsymbol{Q}(x)$ is initially known, and so is the steady state discharge through the side discharge valve transient generator. The pipeline is excited into a transient state by abruptly shutting the side discharge valve at $t = 0$ and where the discharge perturbation through the valve $\boldsymbol{Q_g}(x_{\mathrm{T1}})$ is measured. The two adjacent pressure transducers are installed in close proximity, so it is assumed that the pipe section between the two transducers has a uniform condition. Prior information of this uniform section is assumed to exist, that is such that properties of reaches (i.e. internal diameter) between T1 and T2 $[\boldsymbol{P}(x), x_{T1} < x < x_{T2}]$ are initially known.

The problem is formulated as follows: given the measured head variations $\boldsymbol{H}(x_{\mathrm{T1}})$, $\boldsymbol{H}(x_{\mathrm{T2}})$ (the time series of head measurements at two transducers T1 and T2) and discharge perturbation $\boldsymbol{Q_g}(x_{\mathrm{T1}})$ and known pipe properties between two transducers $\boldsymbol{P}(x), x_{T1} < x < x_{T2}$, the objective is to estimate the properties of pipe sections outside of two transducers $\boldsymbol{P}(x), x < x_{T1}$ and $\boldsymbol{P}(x), x > x_{T2}$.

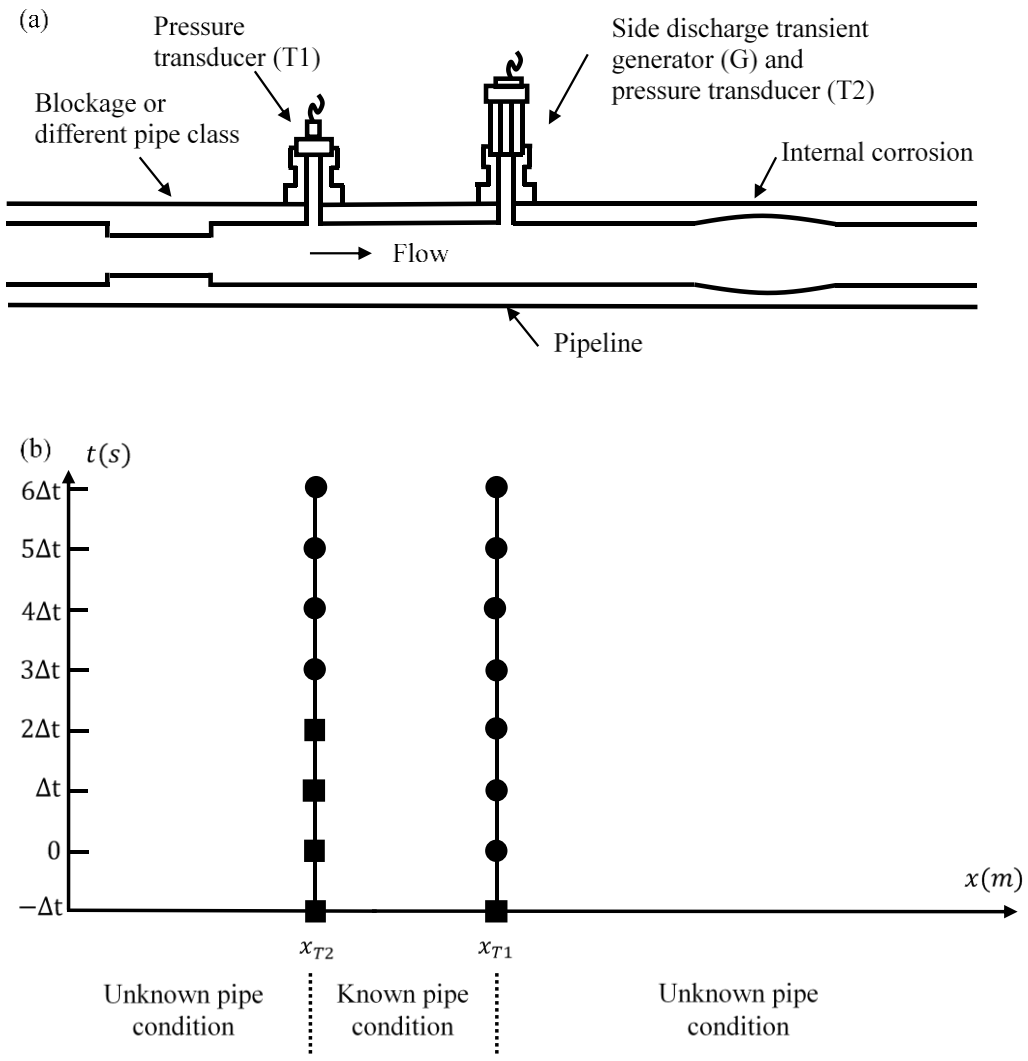

Figure 4.1(a) Configuration of the pipeline for the RMOC analysis, (b) discretization on an *x*-*t* plane

4.3 The generalized RMOC

4.3.1 Overview

The ultimate goal of the new generalized RMOC algorithm is to calculate the pipe properties (for example, hydraulic impedance and wall thickness) along pipelines, given measured head variations at two adjacent transducers and

known properties of pipeline section between the two transducers. Three steps, which are illustrated in the *x-t* plane in Fig. 4.2, are involved in the algorithm. In Step 1, the pipe section between two transducers is discretized and the properties of each reach are determined. In Step 2, the flow variations in time corresponding to the two transducer locations are calculated. Finally, Step 3 is initiated by combining the measured head variations and calculated flow variations at two transducers locations. In Step 3, each reach is reconstructed successively (one reach at a time) by determining its impedance. These steps are outlined in detail in the following.

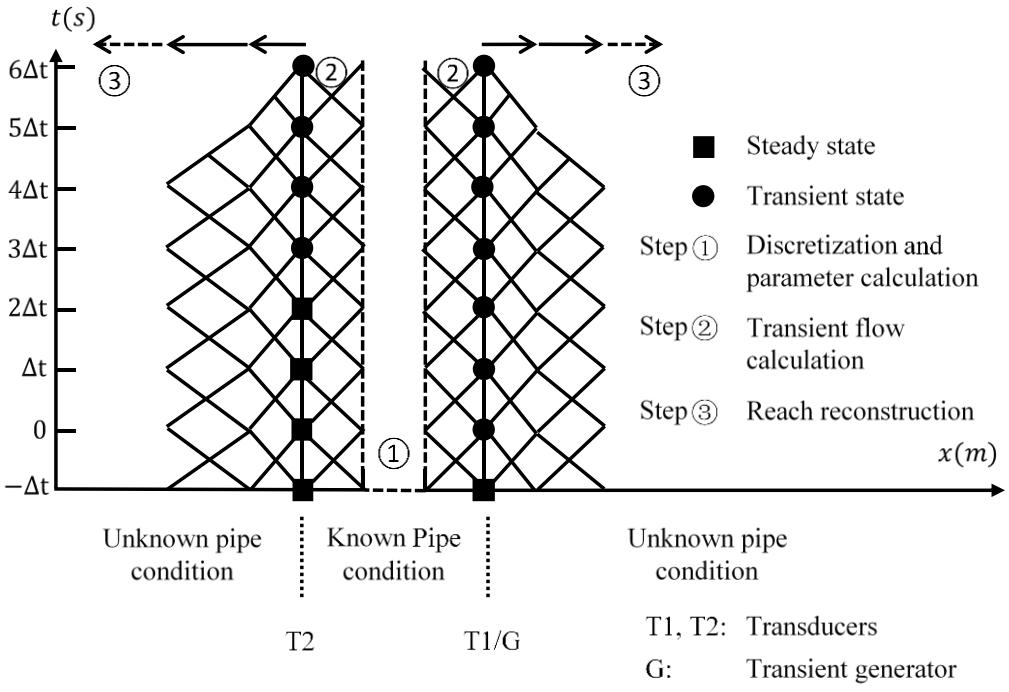

Figure 4.2 Illustration of the generalized RMOC algorithm on an *x-t* plane

4.3.2 Step 1. Discretization of the grid between two transducers

The two adjacent transducers are placed in close proximity, and the pipe section between two transducers is assumed to be of uniform condition. The wave speed of the transient wave in the pipe section can be calculated from the travel time difference between the two transducers

$$a_0 = \frac{L}{t_{T2} - t_{T1}} \tag{4.1}$$

where L is the length of the pipe section between the two transducers, t_{T1} and t_{T2} are the generation, or arrival time, of the transient wave at the transducers, and they can be read from the measured head traces.

The pipe section between two transducers is discretized based on the user selected time step Δt. The time step Δt can be multiple sampling intervals of measured data (i.e. a down sampling of the original data), and the finest resolution is achieved when Δt is equal to the sampling interval of the measured head variations. The number of discretized reaches between two transducers is determined by

$$N_{T1-T2} = \frac{t_{T2} - t_{T1}}{\Delta t} \tag{4.2}$$

For simplicity for this illustration, the number of reaches between two transducers N_{T1-T2} is assumed to be 3, and the x-coordinates of the transducers T1 and T2 are denoted as x_0 and x_{-3} hereon ($x_{\mathrm{T1}} = x_0, x_{\mathrm{T2}} = x_{-3}$).

The internal diameter of the three reaches are approximated by the internal diameter of the intact pipe D_0. The impedance of each of the three reaches can be determined by:

$$B_0 = \frac{a_0}{gA_0} \tag{4.3}$$

where g = the gravitational acceleration and A_0 = internal cross-sectional area of the pipe reach.

The reach resistance between the two transducers for each of the three reaches is determined based on the steady state head measurements recorded by two transducers:

$$R_0 = {[H(x_0, 0) - H(x_{-3}, 0)]}/{3Q_1^2} \tag{4.4}$$

The steady state heads at the nodes between two transducers are then determined by

$$H(x_i, 0) = H(x_{i+1}, 0) + R_0 Q_1^2 \ (i = -1, \cdots, -3) \tag{4.5}$$

4.3.3 Step 2. Transient flow calculations at the two transducer locations

The purpose of this step is to calculate the transient flow variations in time at the nodes where transducers are installed. This is achieved by modelling the grid between two transducers, which is equivalent to MOC modelling with head measurement boundaries, given the known steady-state head and flow, measured head $\boldsymbol{H}(x_{-3})$ and $\boldsymbol{H}(x_0)$, as shown in Fig. 4.3.

For any interior node between two transducers, the calculation of head and flow is undertaken using the MOC by combining two compatibility equations.

Node $(x_{-2}, 0)$ in Fig. 4.3(b) is used as an example for illustration, two compatibility equations along the characteristics lines are:

$$\begin{aligned} C^{+}: \mathrm{H}(x_{-2}, 0) - \mathrm{H}(x_{-3}, -\Delta\mathrm{t}) \\ + B_0[\mathrm{Q}(x_{-2}, 0) - \mathrm{Q}(x_{-3}, -\Delta\mathrm{t})] \\ + R_0\mathrm{Q}(x_{-2}, 0)|\mathrm{Q}(x_{-3}, -\Delta\mathrm{t})| = 0 \end{aligned} \tag{4.6}$$

$$\begin{aligned} C^{-}: \mathrm{H}(x_{-2}, 0) - \mathrm{H}(x_{-1}, -\Delta\mathrm{t}) \\ - B_0[\mathrm{Q}(x_{-2}, 0) - \mathrm{Q}(x_{-1}, -\Delta\mathrm{t})] \\ - R_0\mathrm{Q}(x_{-2}, 0)|\mathrm{Q}(x_{-1}, -\Delta\mathrm{t})| = 0 \end{aligned} \tag{4.7}$$

The head $\mathrm{H}(x_{-2}, 0)$ and the flow $\mathrm{Q}(x_{-2}, 0)$ are the only two unknown variables in Eqs. (4.6-4.7), thus they can be determined.

For any node where the transducers are installed, the calculation of flow is same as the MOC with a known head boundary and only one compatibility equation. For example, flow at the node $(x_0, 0)$ in Fig. 4.3(c) is determined by analyzing the compatibility equation along the characteristics line:

$$\begin{aligned} C^{+}: \mathrm{H}(x_0, 0) - \mathrm{H}(x_{-1}, -\Delta\mathrm{t}) \\ + B_0[\mathrm{Q}_u(x_0, 0) - \mathrm{Q}(x_{-1}, -\Delta\mathrm{t})] \\ + R_0\mathrm{Q}_u(x_0, 0)|\mathrm{Q}(x_{-1}, -\Delta\mathrm{t})| = 0 \end{aligned} \tag{4.8}$$

where Q_u represents the flow upstream of the transient generation node. Given that $\mathrm{H}(x_0, 0)$ is measured, $\mathrm{Q}_u(x_0, 0)$ is the only unknown variable in the Eq. (4.8), so it can be determined.

The flow downstream of the transient generation node $\mathrm{Q}_d(x_0, 0)$ can be determined by the continuity equation, given that the discharge into atmosphere through the generator $\mathrm{Q}_g(x_0, 0)$ is known (see "Problem formulation"), as

$$\mathrm{Q}_d(x_0, 0) = \mathrm{Q}_u(x_0, 0) - \mathrm{Q}_g(x_0, 0) \tag{4.9}$$

By the time marching process of the MOC, flow vector $\boldsymbol{Q}(x_{-3})$ and $\boldsymbol{Q_d}(x_0)$ can be determined.

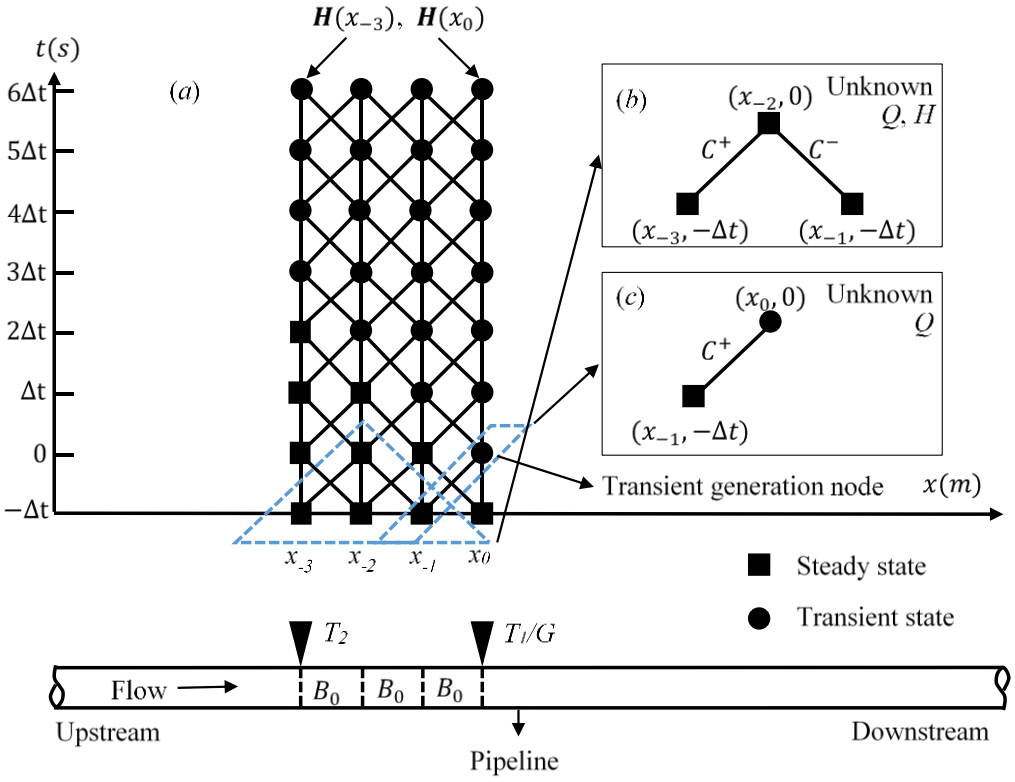

Figure 4.3 Calculations for the grid between the two transducers (Step 2)

Now at the spatial locations of $x = x_{-3}$ and $x = x_0$, where two transducers are installed, both flow and head variations are known, and they will be used to initiate the reach reconstruction (Step 3) in both the upstream and downstream directions, which is explained in the following section.

4.3.4 Step 3. Reach reconstruction

4.3.4.1 First reach reconstruction (Reach 1 in Fig. 4.4)

The reconstruction of the first unknown reach on the downstream side of T1 is illustrated in Fig. 4.4 by analyzing the extremely short negative characteristic line C^- in Fig. 4.4(b). In Fig. 4.4(b), δ is a small positive time step but tends to zero. As a result, the length of the C^- characteristic line is short. The nodes linked by the extremely short characteristic line C^- are the node $(x_0, 0)$, which is the transient generation node, and the node $(x_0 + \delta a_1, -\delta)$, which has the steady state conditions. They are very close such that the effect of friction is negligible, so the compatibility equation on the extremely short characteristic line C^- is:

$$C^-: \mathrm{H}(x_0, 0) - \mathrm{H}(x_0 + \delta a_1, -\delta) - B_1[\mathrm{Q}(x_0, 0) - \mathrm{Q}(x_0 + \delta a_1, -\delta)] = 0 \quad (4.10)$$

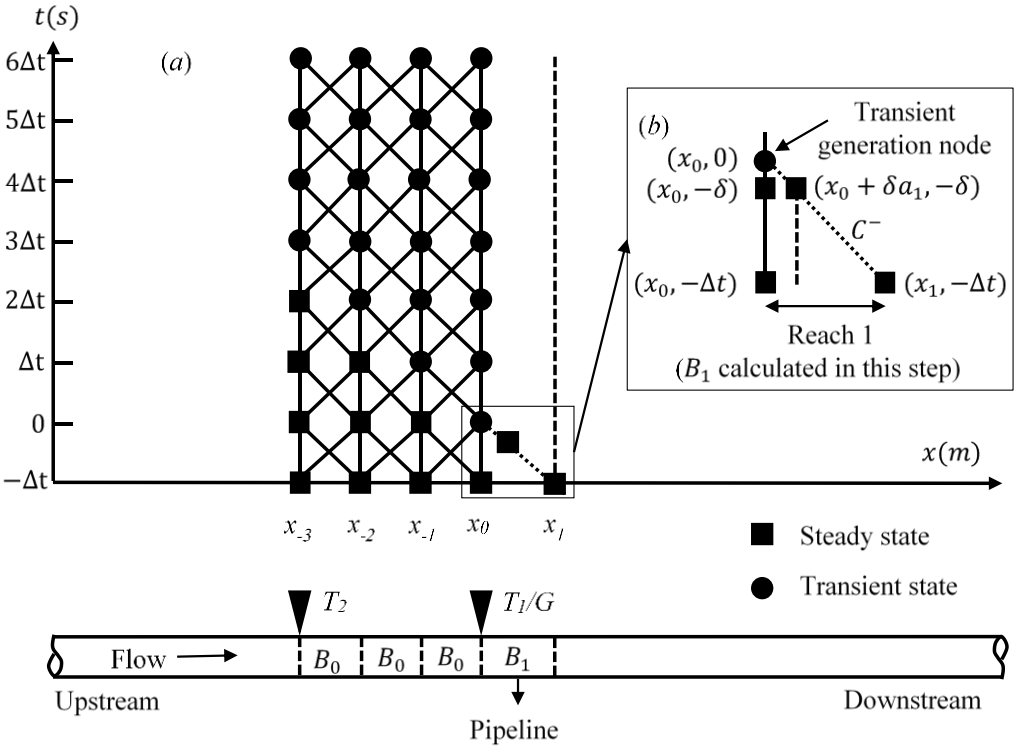

Figure 4.4 Reach reconstruction on the right side of transducer T1 (Step 3, calculation of B_1 for reach 1)

In Eq. (4.10), $\mathrm{H}(x_0, 0)$ is known, and $\mathrm{Q}(x_0, 0)$ was calculated in Step 2. The node $(x_0 + \delta a_1, -\delta)$ is at steady state conditions, thus $\mathrm{Q}(x_0 + \delta a_1, -\delta)$ is equal to the steady-state flow downstream of the transient generator $Q(x > x_0)$, and the steady state head $\mathrm{H}(x_0 + \delta a_1, -\delta)$ is approximated by $\mathrm{H}(x_0, -\delta)$, considering the short length between node $(x_0 + \delta a_1, -\delta)$ and $(x_0, -\delta)$. $\mathrm{H}(x_0, -\delta)$ is equal to $\mathrm{H}(x_0, -\Delta t)$ since the measurement remains until next measurement occurs on the next discrete time point. So, B_1 is the only unknown in Eq. (4.10), and thus it can be directly determined.

4.3.4.2 Second reach reconstruction (Reach 2 in Fig. 4.6)

The second reach on the right of T1 is reconstructed in this section. Firstly, the head and flow vectors at the next spatial location x_1 [$\mathbf{H}(x_1)$ and $\mathbf{Q}(x_1)$] are calculated, as shown in Fig. 4.5. Next the second reach is reconstructed by analyzing a single characteristic line linking the transient arrival node at the next spatial location and a steady state node, as shown in Fig. 4.6 (again a short C^- characteristic line is used for the calculation).

The temporal head and flow variation vectors (i.e. the time-series of head and flow) at the next spatial node x_1 [$\boldsymbol{H}(x_1)$ and $\boldsymbol{Q}(x_1)$] are determined by a process similar to the time marching process in the MOC except for the direction. In the MOC, the time marching process is usually performed along time axis. However, in this algorithm it is performed along the spatial axis.

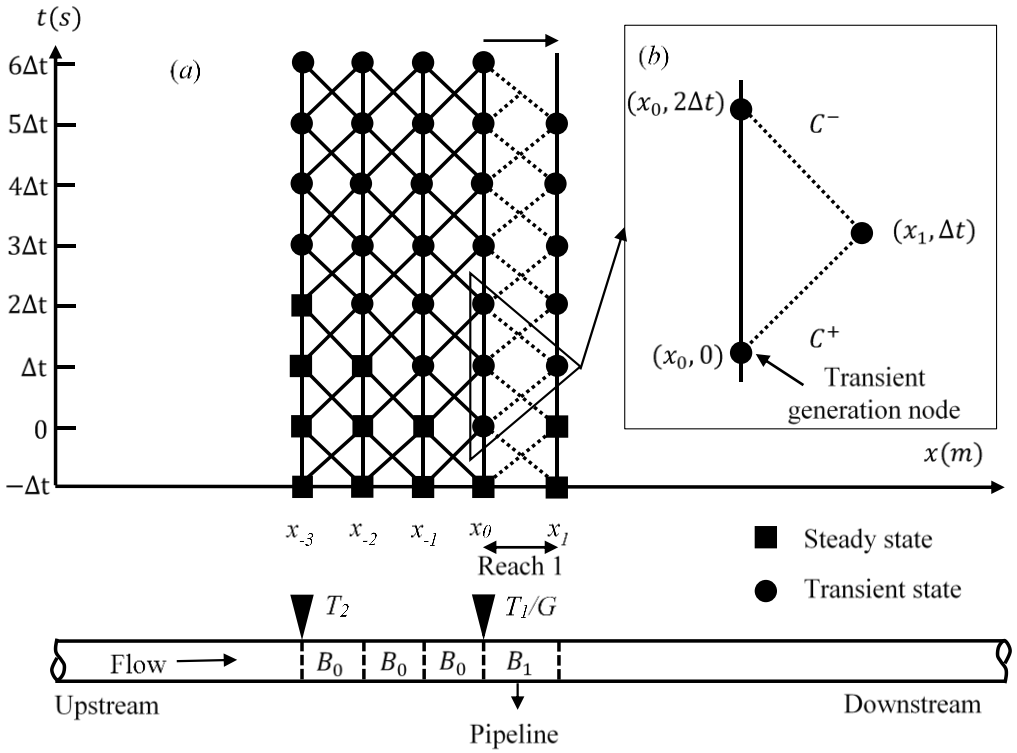

Figure 4.5 Head and flow calculation of the next spatial location on the right side of the transducer T1 (Step 3 continued)

The calculation of $\mathrm{H}(x_1, \Delta\mathrm{t})$ and $\mathrm{Q}(x_1, \Delta\mathrm{t})$ by the two compatibility equations is highlighted in the box in Fig. 4.5(b), as an example. Two compatibility equations along the two characteristics lines are:

$$C^-: \mathrm{H}(x_0, 2\Delta\mathrm{t}) - \mathrm{H}(x_1, \Delta\mathrm{t}) - B_1[\mathrm{Q}(x_0, 2\Delta\mathrm{t}) - \mathrm{Q}(x_1, \Delta\mathrm{t})] - R_1\mathrm{Q}(x_0, 2\Delta\mathrm{t})|\mathrm{Q}(x_1, \Delta\mathrm{t})| = 0 \quad (4.11)$$

$$C^+: \mathrm{H}(x_1, \Delta\mathrm{t}) - \mathrm{H}(x_0, 0) + B_1[\mathrm{Q}(x_1, \Delta\mathrm{t}) - \mathrm{Q}(x_0, 0)] + R_1\mathrm{Q}(x_1, \Delta\mathrm{t})|\mathrm{Q}(x_0, 0)| = 0 \quad (4.12)$$

B_1 is already known after the previous sub-step in Step 3 (the first reach reconstruction). The head and flow vectors at the spatial location of x_0 are all known, as they are either measured or calculated in Step 2. So, $\mathrm{H}(x_1, \Delta\mathrm{t})$ and $\mathrm{Q}(x_1, \Delta\mathrm{t})$ are the only two unknown variables in Eqs. (4.11-4.12), thus they can be calculated. Applying this approach to all other nodes, the temporal head and flow vector at the spatial location of x_1, $\mathbf{H}(x_1)$ and $\mathbf{Q}(x_1)$ values, can be determined.

Notice that for spatial location $x = x_1$, the transient wave front arrives when $\mathrm{t} = \Delta t$. The determined head and flow at the transient arrival node [$\mathrm{H}(x_1, \Delta\mathrm{t})$ and $\mathrm{Q}(x_1, \Delta\mathrm{t})$] enables reconstruction of the next reach. Similarly to the first reach reconstruction, the impedance B_2 is determined by analyzing a single extremely short characteristic line linking the transient arrival node $(x_1, \Delta\mathrm{t})$ and a steady state node, which is highlighted in the box in Fig. 4.6(b). The analysis is similar to the analysis in the first reach reconstruction. The compatibility equation on the characteristic line is

$$C^-: \mathrm{H}(x_1, \Delta\mathrm{t}) - \mathrm{H}(x_1 + \delta a_2, \Delta\mathrm{t} - \delta) - B_2[\mathrm{Q}(x_1, \Delta\mathrm{t}) - \mathrm{Q}(x_1 + \delta a_2, \Delta\mathrm{t} - \delta)] = 0 \quad (4.13)$$

The impedance B_2 can be solved since it is the only unknown variable in Eq. (4.13).

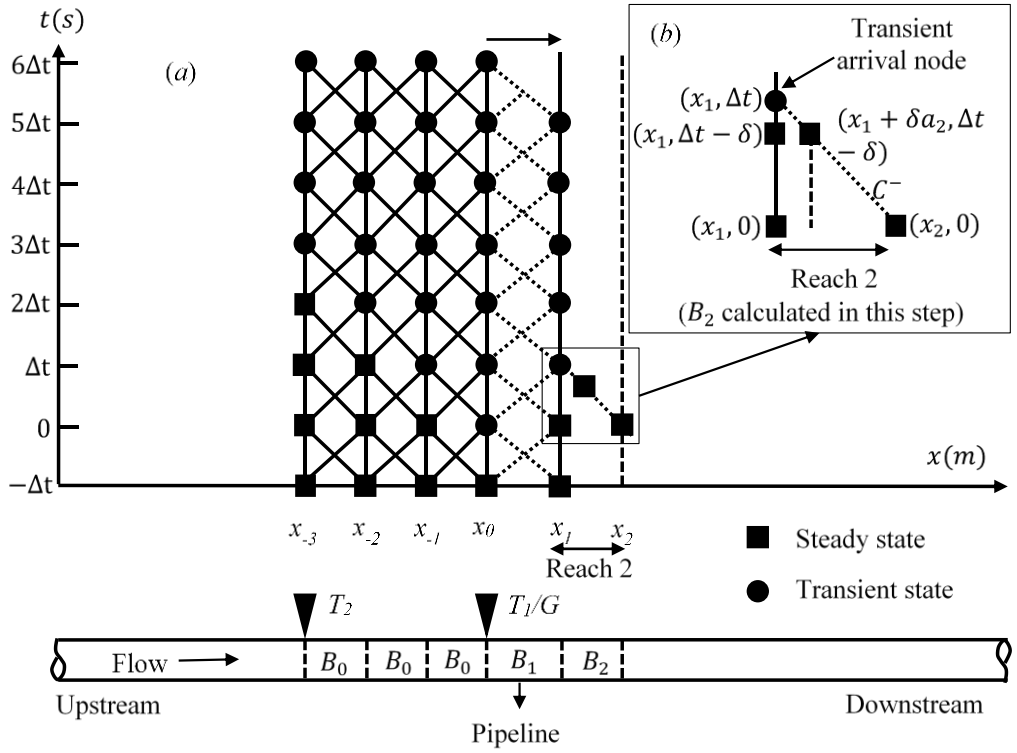

Figure 4.6 Second reach reconstruction on the right side of transducer T1 (Step 3, calculation of B_2 for reach 2)

4.3.4.3 Subsequent reach reconstruction

The subsequent reaches are reconstructed successively, in a similar way to the second reach reconstruction outlined above. The recursive process is performed in two directions: from T1 towards the right and from T2 towards the left. This recursive process is terminated when all reaches, which are relevant to the transient head measurements recorded by two transducers are reconstructed.

4.3.5 From impedance to wall thickness

At this point in the algorithm, the impedance distribution along the pipeline has been estimated so far. Other properties, such as wall thickness, diameter, wave speed and length of each reconstructed reach are determined in this section.

The wave speed of a pipe can be determined by (Wylie et al., 1993, Chaudhry, 2014):

$$a = \sqrt{\frac{K/\rho}{1 + (K/E)(D/e)c_1}} \tag{4.14}$$

where K = the bulk modulus of elasticity of the fluid, ρ = the density of fluid, E = Young's modulus of the pipe wall, D = the internal diameter of the pipe section, e = the wall thickness of the pipe section and c_1 = restraint factor. Considering the definition of impedance B [Eq. (4.3)] and wave speed a [Eq. (4.14)], the diameter (internal diameter D or external diameter D_e) and wall thickness e are coupled in the impedance B. To enable wall thickness estimation, an assumption that either the internal diameter or external diameter of the pipe reach is known has to be made. In the cases where a lack of prior information impedes calculation of wall thickness (for example, Young's modulus or restraint factor is not well known, nominal internal or external diameter is not known), the analysis can be focused on the impedance distribution to identify anomalous pipe sections.

If the internal diameter D is known, the wall thickness can be determined by combining Eq. (4.3) and Eq. (4.14) explicitly:

$$e = \frac{1}{\left(\frac{16K}{\rho g^2 \pi^2 B^2} - D^4\right)\frac{E}{KcD^5}} \tag{4.15}$$

If the external diameter D_e is known, the wall thickness can be determined implicitly by Newton's method. The implicit equation between external diameter D_e and wall thickness e is:

$$\left(1 - \frac{2Kc}{E}\right)(D_e - 2e)^4 e + \frac{Kc}{E} D_e (D_e - 2e)^4 - \frac{16K}{\rho g^2 \pi^2 B^2} e = 0 \tag{4.16}$$

After the wall thickness is determined, the wave speed of each reconstructed reach can be calculated by Eq. (4.14), and the length can be calculated by $\Delta x_i = a_i \Delta t$.

4.4 Numerical verification

To verify the proposed method, a numerical experiment is conducted on a Reservoir-Pipe-Valve (PRV) system, which is depicted in Fig. 4.7. The pipe is assumed to have a uniform external diameter of 600 mm and a uniform Darcy Weisbach friction factor of 0.02. The wall thickness of the pipe is 9 mm, except for three sections with different wall thicknesses. A side-discharge valve, which is installed in the middle of the pipeline (G in Fig. 4.7), is shut instantaneously to generate a transient. A transient is generated by shutting down the valve which is installed at the generator (G in Fig. 4.7). The first transducer T1 is installed at G and the second transducer T2 is in a proximity of 3 m. The numerically generated head measurements at T1 and T2 result from a MOC simulation of the pipeline with a time step of $\Delta t = 0.001\ s$.

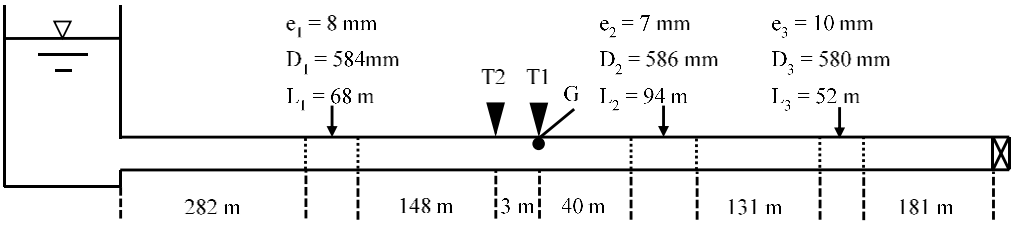

Figure 4.7 Pipeline configuration for the numerical experiment

It is assumed that the external diameter and the wall thickness of the 3 m section between T1 and T2 are known as prior information, and they are the true values, 600 mm and 9 mm respectively. The RMOC approach is applied to the numerically generated head measurements to estimate the impedance distribution along the pipeline. The wall thickness distribution is achieved by Eq. (4.16) after the impedance of each reach is estimated, under the assumption that the pipeline has a uniform external diameter.

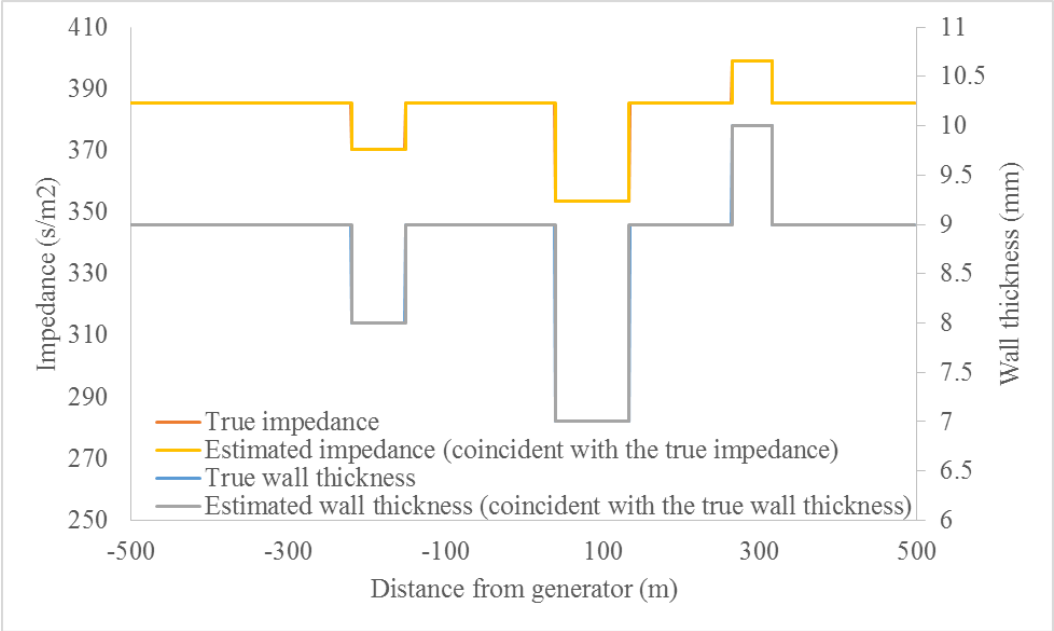

Figure 4.8 Estimated impedance and wall thickness distributions along the pipeline by reconstructive MOC for the numerical experiment

The estimated impedance and wall thickness distributions are given in Fig. 4.8. Three sections with different wall thickness are identified successfully. An exact reconstruction is achieved (they are error free).

4.5 Laboratory verification

Laboratory experiments have been conducted in the Robin Hydraulics Laboratory at the University of Adelaide to verify the RMOC approach. The experimental data has been also used by Shi et al. (2017) for verification of a wave separation algorithm.

4.5.1 Experimental system configuration

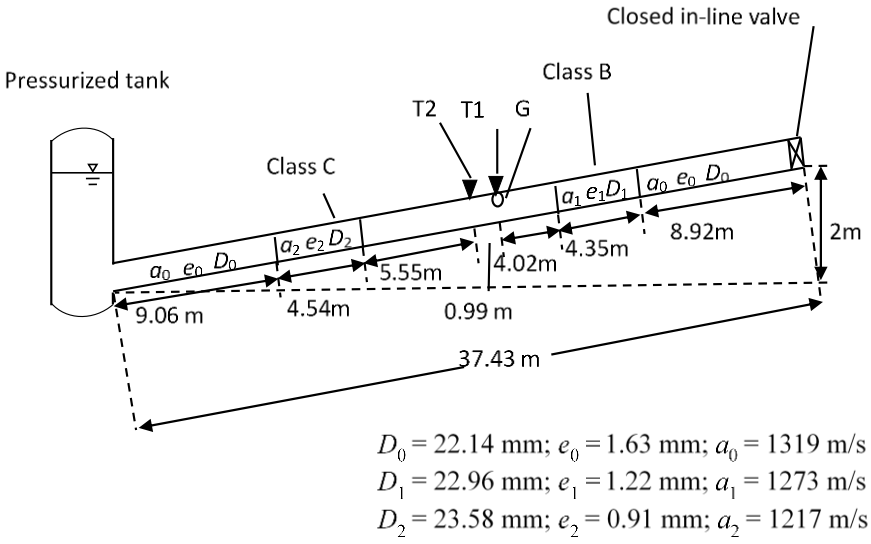

Figure 4.9 Laboratory system layout

The configuration of the laboratory system is depicted in Fig. 4.9. A 37.43 m copper pipe is bounded by a pressurized tank upstream and a closed in-line valve downstream. The pipeline has a uniform external diameter of 25.4 mm.

The pipeline has a wall thickness of 1.63 mm and an internal diameter of 22.14 mm, except for two sections of different class pipes (the parameters of the two sections can be found in Fig. 4.9). A solenoid valve is installed at the generator to excite the system into a transient-state. Two transducers T1 and T2 are installed at proximity of 0.99 m apart. The sampling rate of the head measurements by transducers is 20 kHz.

4.5.2 Preprocessing of the measured head trace

The head measurement at T1 and T2 are given in Fig. 4.10. The first part of head trace, that occurs prior to the reflections from the boundary, has already covered the whole pipeline, so this 0.026 s head trace was used as the measured data in the RMOC. The time duration of the wave front T_w is about $2 \times 10^{-3} s$ which is due to the time duration of valve maneuver to generate the transient. The non-sharp wave front also resulted in the non-sharp reflections on the head trace, which can be found in the zoomed-in plot in Fig. 4.10. It is noted that if possible, a sharp wave front and wave reflections are preferable in the implementation of RMOC algorithm.

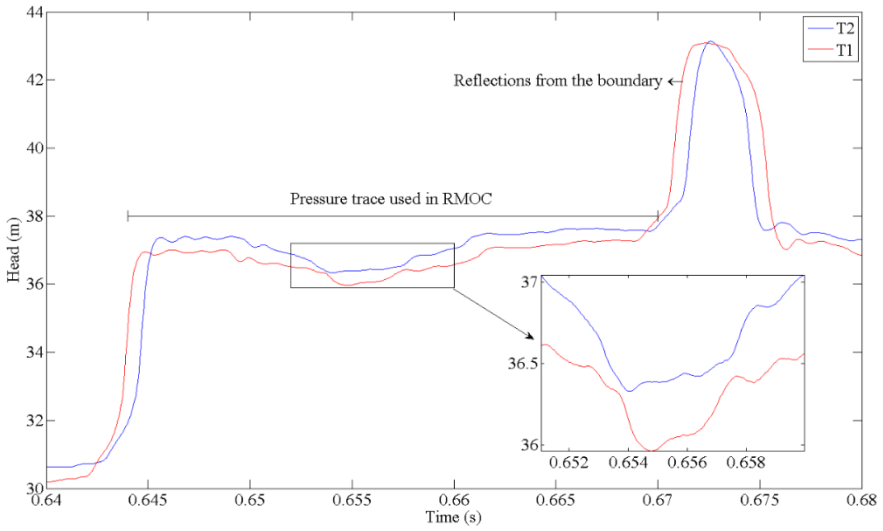

Figure 4.10 Head measurements at T1 and T2

In order to sharpen the data, the step response function (SRF), which is the response of a pipeline system to a theoretical step input transient wave, is estimated first before applying the RMOC algorithm. A detailed description of the SRF estimation can be found in Gong et al. (2014) and Ljung (1998).

Given the induced flow perturbation at the generator as the input and raw head measurements as the outputs, the SRF of the system is estimated (Fig. 4.11). It can be seen that the duration of wave front T_w in SRF is reduced to be roughly $1 \times 10^{-3} s$, which is half of the duration in the raw data. Comparing the zoomed-in plots in both Fig. 4.10 and Fig. 4.11, the edges of wave reflections in the SRF are also sharper than those in the raw data.

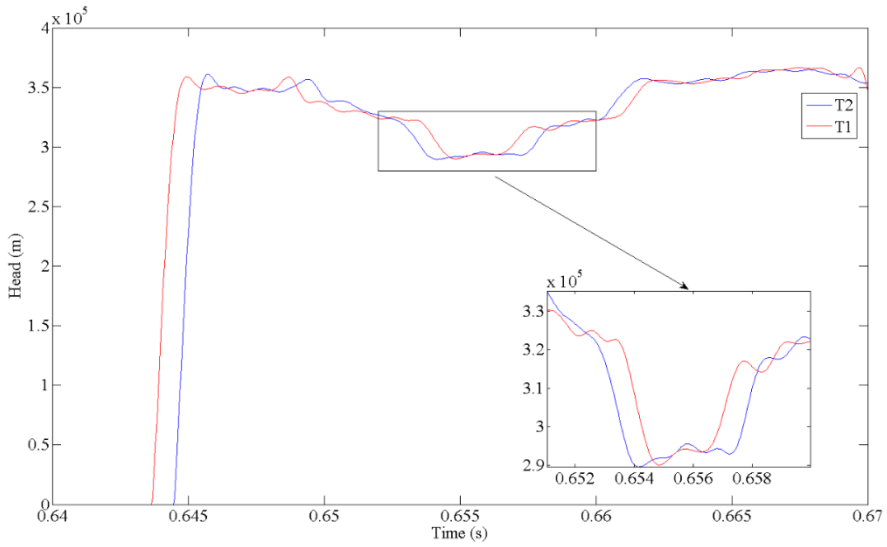

Figure 4.11 Step response function (SRF) at T1 and T2 estimated from raw head measurements

4.5.3 Results and discussion

After preprocessing data, the reconstructive MOC was applied to the SRF, of which the time duration is 0.026 s (as explained previously) and the time step is equal to the data sampling interval $5 \times 10^{-5} s$. This results in a pipeline discretization of 560 reaches and a reach length of about 0.066 m ($\Delta x = a\Delta t$, where $a = a_0$). After the impedance and wall thickness of each reach was estimated, a 40-point median filter (corresponding to a length of 2.6 m) is applied to smooth the results. The estimated impedance and wall thickness distribution after filtering are given in Fig. 4.12.

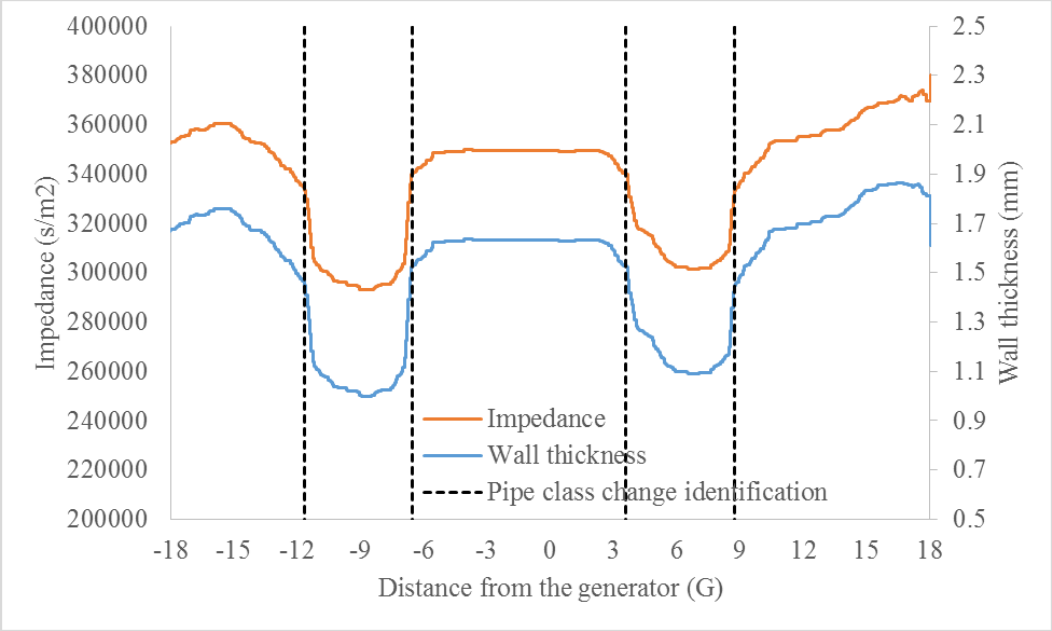

Figure 4.12 Estimated impedance and wall thickness distributions by reconstructive MOC for the laboratory experiment.

It can be seen from Fig. 4.12 that four significant pipe class change interfaces are successfully identified (see dashed line in Fig. 4.12) thus, the location and length of pipe sections are determined. The average wall thicknesses of class B pipe section and class C pipe section are estimated by averaging relevant values of individual reaches. The estimated wall thickness, length, distance from the generator and their corresponding relative errors are given in Table 1. Except for one occurrence of 14.93%, all other relative errors are below 7%, indicating that reconstructive MOC worked well in a laboratory environment.

Table 4.1 Estimated wall thickness, length, distance of two sections and their corresponding relative errors

	Class C pipe section			Class B pipe section		
	Wall thickness (mm)	Length (m)	Distance from G (m)	Wall thickness (mm)	Length (m)	Distance from G (m)
Theoretical values	0.91	4.54	6.54	1.22	4.54	4.02
Estimated values	1.05	4.53	6.79	1.14	4.34	4.21
Relative error*	14.93%	0.21%	3.83%	6.22%	4.44%	4.69%

*Relative error = | (estimated value – theoretical value) / theoretical value| × 100%

4.6 Conclusions

A generalized reconstructive MOC algorithm has been developed for estimating impedance and wall thickness distributions along single pipelines, which are indicative of pipeline condition. The requirement of a dead-end boundary and a head transducer upstream of the dead-end boundary by the previously developed RMOC is relaxed. Instead, two adjacent head transducers, which can be installed any location along the pipeline, are used to record head variations. Based on the measured head variations by the two transducers and known impedance of pipe section between the two transducers, the impedances of the pipe sections outside of two transducers are analytically and uniquely determined by the proposed generalized RMOC presented in this paper. The equations used to calculate the wall thickness from impedance are also derived in this paper, given that the external, or internal, diameter of pipelines are known. The algorithm is verified by

numerical and laboratory experiments. In the numerical experiments, three wall thickness sections were successfully identified, without any error. In the laboratory experiments, two wall thickness sections were successfully identified, including their size and location. Except for one occurrence of one section with a relative error of 14.93%, all other relative errors are all under 7%, indicating that the generalized reconstructive MOC algorithm has worked well in a laboratory environment.

Chapter 5

Sensor placement strategy for pipeline condition assessment using inverse transient analysis

(Journal Paper 4)

Zhang, C., Gong, J., Lambert, M. F., Simpson, A. R. & Zecchin, A. C.

School of Civil, Environmental and Mining Engineering, the University of Adelaide, Adelaide, SA 5005 Australia

Water Resources Management, (submitted).

This page is intentionally blank.

Statement of Authorship

Title of Paper	Sensor placement strategy for pipeline condition assessment using inverse transient analysis
Publication Status	☐ Published ☐ Accepted for Publication ☑ Submitted for Publication ☐ Unpublished and Unsubmitted work written in manuscript style
Publication Details	Zhang, C., Gong, J., Lambert, M. F., Simpson, A. R. & Zecchin, A. C. 2018 "Sensor placement strategy for pipeline condition assessment using inverse transient analysis" Journal of Water Resources Planning and Management, under review.

Principal Author

Name of Principal Author (Candidate)	Chi Zhang		
Contribution to the Paper	Conception and design of the project Analysis and interpretation of research data Draft the paper		
Overall percentage (%)	75%		
Certification:	This paper reports on original research I conducted during the period of my Higher Degree by Research candidature and is not subject to any obligations or contractual agreements with a third party that would constrain its inclusion in this thesis. I am the primary author of this paper.		
Signature		Date	02/03/2018

Co-Author Contributions

By signing the Statement of Authorship, each author certifies that:

i. the candidate's stated contribution to the publication is accurate (as detailed above);

ii. permission is granted for the candidate in include the publication in the thesis; and

iii. the sum of all co-author contributions is equal to 100% less the candidate's stated contribution.

Name of Co-Author	Jinzhe Gong		
Contribution to the Paper	Conception and design of the project Analysis and interpretation of research data Critically revising the paper so as to contribute to the interpretation		
Signature		Date	02/03/2018

Name of Co-Author	Martin Lambert		
Contribution to the Paper	Conception and design of the project Analysis and interpretation of research data Critically revising the paper so as to contribute to the interpretation		
Signature		Date	2/3/18

Name of Co-Author	Angus Simpson		
Contribution to the Paper	Conception and design of the project Analysis and interpretation of research data Critically revising the paper so as to contribute to the interpretation		
Signature		Date	2 Mar. 2018

Name of Co-Author	Aaron Zecchin		
Contribution to the Paper	Conception and design of the project Analysis and interpretation of research data Critically revising the paper so as to contribute to the interpretation		
Signature		Date	2/3/2018

Please cut and paste additional co-author panels here as required.

Abstract

Inverse transient analysis (ITA) has been proven to be a useful technique for pipeline condition assessment, such as leak detection and pipe wall thickness estimation. The effectiveness and accuracy of the inverse analysis are dependent on the sensor placement design, however, previous research on this topic is limited. This paper investigates how the number and location of pressure sensors affects the accuracy and robustness of the ITA approach. An analytical analysis demonstrates that pressure measurements by only two sensors are insufficient to uniquely identify the wave speeds along the pipe, unless the pipe condition in-between the sensors is accurately known (which is often difficult to determine under field conditions). To find the optimal location for a third sensor, numerical studies are conducted to determine the sensitivity of pressure responses at various pipe locations to variations in wave speed values. Multiple ITA cases where three sensors are placed in different locations are also conducted to explore how the locations of sensors affects the accuracy and robustness of ITA. A key observation, consistent with both the sensitivity analysis and the ITA case studies, is that given that the first two sensors are N reaches apart (i.e. N pipe segments in the inverse model), the third sensor should not be placed at nodes that are separated from any of the first two sensors by an integer multiple of N reaches.

This page is intentionally blank.

5.1 Introduction

Water distribution systems are one of the most important types of infrastructure in modern cities. The gradual deterioration as systems age leads to failure of pipelines, which may have severe consequences in terms of water resources loss, disruption to traffic and the wider community, repair costs and compensation claims. Developing an efficient and reliable pipeline condition assessment approach is essential to decision-making involving inspection, rehabilitation or replacement of pipelines. Fluid transient-based methods are promising for the detection of anomalies (Lee et al., 2006, Gong et al., 2012, Duan et al., 2013, Meniconi et al., 2013) and condition assessment (Stephens et al., 2013, Gong et al., 2015, Shi et al., 2017) in water distribution systems due to their non-invasive and cost-effective nature. Among the fluid transient-based methods, Inverse Transient Analysis (ITA), a popular transient-state calibration method, has been intensively studied in the past few decades (Liggett and Chen, 1994, Vítkovský et al., 2007, Kim, 2008, Covas and Ramos, 2010, Stephens et al., 2013, Zecchin et al., 2013, Zhang et al., 2018a).

Even though the successful applications of ITA in hydraulic laboratories and the field are available in the literature, it has also been observed that ITA can suffer the problem of multiple solutions. In this case the seemingly reasonable match between the measured transient pressure response and the predicted transient pressure response is achieved by the calibrated model, however, the parameter estimation accuracy was poor. That is to say that multiple and disparate parameter estimates yield the same inverse model objective (e.g. sum of squared errors). This issue is also termed the identifiability problem

(Ljung, 1998), This problem was illustrated by a numerical case study by Zhang et al. (2018b). Jung and Karney (2008) attributed this problem to the lack of data, while Kapelan et al. (2004) proposed to improve the ill-condition state of the problem by incorporating prior information. Instead of increasing the data or incorporating prior information, Zhang et al. (2018b) proposed a multiple stage algorithm to identify the wave speed parameters by strategically limiting the extent of the search-space for reaches identified as non-anomalous. Despite this work, the mechanism behind the identifiability problem is still not clear. This paper proposes that the identifiability problem is intimately related to the sensor placement design.

Sensor placement design plays a crucial role in model calibration (Savic et al., 2009). The objective of sensor placement design is to collect data that, when used, will yield the best results. A proper sensor placement design will avoid collection of redundant data, i.e. data whose information is already contained within other measurements. Recently, the proliferation of smart water network installations makes Sensor placement design even more important. For example, the South Australia Water Corporation in Adelaide, Australia has invested more than 4 million dollars on smart technologies in Adelaide's central business district, including installing smart sensors to track water flow and pressure (sampled at high frequencies), so that potential leaks and bursts can be prevented before they cause disruption. Since these sensors are permanently installed, the study of sensor placement design can ensure that sensors are placed in the right, and even optimal, locations.

The problem of sensor placement design for steady-state hydraulic model calibration has previously attracted attention. Bush and Uber (1998) proposed

general sensitivity based methods to rank the locations available for measurement. Sensitivity based methods have been the building blocks of much of the following research, however, instead of ranking according to the sensitivity, many researchers treated the sensor placement design problem as an optimization problem (Meier and Barkdoll, 2000, Lansey et al., 2001, Do et al., 2016), in which evolutionary algorithms, such as a genetic algorithm (GA), were employed to minimize a parameter-covariance-metric based objective function. In addition, Kapelan et al. (2005) proposed a second objective function of minimizing the number of sensors. Thus, the sensor placement design problem was formulated as a multiple-objective problem. This was solved by a GA (Kapelan et al., 2005) and by an adaptive neural network (Behzadian et al., 2009).

In contrast, research on sensor placement design for transient hydraulic model calibration is very limited (Savic et al., 2009). Liggett and Chen (1994) suggested that pressures should be measured at the most sensitive locations in networks. Vítkovský et al. (2003) treated the transient-state sensor placement design as an optimization problem, in which a GA was used to minimize or maximize three different indicators. However, no one has investigated the relation between the sensor placement design and the problem of multiple solutions.

This paper investigates how the sensor placement design (number and location of measurement stations) affects the problem of multiple solutions in ITA. This paper is organized as follows: the problem of sensor placement design and identifiability is formulated first. This is followed by an analytical analysis to demonstrate that two pressure sensors are not able to uniquely

identify wave speed parameters along pipelines. Then a sensitivity analysis is conducted to determine the location where the pressure is the most sensitive to wave speed variations to install a third sensor. Multiple scenarios are investigated that involve three sensors installed in different locations to investigate how the locations of three sensors affects the accuracy and robustness of ITA results. Finally, conclusions are drawn based on the pattern revealed by the sensitivity analysis and ITA case studies.

5.2 Problem formulation

The pipeline of interest depicted in Fig. 5.1 is discretized into *M* reaches (consider *M* is even, without loss of generality). The discretization is based on a uniform time step Δt, instead of a fixed reach length Δx. Assuming that the pipeline is excited into a transient state by a flow perturbation at node $x_{M/2}$ at time t_0 (point A in Fig. 5.1), there will be *M* reaches, centered on the $x_{M/2}$ point, contributing to the first $M-1$ transient pressure measurements $\mathbf{H}(x_{M/2})$ at the transient generator. The length of each reach is the distance that the transient wave travels in each time step, thus is determined by $\Delta x_i = a_i \Delta t$. The discretization based on the time step Δt eradicates the need for interpolation in numerical modelling using the method of characteristics (MOC), and enables an analytical analysis of the identifiability problem.

The unknown parameters (in this research, it is assumed that the pipeline has a uniform internal diameter, and wave speeds are the unknown parameters representing pipeline condition) of *M* reaches require estimation. The pressure response on the edges or inside the polygon bounded by *A*, *B*, *C*, and *D* are

only dependent on the M wave speeds (a_1 to a_M) in the pipe section of interest. The M – 1 nodes linking M reaches are potential locations for placing pressure transducers, which record the pressure response of the pipeline after the transient excitation.

Several researchers have utilized pressure measurements to assess pipeline condition by ITA-based approaches (Stephens et al., 2013, Zhang et al., 2018b). The question remains that from the M – 1 potential locations for sensors, how many sensors are required and how are these sensors best placed to identify the unknown parameters.

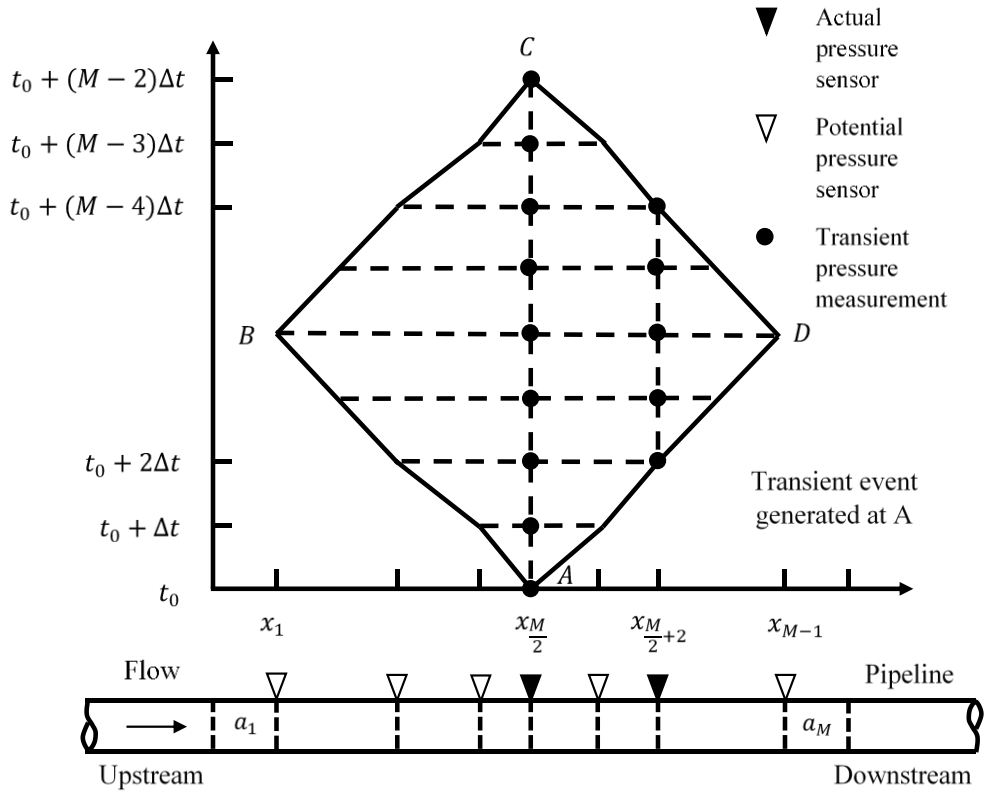

Figure 5.1 The parameters to be calibrated, potential locations for sensors and the pressure measurements

5.3 Multiple solutions with two sensors

One sensor only is not sufficient to uniquely identify the wave speed distribution of a pipeline, since it is impossible to tell which direction the transient wave reflections comes from. This section investigates whether two sensors are sufficient for uniquely identifying the wave speed distribution of a pipeline by an analytical analysis using Reconstructive Method of Characteristics (RMOC). RMOC was first proposed by Gong et al. (2014) to calculate the impedance distribution along a pipe using transient pressure responses measured in the pipeline close to a dead-end, and a MOC analysis backward in time. RMOC was then generalized by Zhang, et al. (2018c), where the pipeline impedance can be estimated by pressure measurements at two adjacent sensors at interior points along the pipe.

Given that pressures are measured by two sensors and pipe parameters between the two sensors are known, the RMOC can analytically and uniquely determine the remaining pipe parameters upstream and downstream of the two sensors. For example, if pressure is measured by two sensors at the node $x_{M/2}$ and the node $x_{M/2+2}$ with the measurements described by $\mathbf{H}(x_{M/2})$ and $\mathbf{H}(x_{M/2+2})$ (solid dots in Fig. 5.1), with the pipe parameters $a_{M/2+1}$ and $a_{M/2+2}$ between the two sensors are known, all the other wave speeds can be analytically and uniquely calculated by the RMOC (Zhang, et al., 2018c). The reader can refer to Zhang, et al. (2018c) for more details of the RMOC algorithm.

Multiple solutions for an ITA problem exist if numerical pipe models with different parameters generate the same pressure response at all the

measurement stations, as the ITA objective is based on the model predictions only at these points. A numerical experiment is used to illustrate multiple ITA solutions with two sensors for three different scenarios of assumed wave speed parameter values between the sensors.

5.3.1 Example Outline

The Reservoir-Pipe-Valve system, which is used in the numerical experiment, is depicted in Fig. 5.2. The reservoir at the upstream of the pipe has a constant head of 30 m. The valve at the downstream of the pipe has a constant discharge of 0.0001 m^3/s. The 1280 m pipe is assumed to have a diameter of 0.6 m, a constant Darcy-Weisbach friction factor of 0.02 and a constant wave speed of 1000 m/s throughout the pipe. The pipe is discretized into $N = 128$ reaches using a time step of 0.01 s, which results in the length of each reach is 10 m. A side-discharge valve is installed at the center of the pipe (Node 65, which is referred as N65 hereafter), and it has a steady state discharge of 0.05 m^3/s. The valve is closed instantaneously at time $t = 0.01$ s to generate a step transient pressure wave. To record pressure responses, two sensors M1 and M2 are placed at N65 and N68, respectively. Pressure responses at these two sensors were generated by forward MOC simulations with a time step of $\Delta t = 0.01$ s.

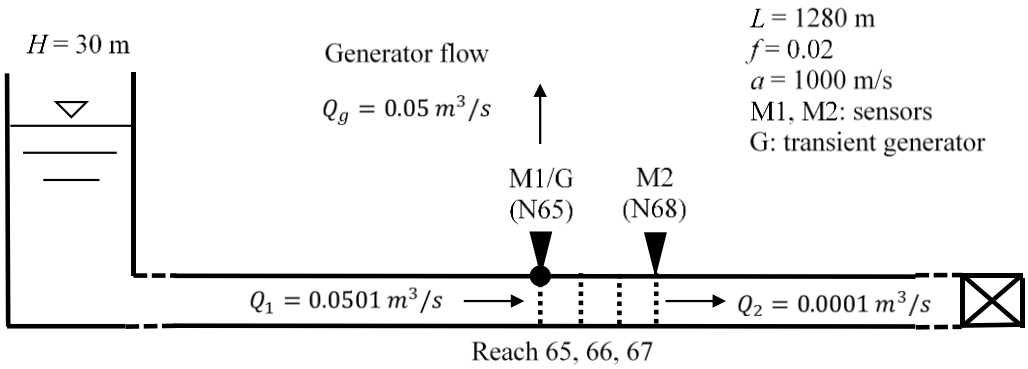

Figure 5.2 Reservoir-Pipe-Valve system

Together with the two numerically generated pressure traces at the two sensors (both are almost flat since there are no transient wave reflections), three wave speed scenario sets for the pipe reaches in-between the two sensors were input for the RMOC approach to calculate the wave speed distribution outside of the sensor pair. For reaches 65, 66 and 67 in-between the two sensors (in Fig. 5.2) the three scenarios are given by the wave speeds $A_1 = [1000, 1000, 1000]$ m/s, $A_2 = [1000, 990, 1000]$ m/s and $A_3 = [1000, 1010, 1000]$ m/s, respectively.

5.3.2 Example Results

The wave speed distributions determined for each of three input scenarios listed above using the RMOC are given in Fig. 5.3.

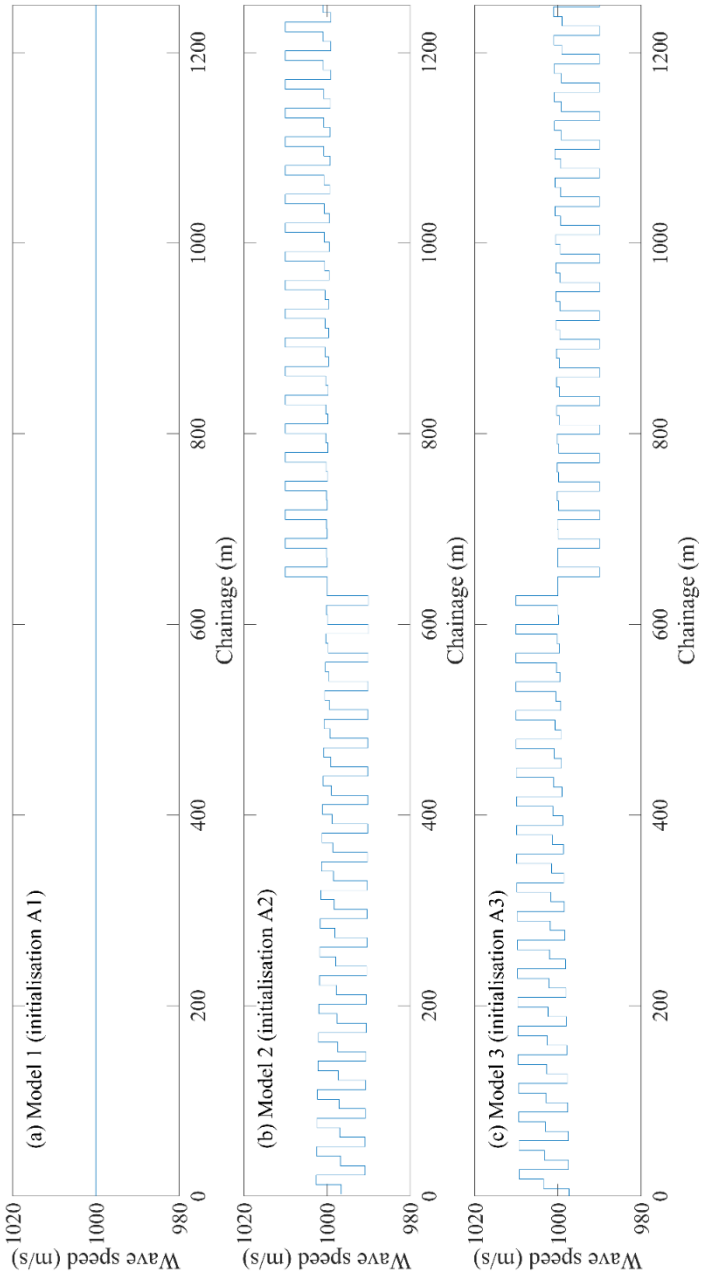

Figure 5.3 Three wave speed distributions calculated by RMOC with the same set of pressure response at two sensors but different wave speed initializations between sensors (a) model 1 with A1; (b) model 2 with A2; (c) model 3 with A3

Wave speeds calculated by RMOC for scenario A_1 result in a uniform wave speed distribution along the pipe, confirming that if $[a_{65}, a_{66}, a_{67}]$ are known to be the correct values, the other wave speeds will be calculated correctly. However, as seen in Figs 5.3(b) and 5.3(c), if $[a_{65}, a_{66}, a_{67}]$ are different from the correct values, as is the case for scenarios A_2 and A_3, the other wave speed parameters along the length of the pipe will have significant variations from the true values A repeated pattern is found in Figs 5.3(b) and 5.3(c) and it is inversely reflected about the transient generated. It is very likely that the wave reflections created by the wave speed variations cancelled out at the two existing sensors locations. The observed wave speed variations compensate for the error in the assigned wave speeds in the internal reaches between the two transducers, so that the determined model with incorrect input information still produces pressure responses that match those measured by the two sensors exactly.

The pressures responses at the sensor M2 (N68) for the three scenarios are calculated using the MOC. It is confirmed by Fig. 5.4 that despite the differences in the wave speeds in the three models (in Fig. 5.3), these models had the same pressure traces at M1 and M2. Considering the narrow range of the *y*-axis (0.15 m in Fig. 5.4), the three lines are still indistinguishable, demonstrating that the three models have the same pressure traces at M2, as expected. The pressure responses at M1 for the three models are also identical.

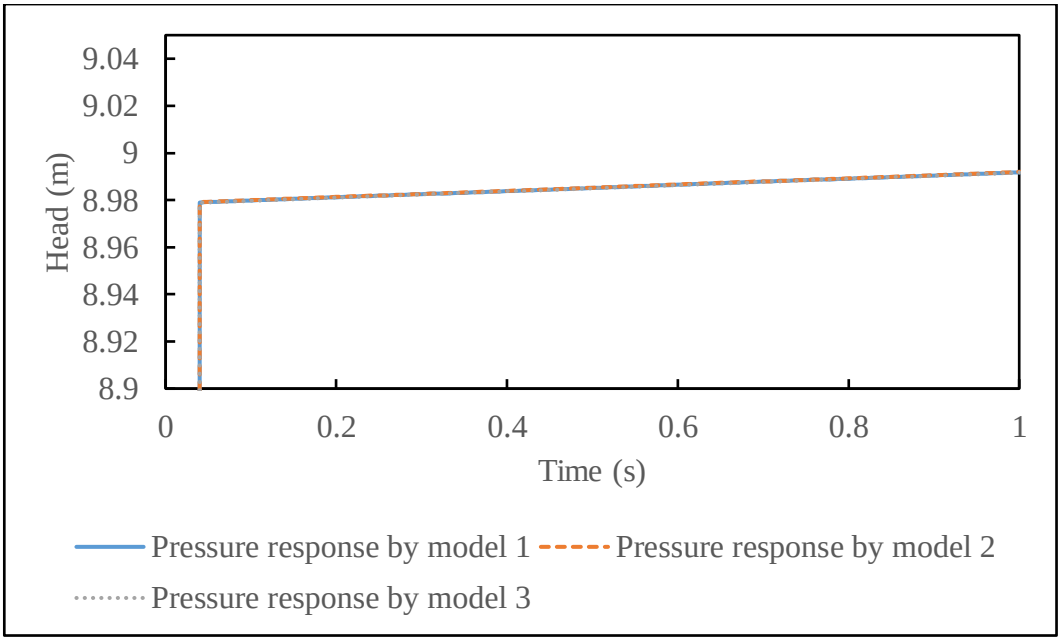

Figure 5.4 Predicted pressure traces of three models at M2 (N68)

5.3.3 Example Discussion and Analysis

There can be an infinite number of wave speed initialization arrangements for the reaches between the two placed sensors. For any initialization, the RMOC method can analytically determine a model that produces the same pressure traces at each of the two sensors. This demonstrates that there can be infinite pipe models which produce exact the same pressure responses at two sensors.

An interesting phenomenon is revealed when inspecting the predicted pressures at node N61 (given in Fig. 5.5) and N62 (given in Fig. 5.6) of the three models. It is not surprise that at N61, the model 1 with a uniform wave speed distribution has a flat pressure trace, the model 2 and 3 with oscillations in wave speed distributions have pressure trace with oscillations. However, it is surprising to see that at N62, the three models have almost the same pressure traces.

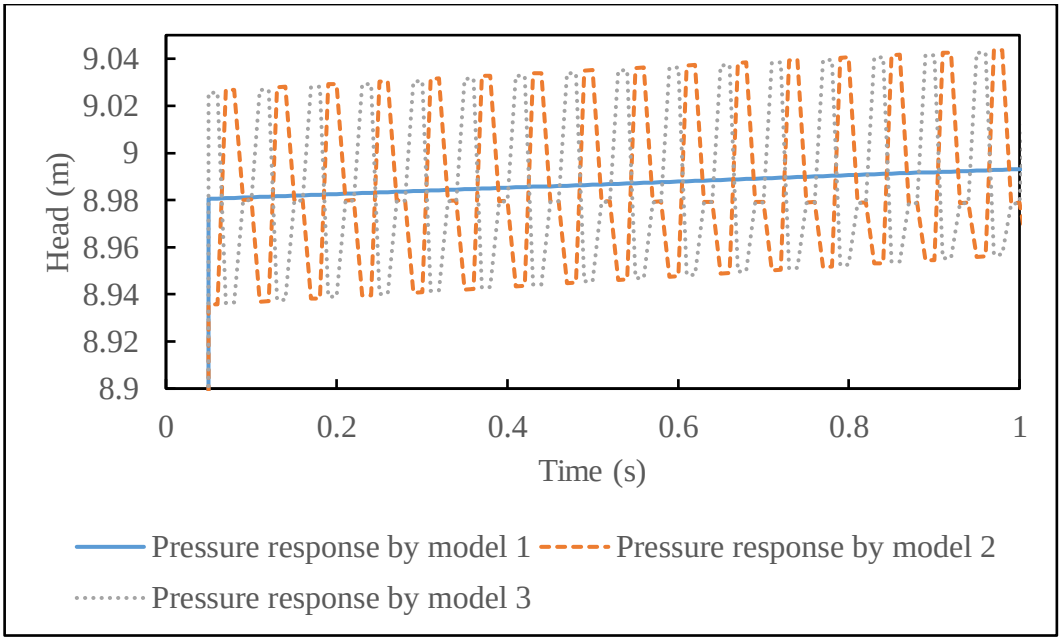

Figure 5.5 Predicted pressure traces of three models at N61

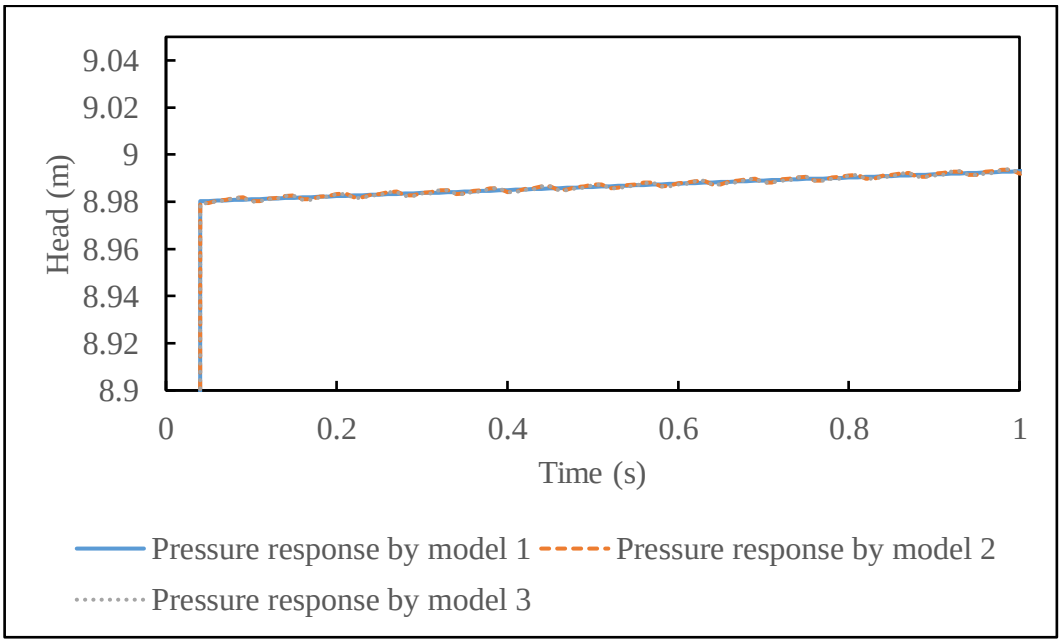

Figure 5.6 Predicted pressure traces of three models at N62

This discovery is meaningful and valuable. The results indicate that the information carried by the pressure measurement at N62 is redundant, as it provides no further information concerning the system identifiability other than the information contained within the pressure measurements at N65 and

N68. Given that two sensors are already placed at N65 and N68, if the third sensor is placed at the nodes at N62, the parameter estimation (using any transient-based method based on three sensors) will still suffer from the problem of multiple solutions. However, if the third sensor is placed at N61, the pressure trace at this node will provide extra information. That is, the differences between the three models are manifest at this point as the wave forms from different models do not cancel each other out at this point, meaning that the parameters are likely to be uniquely identified by transient-based methods. The sensor placement, even one node away (from N62 to N61), can make a significant difference in the identifiability of parameter estimation.

To summarize, this section demonstrates by example that two sensors are insufficient to uniquely identify the wave speed distribution along the pipeline. To enhance the identifiability, a third sensor is required. The location of third sensor plays a significant role in the problem of identification and is further explored in the following sensitivity analysis.

5.4 Sensitivity analysis for the placement of the third sensor

To systematically explore the best location for the placement of the third sensor, a sensitivity analysis is conducted. The third sensor should be placed at the location where the pressure response is most sensitive to changes in the wave speed values. A sensitivity matrix **J**, representing the sensitivity of transient pressure to wave speed, is defined as:

$$\mathbf{J} = \begin{bmatrix} \frac{\partial \mathbf{H}_1}{\partial a_1} & \cdots & \frac{\partial \mathbf{H}_1}{\partial a_{Nr}} \\ \vdots & \ddots & \vdots \\ \frac{\partial \mathbf{H}_{Nn}}{\partial a_1} & \cdots & \frac{\partial \mathbf{H}_{Nn}}{\partial a_{Nr}} \end{bmatrix} \tag{5.17}$$

where N_r = the number of reaches between the two existing sensors; N_n = the number of potential nodes for the placement of the third sensor; $\mathbf{H}_j = [H_{j,1} \quad \cdots \quad H_{j,Np}]$ is the temporal vector of transient pressure values at the *j*th node; N_p = the number of effective transient pressure data points at the *j*th node.

In this research, the derivatives $\frac{\partial \mathbf{H}_j}{\partial \mathrm{a}_i}$ (elements of **J**, representing the sensitivity of the pressure at *j*th node to the parameter of *i*th reach) are calculated by the finite difference method (Lansey et al., 2001):

$$\frac{\partial \mathbf{H}_j}{\partial a_i} \approx \frac{\mathbf{H}_j(\mathbf{a}') - \mathbf{H}_j(\mathbf{a})}{\Delta a_i} \tag{5.2}$$

where $\mathbf{H}_j(\mathbf{a}) =$ pressure prediction of the benchmark model, at the *j*th pipe node, $\mathbf{a}$ = wave speed vector of the benchmark model, Δa_i = perturbation in the *i*th wave speed a_i, and $\mathbf{a}'$ = wave speed vector associated with the added wave speed perturbation.

In this paper, wave speed perturbations are introduced one at a time into the N_r pipe reaches between the two existing sensors. The wave speeds of the reaches outside the sensor pair are calculated by the RMOC, which is embedded in the sensitivity analysis:

$$\mathbf{a}' = f_{\mathrm{RMOC}}(\mathbf{a_s} + \Delta\mathbf{a}) \tag{5.3}$$

where $\mathbf{a}'$ is the determined wave speed vector by the RMOC, $\mathbf{a_s}$ is a subset of $\mathbf{a}$ and represents the wave speeds between two sensors in the benchmark

model and $\Delta\mathbf{a}$ is the perturbation vector in which the only non-zero element is Δa_i (the perturbation introduced to the *i*th wave speed).

The average sensitivity of the pressure at the *j*th node to *i*th wave speed is denoted as $S_{j,i}$ (j = 1,…, N_n-1, and i = 1,…, N_r) and defined by:

$$S_{j,i} = \frac{1}{N_p}\sum_{k=1}^{N_p}\left|\frac{\partial H_{j,k}}{\partial \mathrm{a}_i}\right| \tag{5.4}$$

Overall, the averaged sensitivity matrix **S** (the assemblies of elements $S_{j,i}$), representing the sensitivity of pressure response at each node to each wave speed between two sensors, is the outcome of the calculation. To calculate the matrix **S**, the following procedure is used: (Step 1) simulate the transient response of the benchmark model by the MOC; (Step 2) calculate the wave speeds for the model with a wave speed perturbation in one of the reaches between the two sensors by the RMOC as the perturbed model; (Step 3) simulate the transient response of the perturbed model by MOC; (Step 4) calculate the derivatives by Eq. (5.2); (Step 5) calculate average sensitivity at each potential location $S_{j,i}$by Eq. (5.4).

5.4.1 Preliminaries for sensitivity analysis

The sensitivity analysis was conducted on the same system as used in the previous section (Fig. 5.2). The pipe model used in the sensitivity analysis (L = 1280 m, a = 1000 m/s, D = 600 mm and f = 0.02) is referred to as the uniform wave speed model. In addition, as a second example, a 1248.6 m pipe with a uniform diameter of 749.5 mm and a uniform friction factor of 0.02, but continuously varied wave speeds (to represent a real world complex pipe

condition), is used as a variable wave speed model. The wave speed variations of the variable wave speed model are given in Fig. 5.7. The pipe of the variable wave speed model is also discretized into 128 reaches, where the length varies for each reach and is determined by $\Delta x_i = a_i \Delta t$.

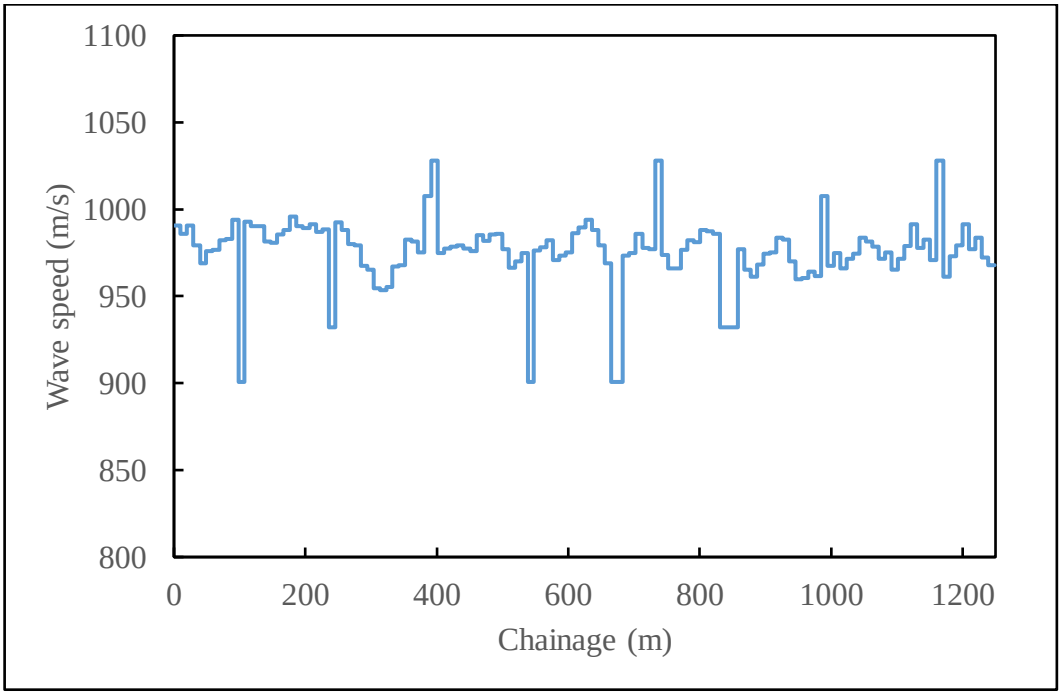

Figure 5.7 Wave speed distribution along the pipe in the variable wave speed model (L = 1248.6 m)

To further generalize the analysis, in both the uniform and variable wave speed models, two different sensor placements scenarios are considered. The first two sensors are placed at node 65 (N65) and node 68 (N68) in scenario (a), and at node 65 (N65) and node 70 (N70) in scenario (b). Nodes 30 – 100 [except for N65 and N68 in scenario (a), and N65 and N70 in scenario (b)] are potential locations for placing the third sensor.

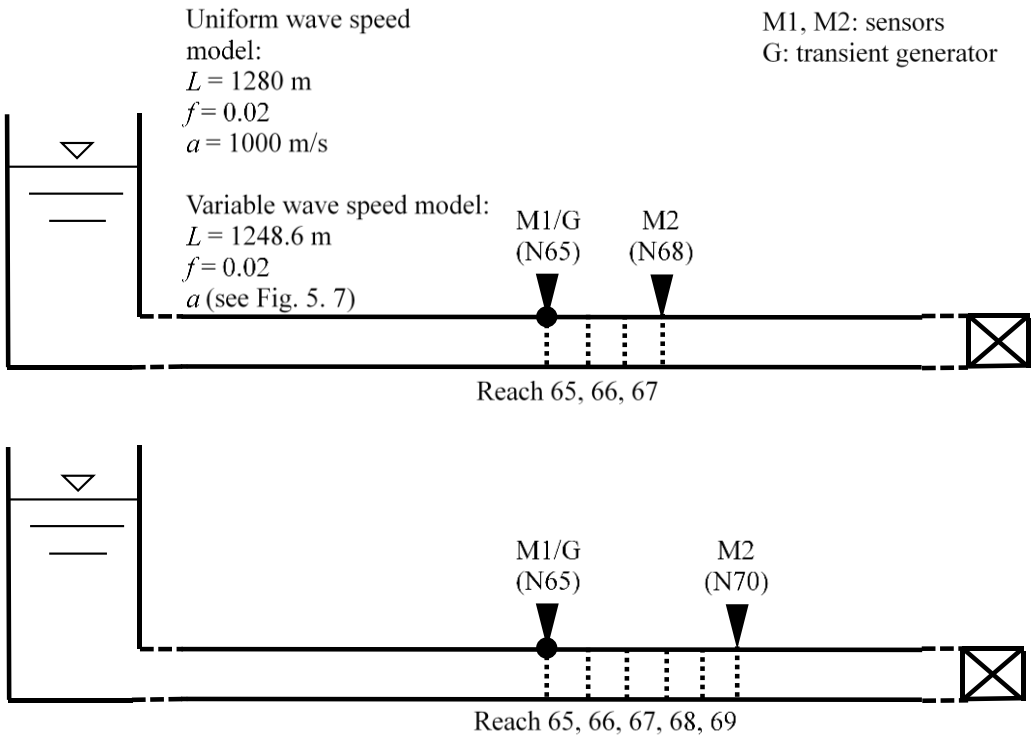

Figure 5.8 (a) First two sensors are placed at N65 and N68; (b) first two sensors are placed at N65 and N70

5.4.2 Results and discussions

Fig. 5.9 shows the sensitivity $S_{j,i}, (j = 30, \cdots, 100, i = 65, 66, 67)$ in scenario (a) for the uniform wave speed model. The sensitivity values at N65 and N68 to the three reaches were all zero, because the RMOC guarantees that all the models determined have exactly the same traces as the benchmark model at these two nodes. Besides these two nodes, Fig. 5.9 shows that the sensitivity values at the nodes that are every three reaches apart from N65 (which is equal to the number of reaches in-between the two placed sensors), are close to zero. The extremely low sensitivity indicates that pressure traces at these nodes are redundant – the information provided at these nodes is already contained within the pressure responses recorded by the first two sensors at

N65 and N68. As a result, for the purpose of parameter estimation by utilizing the pressure traces, the third sensor should not be placed at these nodes. The sensitivity values at other nodes are relatively similar to each other, and they are much larger than those at the nodes which are three reaches apart from N65 and N68. Also, at a certain node, the sensitivities values to different reaches in-between two existing reaches (i.e. reach 65, 66 and 67 in Fig. 5.9) are in the same level. In the following discussion, only the average sensitivities (sensitivities of the pressure response at each node to all wave speed parameters between the existing sensors) is presented for simplicity.

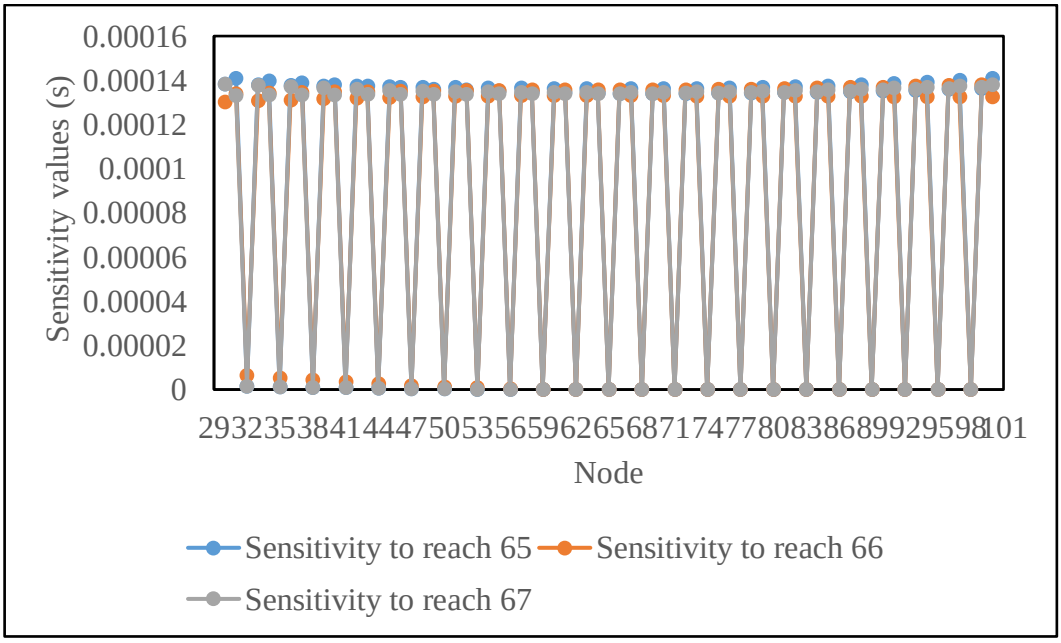

Figure 5.9 Sensitivity of pressure response in scenario (a) for the uniform wave speed model

Fig. 5.10 shows the average sensitivity S_j $(j = 30, \cdots, 100)$ of scenario (b) for the uniform wave speed model. The similar pattern of low sensitivity is observed but with a different spacing between the insensitive points. That is the sensitivity at the nodes that are apart from N65 with an integer multiple of five is extremely low to changes in the wave speeds. Once again, the spacing

of the pattern equals to the number of reaches in-between the two existing sensors. Therefore, the third sensor should not be placed at these nodes when the first two sensors are placed on the N65 and N70.

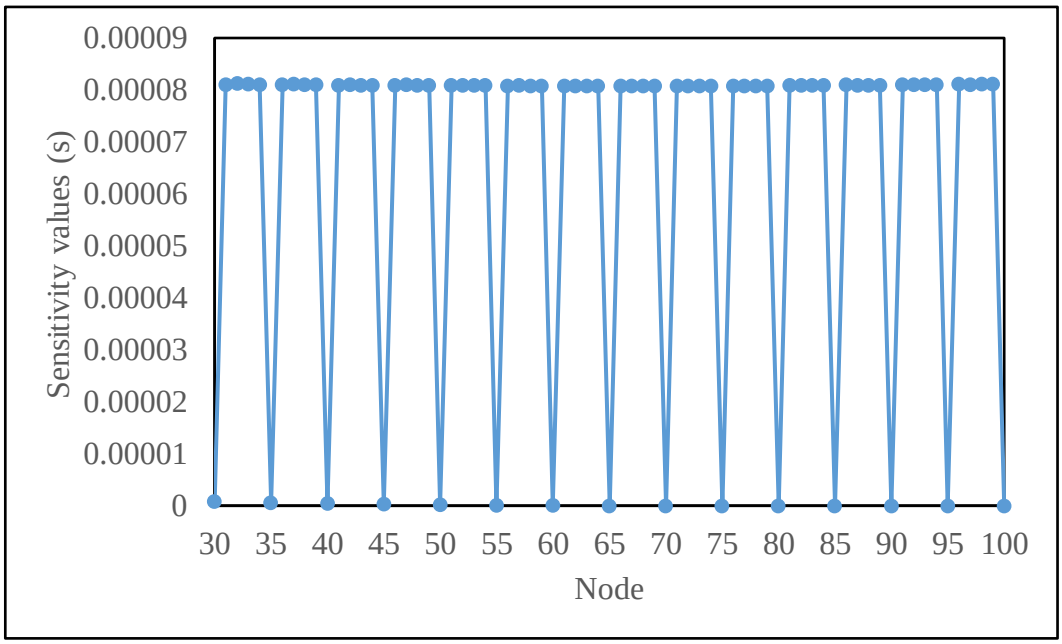

Figure 5.10 Sensitivity of pressure response in scenario (b) for the uniform wave speed model

The sensitivity analysis is also carried out on the variable wave speed model. The average sensitivity of the pressure response at different nodes to the wave speeds of the reaches between the existing two sensors are given in Fig. 5.11 and Fig. 5.12 for the two scenarios as discussed previously [the first two sensors are placed at N65 and N68 (three reaches apart) in scenario (a), and at N65 and N70 (five reaches apart) in scenario (b)]. Consistent with the pattern in Fig. 5.9 and Fig. 5.10, the pattern of periodic low sensitivity is further observed. Sensitivity of the pressure responses to changes in wave speeds at some particular nodes, which are apart from the first two sensors with an integer multiple of the number of reaches between the sensors, are extremely low. The sensitivity values at other nodes are all significantly larger, and their

relative size varies with the scenarios explored [scenarios (a) and (b) in Fig. 5.8]. No general conclusion can be drawn on which node is superior to others, just that there exists a pattern in the locations of the low sensitive nodes.

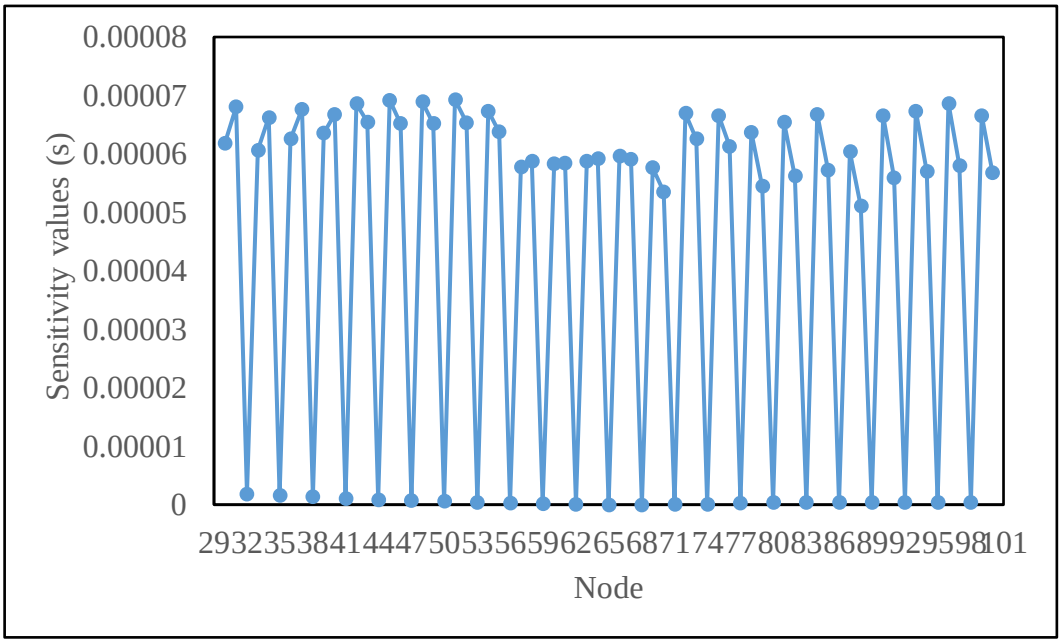

Figure 5.11 Sensitivity of pressure response in scenario (a) for the variable wave speed model

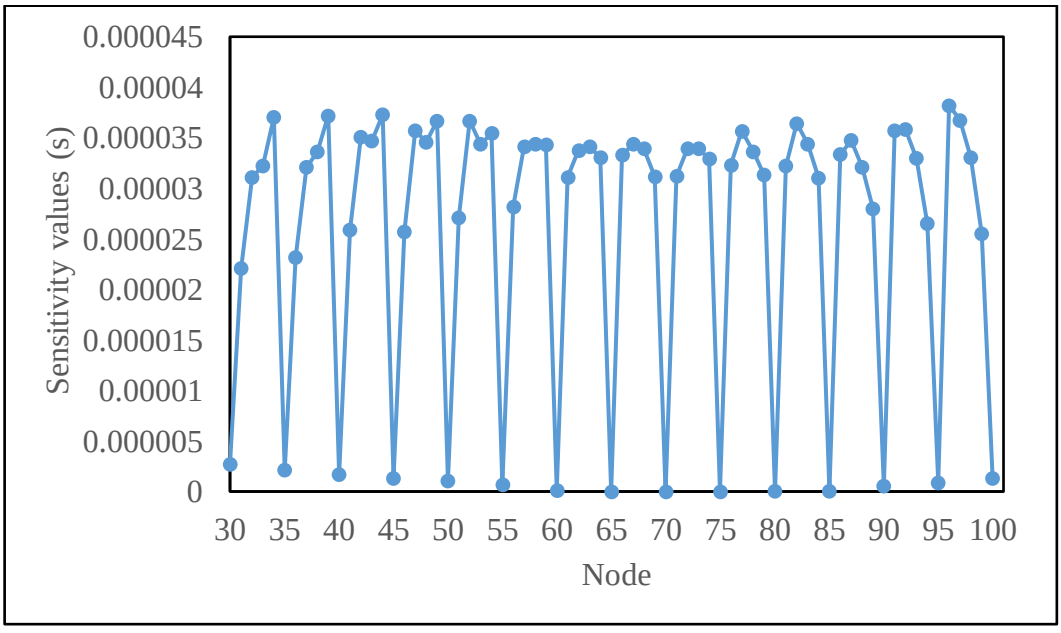

Figure 5.12 Sensitivity of pressure response in scenario (b) for the variable wave speed model

By the sensitivity analysis, a pattern is revealed. Given that the first two sensors are *N* reaches apart, the pressure response at the nodes which are a grid distance from any of the two sensors by an integer multiple of *N* reaches, is not sensitive to the wave speed changes, thus the third sensor should not be placed at these nodes.

5.5 ITA case studies

In this section, the pattern identified in the previous sensitivity analysis is confirmed by conducting inverse transient analysis (ITA) on different cases. In select cases, the third sensor is placed on the node which is at a grid distance from one of the first two sensors by an integer multiple of *N* reaches, while in other cases the third sensor is not (for brevity, referred as integer multiple location case and non-integer multiple location case, respectively). The results show that ITA performances are significantly different between integer multiple and non-integer multiple location cases.

5.5.1 Numerical Experiment Preliminaries

The Reservoir-Pipe-Valve system used in the ITA case studies is the same used in the sensitivity analysis (Fig. 5.2). Ten scenarios for each pipe model (uniform and variable wave speeds) are considered where the different placements of the three sensors in each case are given in Fig. 5.13. This results in a total of 20 case studies.

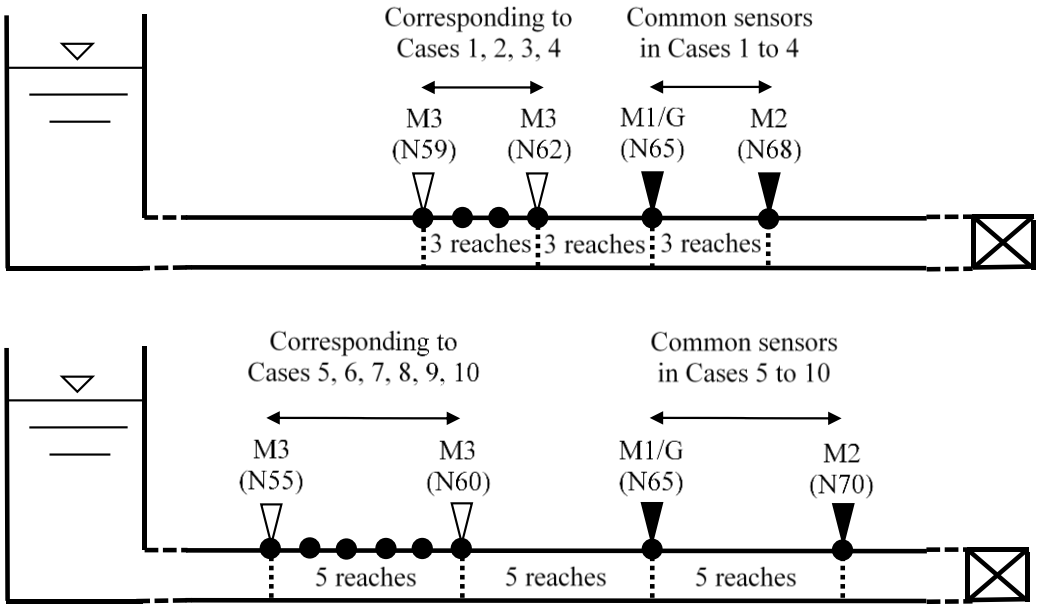

Figure 5.13 Sensor placements of the 10 cases

In Cases 1 to 4, two common sensors are placed on N65 and N68. Four candidate locations for the third sensor, N59 to N62 (four consecutive black dots in Fig. 5.13), result in the four cases. Among the four cases, Case 1 (the third sensor at N62) and Case 4 (the third sensor at N59) are non-identifiable cases. In Cases 5 to 10, two common sensors are placed on N65 and N70. Six candidate locations for the third sensor, N55 to N60 (black dots in Fig. 5.7), result in the six cases. Among the six cases, Case 5 (third sensor at N55) and Case 10 (third sensor at N60) are non-identifiable cases. From hereon, cases for the uniform wave speed model are denoted with a "U" (e.g. Case 5.U), and cases for the variable wave speed model are denoted with a "V" (e.g. Case 5.V).

For the ITA, it is assumed that the friction factor was known to be the assumed value of 0.02, and wave speeds of 128 reaches are the parameters to

be calibrated. A flexible grid (Zhang et al., 2018a) as described in Fig. 5.1 is used in the ITA to eradicate the need for interpolation. To ensure the distance between any two sensors, which varies during iterations in the ITA due to the adaption of a flexible grid, to be the fixed known value, the wave speed of one reach between the two sensors is calculated by the known distance and the calibrated wave speeds of other reaches. In this way, the distance between any two sensors is fixed and the number of decision variable is reduced from 128 to 126. Search spaces for the wave speed are set to be in the range [950 m/s, 1000 m/s] and [850 m/s, 1100 m/s] for the simple and complex pipe model, respectively. Particle Swarm Optimization (PSO) (Poli et al., 2007, Zecchin et al., 2013) is used as the optimizer to minimize the objective function. The number of PSO particles and the number of iterations are set to be 500 and 5000, respectively. All results presented below are based on 10 independent trials starting from different random number seeds.

5.5.2 Results and discussion

Results of Cases 5 and 6 for the uniform wave speed model (Cases 5.U and 6.U), and Cases 5 and 6 for the variable wave speed model (Cases 5.V and 6.V), are discussed in detail as they illustrate trends common to all cases. Cases 5.U and 5.V are two non-identifiable cases, and Cases 6.U and 6.V are two identifiable cases. At the end of this section, the other cases are briefly discussed.

5.5.2.1 Results for the uniform wave speed Cases 5.U and 6.U

The relative errors of 10 independent trials in Cases 5.U and 6.U are presented as boxplots in Fig. 5.14. The relative error of the wave speed estimates in each reach is calculated by:

$$e = \frac{\tilde{a} - a}{a} \times 100\% \tag{5.5}$$

where a is the true wave speed, and $\tilde{a}$ is the wave speed estimate.

As seen in Fig. 5.14, the relative error of estimates in Case 6.U are more centered on 0%, compared to those in Case 5.U. The box plot of Case 6.U has a significantly reduced average IQR (interquartile range) of 0.45%, compared with 0.67%, which is the average IQR of Case 5.U. A reduced IQR means less variation in the parameter estimates, implying that the calibration objective function for Case 6.U is more informative about the global optimal parameter estimate than is the objective function for Case 5.U. The estimates of Case 6.U also have fewer outliers, and the relative errors are limited to the range of ±2%. However, the outliers of the relative errors of Case 5.U are spread over the range of ±5%. As the distance from the generator increases, the estimate accuracy reduces (see the outliers and increased IQR in the first and last few reaches).

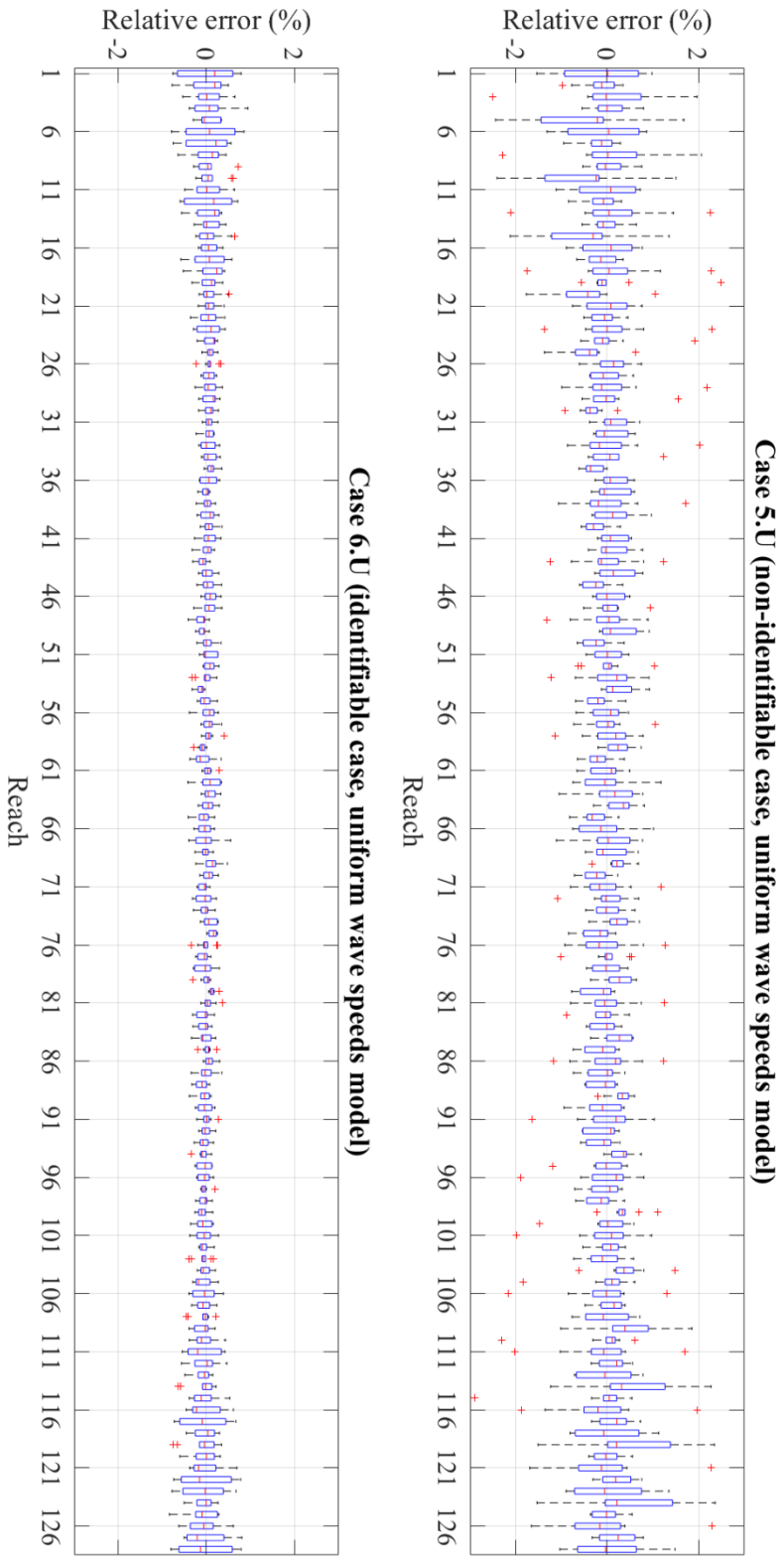

Figure 5.14 Box plot of the wave speed estimates from Case 5.U and 6.U. The horizontal axis indicates the reach number

It is also worth pointing out that according to the box plots for Case 5.U in Fig. 5.14, if the wave speed of one reach on the left hand side of the transient generator is underestimated, then its counterpart on the right hand side is overestimated (see the existence of outliers and the estimates with large IQR, they are inversely reflected about the generator location). From this pattern, it is believed that an overestimated wave speed compensates for an underestimated wave speed that is symmetric around generator, providing a reasonable match on integer multiple locations, which is confirmed below in Figs 5.15 and 5.16.

Fig. 5.15 compares the best estimated wave speeds of the 10 trials (ranked in terms of objective function) for Cases 5.U and 6.U, and Fig. 5.16 shows the pressure responses at the generator. The best estimated wave speeds of Case 5.U have multiple distinct outliers, which are inversely reflected about the generator location. To the contrary, the best estimated wave speeds of Case 6.U are all in the interval of [995 m/s to 1005 m/s], which is centered around the true wave speeds of 1000 m/s.

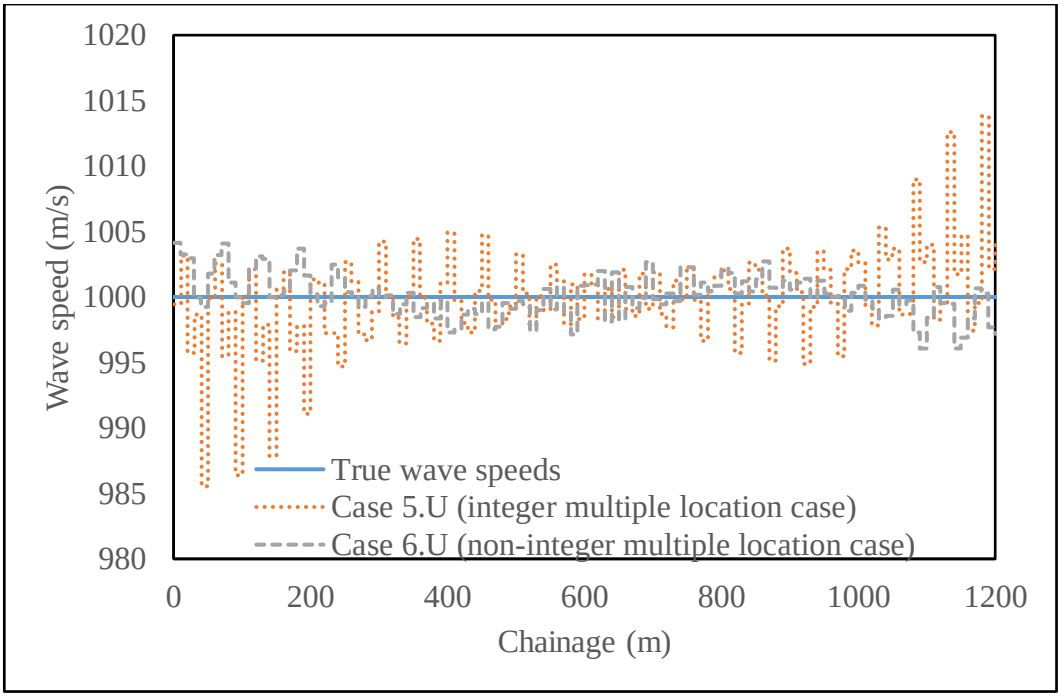

Figure 5.15 Comparison of true wave speeds and the best estimated wave speeds from 10 ITA trials for the uniform wave speed model Case 5.U and Case 6.U.

The predicted pressure responses at the transient generator (N65) by the best calibrated model in Cases 5.U and 6.U are given in Fig. 5.16. The range of the *y*-axis has been zoomed into a 0.1 m interval, and it is noted that the discrepancy between the predicted response and the measured response is less than 0.01 m, which might be undetectable in the field. Despite the existence of multiple incorrect wave speed estimates (in Fig. 5.14), the calibrated model of Case 5.U still provides a reasonably good match between its predicted pressure response and the measured pressure response, hence confirming that fact that the calibration objective for Case 5.U is not sufficiently informative to provide accurate parameter estimates.

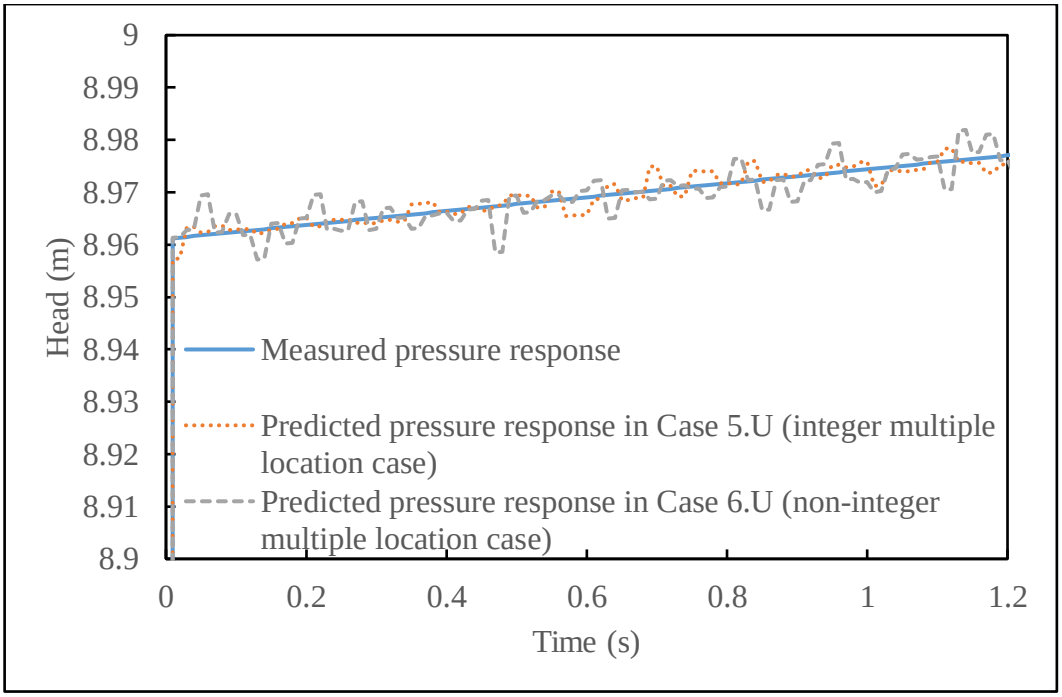

Figure 5.16 Comparison of measured pressure trace for the uniform wave speed model at the generator and predicted pressure traces obtained by the best estimated wave speeds among 10 ITA trials for the uniform wave speed model Case 5.U and Case 6.U.

5.5.2.2 Results for the variable wave speed Cases 5.V and 6.V

The results of 10 independent trials for Case 5 (integer multiple locations case) and Case 6 (non-integer multiple locations case) on the variable wave speed model (referred to as Case 5.V and Case 6.V) are summarized in the box plots in Fig. 5.17. Consistent with the results of the uniform wave speed case, the ITA performance for Case 6.V (identifiable case) is better than that for Case 5.V (non-identifiable case), indicated by the significantly smaller average IQR and significantly reduced outliers. The feature that if a wave speed of one reach on the left hand side of the transient generator is underestimated, then its counterpart on the right hand side is overestimated is also observed in the box plots in Fig. 5.17.

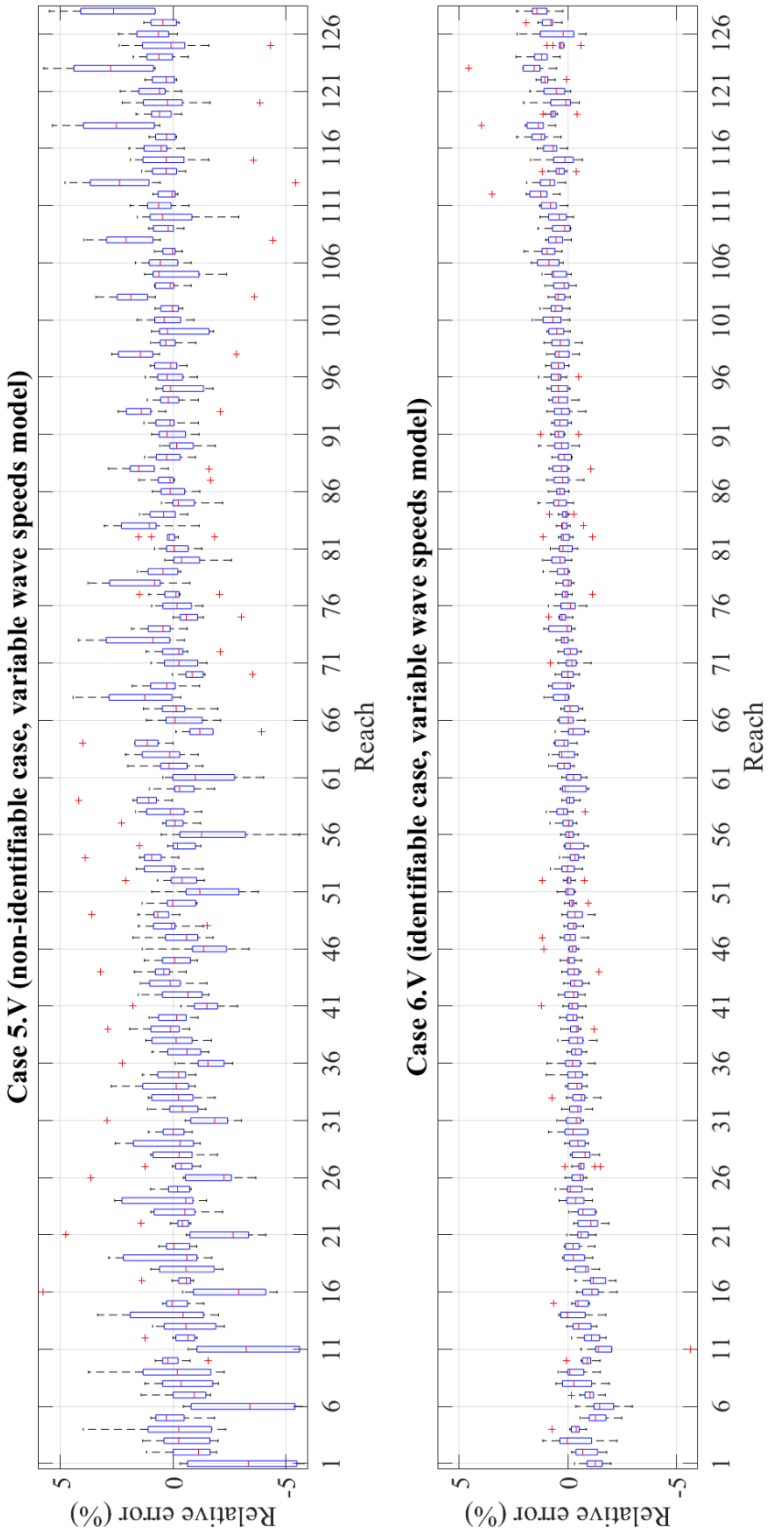

Figure 5.17 Box plot of the wave speed estimates from Case 5.V and 6.V. The horizontal axis indicates the reach number.

Fig. 5.18 and Fig. 5.19 compare the best estimated wave speeds of 10 ITA trials for Case 5.V and Case 6.V, and their corresponding pressure responses at the generator. Despite a reasonable match for both cases in Fig. 5.19, the best estimated wave speeds for Case 5.V have numerous extrema that do not exist in the true wave speed set (termed "false positives" as they are sections that are likely to be identified as anomalies, when they are actually not anomalies. Section A, B, C and D are examples). However, the wave speed estimates in Case 6.V in Fig. 5.18 are closer to the true wave speeds, and the false positives A, B, C and D are eliminated.

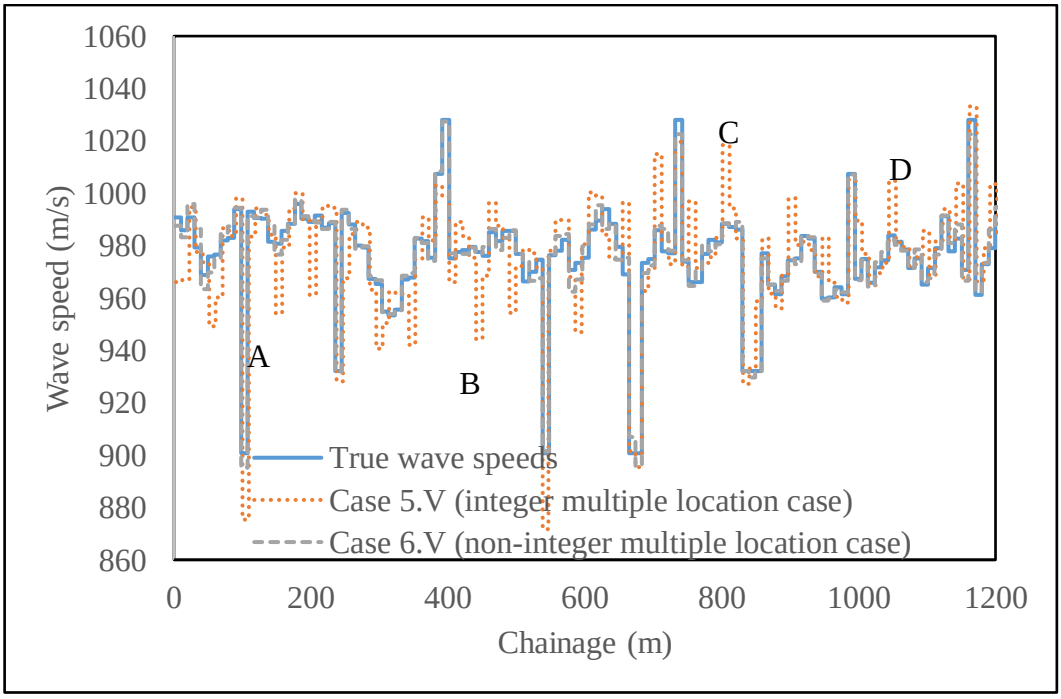

Figure 5.18 Comparison of true wave speeds and the best estimated wave speeds from 10 ITA trials for the variable wave speed model Case 5.V and Case 6.V.

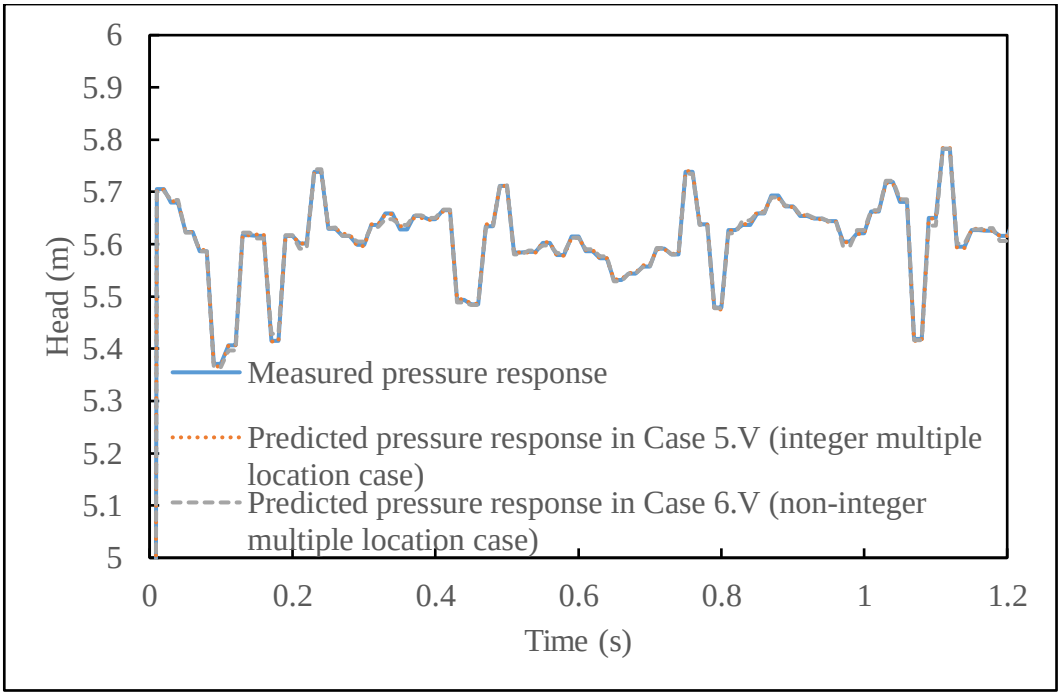

Figure 5.19 Comparison of measured pressure trace for the variable wave speed model at the generator and predicted pressure traces obtained by the best estimated wave speeds from 10 ITA trials for the variable wave speed model Case 5.V and Case 6.V.

5.5.2.3 Overall results summary

The results of all cases for both pipe models are now presented. The estimates relative errors for each case are presented as boxplots in Fig. 5.20 (Note that for each case, there are 1280 estimates, resulting from 128 variables and 10 independent ITA trials). It can be seen that the non-identifiable cases (in the black dashed boxes) have a much broader minima and maxima points (indicated by the larger whiskers) and many more outliers than those of the identifiable cases. The outliers represent the parameter estimates with great error, and thus they will result in a false positive diagnosis for the purposes of condition assessment (e.g. the sections A, B, C and D in Fig. 5. 18.). This further confirms that ITA performs better in the cases where the sensors are at

non-integer multiple locations. As result, the sensors should be placed at the non-integer multiple locations. Among all the non-integer multiple locations cases, it is difficult to draw a general conclusion as to which one is distinctly better than others, which is consistent with the previous sensitivity analysis.

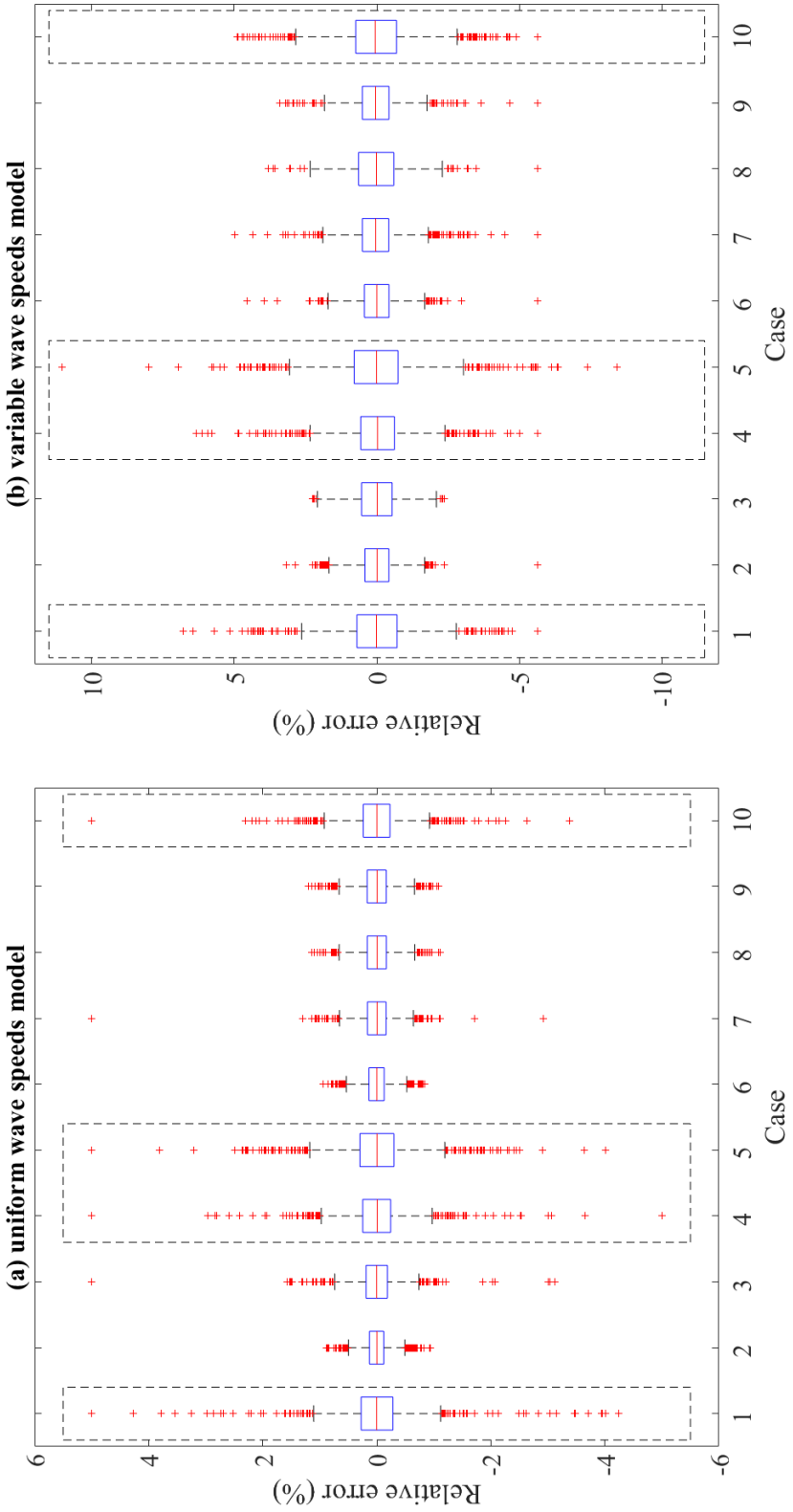

Figure 5.20 Boxplots of all relative errors for all cases

5.6 Conclusions

This research investigates how the number and location of pressure sensors affect the identifiability of the pipeline parameter estimation problem. It has been demonstrated that two pressure sensors are not able to uniquely identify the wave speed distribution along a pipeline using transient-based methods. An infinite number of pipe models with different wave speed distributions can produce exact the same pressure response at the two sensors. A sensitivity analysis has been conducted to investigate where to put a third sensor. It has been shown that, if the first two sensors are N reaches apart, the pressure response at nodes that are an integer multiple of N reaches apart from one of the first two sensors are not sensitive to changes within the wave speed estimates.

This pattern is also confirmed by inverse transient analysis case studies. ITA has been performed on 20 case studies and results have shown that the calibration accuracy is significantly different between integer multiple (non-identifiable) or non-integer multiple (identifiable) location cases. Within the integer multiple locations cases, the estimates were observed to have a consistently greater spread throughout the parameter space, implying that erroneous wave speed estimates are more likely with this spacing of sensors. . Within the non-integer multiple locations cases, the estimates were observed to be more consistent, and have greater accuracy.

The sensitivity analysis together with the ITA case studies have proved demonstrated that, in order to ensure the robustness of parameter estimation and identifiability of the pipeline, given that the first two sensors are N

reaches apart (i.e. *N* pipe segments in the inverse model), the third sensor should not be placed at nodes that are separated from any of the first two sensors by an integer multiple of *N* reaches.

This page is intentionally blank.

Chapter 6

Conclusions

This thesis focuses on the development and analysis of alternative inverse transient analysis (ITA) methods, and the generalisation of the reconstructive method of characteristics (RMOC) for the purpose of large-scale and detailed continuous condition assessment of water distribution transmission mains. This is achieved through a number of avenues including the development of a computationally faster transient simulator (suited for embedment into highly iterative optimisation strategies required for inverse analysis); the development of a novel reach classification and parameter bounding scheme to increase the identifiability of the inverse problem; the investigation of the number and location of pressure transducers required to achieve optimal identifiability for ITA methods; and the generalisation of the RMOC method to utilise two pressure transducers instead of one dead-end boundary and one pressure transducer near the dead-end. The specific contributions of this research are summarised in the next subsection. The recommendations for the future work are also presented.

6.1 Research contributions

In Chapter 2, an efficient transient simulation model has been developed and incorporated into the ITA method to significantly improve computational efficiency. This was achieved through the novel development of a head-based MOC with a flexible grid, which separated the head calculation from the coupled head and flow calculations, and also eliminated the need for interpolation. The proposed ITA method was examined by numerical case studies where 128 decision variables (wave speeds of 128 reaches) were involved. It was shown that the proposed ITA developed in this thesis only requires a quarter of the computational time required by the traditional ITA. The results also have shown that the accuracy of parameter calibration by the proposed ITA was also improved due to the elimination of interpolation errors.

This thesis has explored the issue of the identifiability problem in inverse transient analysis (non-uniqueness of solutions), and proposed strategies to address this issue in Chapter 3. The fast ITA proposed in Chapter 2 was further developed into a multi-stage parameter constraining ITA (ITA_{MP}) to enhance parameter identifiability of high dimensional inverse problems. This was achieved through reach classification and search-space updating. ITA_{MP} iteratively generates sets of parameter estimates and modifies the search-space interval for the generation of subsequent estimates based on identifying a reach as either in a normal or an anomalous state. The parameter estimates for the normal reaches become increasingly concentrated and outliers in the parameter estimates are eliminated, thus the identifiability of parameter values is enhanced. The ITA_{MP} approach

has been applied to a field case study consisting of a 4-km mild steel pipe with cement mortar lining (the Morgan-Whyalla transmission pipeline in South Australia). This 4-km pipeline was discretized into 383 reaches with a resolution of about 10 m. The wave speed estimates of all reaches were compared with the extensive ultrasonic wall thickness measurements with an interval of 5 m. The general agreement between ITA_{MP} results and ultrasonic measurements demonstrates the ability of ITA_{MP} as a screening tool for pipeline condition assessment in real world systems.

The previously developed RMOC has been further generalised in Chapter 4. The generalised RMOC in this thesis utilises two pressure transducers, instead of a dead-end boundary and one pressure transducer near the dead-end boundary, which is difficult to achieve in the field. The ability to assess pipeline condition of the generalized RMOC method was verified by a laboratory experiment, where a 37.5 m copper pipe has two sections with wall thicknesses different from the rest of pipe. The results show that the size and location of the two sections with different wall thicknesses were successfully identified.

In Chapter 5, the relevance of the number and location of pressure transducers to the parameter identifiability of the ITA has been investigated and analysed, Fundamental rules for transducers placement (to avoid problems with identifiability) are outlined. The generalized RMOC developed in Chapter 4 has been used to demonstrate that two transducers are insufficient to identify system parameters if the parameters between two transducers are unknown. In the case of an increase in the number of transducers to three, the sensitivity analysis revealed that if the

first two transducers are *N* reaches apart, the pressure response at nodes that are an integer multiple of *N* reaches from one of the first two sensors are not sensitive to changes within the wave speed values. This also provided insights as to why ITA applications suffer from the identifiability problems when three transducers are placed in integer multiple locations. When the wave speeds between transducers can vary, which is the case in ITA, there were an infinite number of models which provided almost the same pressure responses at the integer multiple locations. This discovery was further confirmed by 20 ITA case studies (in some cases, three transducers are placed in integer multiple locations while in other cases they are not), and it was found that the calibration accuracy was significantly different between integer multiple or non-integer multiple location cases. Within the non-integer multiple locations cases, the parameter estimates were observed to be more consistent, and have greater accuracy.

6.2 Research limitations and future work

In the current research concerning the field verification of ITA_{MP}, although parameters estimated by ITA_{MP} are generally consistent with ultrasonic wall thickness measurements, a few actual anomalous sections were missed by ITA_{MP}. This is likely due to the insufficient dynamic characterisation of the real pipeline system by the elastic model adopted. The unsteady friction and viscoelastic models, which are used to capture

dissipation and dispersion of pressure responses, are rarely used in ITA due to the prohibitive computational cost associated with these models. Preliminary investigations have shown that a viscoelastic model has the potential to be embedded in the head based MOC as developed in Chapter 2, which could result in a model able to account for dispersion in pressure response without dramatically increasing the computational cost. This model might further enhance ITA's capability to assess pipeline condition in the field.

It is a common practice that millions of evaluations are involved in ITA when an evolutionary optimization algorithm is used, which is the case in this thesis (Chapter 2, 3 and 5). Even though the computational efficiency has been significantly increased by the novel forward method developed in Chapter 2, the computational cost required by current ITA is still a concern for complex problems. In order to further enhance computational efficiency, it is worth testing other optimization algorithms (for example, a hybrid optimization algorithm incorporating the gradient-based algorithm) and other forward modeling schemes (for example, the implicit MOC scheme). Strategies such as incorporating prior information and reducing the number of decision variables by merging the reaches identified as in normal state are also recommended to investigate.

In this thesis, the inverse problem is formulated as a deterministic problem, where parameters are considered fixed and unknown. The inverse problem can also be formulated from a Bayesian perspective, where parameters are treated as probabilistic variables having a joint posterior probability density function. A Markov Chain Monte Carlo

(MCMC) based method can be applied to sample from the posterior probability density function. MCMC based methods also have the potential to accomplish parameter estimation and uncertainty assessment simultaneously.

In Chapter 4, the generalized RMOC is validated by a numerical experiment where the synthetic data is noise free. It has also been validated by a laboratory experiment where measurement errors and model error inevitably exist. It is recommended to examine the robustness of the generalised RMOC in a more rigorous way, and further research is also required to verify the generalised RMOC algorithm in field cases.

Chapter 5 reveals the relationship between parameter identifiability and sensor placement by numerical sensitivity analysis and numerical case studies. An implication of the results is that the system is uniquely identifiable when sensors are unevenly placed, and is not uniquely identifiable when sensors are evenly placed. However, explicit or mathematical proof has yet been provided. It is recommended to prove the inverse problem is identifiable or not in the future work. In addition, in field cases where measurement noise and model error are inevitable, the revealed relationship between parameter identifiability and sensor placement needs further confirmation by future research.

References

Adamkowski, A., and Lewandowski, M. (2006). "Experimental examination of unsteady friction models for transient pipe flow simulation." *Journal of Fluids Engineering*, 128(6), 1351-1363.

Afzal, M., and Udpa, S. (2002). "Advanced signal processing of magnetic flux leakage data obtained from seamless gas pipeline." *Ndt & E International*, 35(7), 449-457.

ASCE (2017). "ASCE's 2017 Infrastructure Report Card."

Behzadian, K., Kapelan, Z., Savic, D., and Ardeshir, A. (2009). "Stochastic sampling design using a multi-objective genetic algorithm and adaptive neural networks." *Environmental Modelling & Software*, 24(4), 530-541.

Brunone, B. (1999). "Transient test-based technique for leak detection in outfall pipes." *Journal of water resources planning and management*, 125(5), 302-306.

Brunone, B., and Ferrante, M. (2001). "Detecting leaks in pressurised pipes by means of transients." *Journal of Hydraulic Research*, 39(5), 539-547.

Brunone, B., Ferrante, M., and Meniconi, S. (2008). "Portable pressure wave-maker for leak detection and pipe system characterization." *Journal (American Water Works Association)*, 100(4), 108-116.

Brunone, B., Karney, B. W., Mecarelli, M., and Ferrante, M. (2000). "Velocity profiles and unsteady pipe friction in transient flow."

Journal of water resources planning and management, 126(4), 236-244.

Bureau of Meteorology (2016). "Urban National Performance Report."

Bush, C. A., and Uber, J. G. (1998). "Sampling design methods for water distribution model calibration." *Journal of Water Resources Planning and Management*, 124(6), 334-344.

Capponi, C., Ferrante, M., Zecchin, A. C., and Gong, J. (2017). "Leak Detection in a Branched System by Inverse Transient Analysis with the Admittance Matrix Method." *Water Resources Management*, 1-15.

Chaudhry, M. H. (2014). "Applied Hydraulic Transients."

Chen, L.-C. (1995). *Pipe network transient analysis: the forward and inverse problems*, Cornell University, August.

Colombo, A. F., Lee, P., and Karney, B. W. (2009). "A selective literature review of transient-based leak detection methods." *Journal of Hydro-environment Research*, 2(4), 212-227.

Covas, D., and Ramos, H. (2010). "Case studies of leak detection and location in water pipe systems by inverse transient analysis." *Journal of Water Resources Planning and Management*, 136(2), 248-257.

Covas, D., Stoianov, I., Ramos, H., Graham, N., and Maksimovic, C. (2004). "The dynamic effect of pipe-wall viscoelasticity in hydraulic transients. Part I—Experimental analysis and creep characterization." *Journal of Hydraulic Research*, 42(5), 517-532.

Do, N. C., Simpson, A. R., Deuerlein, J. W., and Piller, O. (2016). "Calibration of water demand multipliers in water distribution systems

using genetic algorithms." *Journal of Water Resources Planning and Management*, 142(11), 04016044.

Duan, H.-F., Ghidaoui, M. S., Lee, P. J., and Tung, Y.-K. (2011). "Relevance of unsteady friction to pipe size and length in pipe fluid transients." *Journal of hydraulic engineering*, 138(2), 154-166.

Duan, H.-F., Lee, P. J., Ghidaoui, M. S., and Tung, Y.-K. (2011). "Extended blockage detection in pipelines by using the system frequency response analysis." *Journal of Water Resources Planning and Management*, 138(1), 55-62.

Duan, H.-F., Lee, P. J., Ghidaoui, M. S., and Tung, Y.-K. (2011). "Leak detection in complex series pipelines by using the system frequency response method." *Journal of Hydraulic Research*, 49(2), 213-221.

Duan, H.-F., Lee, P. J., Kashima, A., Lu, J., Ghidaoui, M., and Tung, Y.-K. (2013). "Extended blockage detection in pipes using the system frequency response: analytical analysis and experimental verification." *Journal of Hydraulic Engineering*, 139(7), 763-771.

Duran, O., Althoefer, K., and Seneviratne, L. D. (2002). "State of the art in sensor technologies for sewer inspection." *Sensors Journal, IEEE*, 2(2), 73-81.

Eberhart, R. C., and Kennedy, J. "A new optimizer using particle swarm theory." *Proc., Proceedings of the sixth international symposium on micro machine and human science*, New York, NY, 39-43.

Ferrante, M., Brunone, B., and Meniconi, S. (2007). "Wavelets for the analysis of transient pressure signals for leak detection." *Journal of hydraulic engineering*, 133(11), 1274-1282.

Ferrante, M., Brunone, B., and Meniconi, S. (2009). "Leak detection in branched pipe systems coupling wavelet analysis and a Lagrangian model." *Journal of Water Supply: Research and Technology-AQUA*, 58(2), 95-106.

Fuchs, H., and Riehle, R. (1991). "Ten years of experience with leak detection by acoustic signal analysis." *Applied Acoustics*, 33(1), 1-19.

Ghazali, M., Beck, S., Shucksmith, J., Boxall, J., and Staszewski, W. (2012). "Comparative study of instantaneous frequency based methods for leak detection in pipeline networks." *Mechanical Systems and Signal Processing*, 29, 187-200.

Ghidaoui, M. S., and Karney, B. W. (1994). "Equivalent differential equations in fixed-grid characteristics method." *Journal of Hydraulic Engineering*, 120(10), 1159-1175.

Ghidaoui, M. S., Karney, B. W., and McInnis, D. A. (1998). "Energy estimates for discretization errors in water hammer problems." *Journal of Hydraulic Engineering*, 124(4), 384-393.

Ghidaoui, M. S., Zhao, M., McInnis, D. A., and Axworthy, D. H. (2005). "A review of water hammer theory and practice." *Applied Mechanics Reviews*, 58(1), 49-76.

Goldberg, D. E., and Wylie, B. E. (1983). "Characteristics method using time-line interpolations." *Journal of Hydraulic Engineering*, 109(5), 670-683.

Gong, J., Lambert, M., Zecchin, A., Simpson, A., Arbon, N., and Kim, Y.-i. (2016). "Field study on non-invasive and non-destructive condition

assessment for asbestos cement pipelines by time-domain fluid transient analysis." *Structural Health Monitoring*, 15(1), 113-124.

Gong, J., Lambert, M. F., Simpson, A. R., and Zecchin, A. C. (2012). "Single-event leak detection in pipeline using first three resonant responses." *Journal of Hydraulic Engineering*, 139(6), 645-655.

Gong, J., Lambert, M. F., Simpson, A. R., and Zecchin, A. C. (2013). "Single-event leak detection in pipeline using first three resonant responses." *J. Hydraulic Eng.*, 139(6), 645-655.

Gong, J., Lambert, M. F., Simpson, A. R., and Zecchin, A. C. (2014). "Detection of Localized Deterioration Distributed along Single Pipelines by Reconstructive MOC Analysis." *Journal of Hydraulic Engineering*, 140(2), 190-198.

Gong, J., Png, G. M., Arkwright, J. W., Papageorgiou, A. W., Cook, P. R., Lambert, M. F., Simpson, A. R., and Zecchin, A. C. (2018). "In-pipe fibre optic pressure sensor array for hydraulic transient measurement with application to leak detection." *Measurement*.

Gong, J., Simpson, A. R., Lambert, M. F., Zecchin, A. C., Kim, Y.-i., and Tijsseling, A. S. (2012). "Detection of distributed deterioration in single pipes using transient reflections." *Journal of Pipeline Systems Engineering and Practice*, 4(1), 32-40.

Gong, J., Stephens, M. L., Arbon, N. S., Zecchin, A. C., Lambert, M. F., and Simpson, A. R. (2015). "On-site non-invasive condition assessment for cement mortar-lined metallic pipelines by time-domain fluid transient analysis." *Structural Health Monitoring*, 14(5), 426-438.

Gong, J., Stephens, M. L., Arbon, N. S., Zecchin, A. C., Lambert, M. F., and Simpson, A. R. (2015). "On-site non-invasive condition assessment for cement mortar–lined metallic pipelines by time-domain fluid transient analysis." *Structural Health Monitoring*, 14(5), 426-438.

Hunaidi, O., Chu, W., Wang, A., and Guan, W. (2000). "Detecting leaks in plastic pipes." *American Water Works Association. Journal*, 92(2), 82.

Hunaidi, O., and Giamou, P. "Ground-penetrating radar for detection of leaks in buried plastic water distribution pipes." *Proc., International Conference on Ground Penetrating Radar*.

Jönsson, L., and Larson, M. (1992). "Leak detection through hydraulic transient analysis." *Pipeline systems*, Springer, 273-286.

Jung, B., Karnev, B., and Lambert, M. (2006). "Benchmark tests of evolutionary algorithms: mathematic evaluation and application to water distribution systems." *J Environ Inform*, 7(1), 24-35.

Jung, B., and Karney, B. (2008). "Systematic exploration of pipeline network calibration using transients." *Journal of Hydraulic Research*, 46(sup1), 129-137.

Kapelan, Z., Savic, D., and Walters, G. (2004). "Incorporation of prior information on parameters in inverse transient analysis for leak detection and roughness calibration." *Urban Water Journal*, 1(2), 129-143.

Kapelan, Z. S., Savic, D. A., and Walters, G. A. (2003). "A hybrid inverse transient model for leakage detection and roughness calibration in pipe networks." *Journal of Hydraulic Research*, 41(5), 481-492.

Kapelan, Z. S., Savic, D. A., and Walters, G. A. (2005). "Optimal sampling design methodologies for water distribution model calibration." *Journal of Hydraulic Engineering*, 131(3), 190-200.

Kim, S. (2007). "Impedance matrix method for transient analysis of complicated pipe networks." *Journal of Hydraulic Research*, 45(6), 818-828.

Kim, S. (2016). "Impedance Method for Abnormality Detection of a Branched Pipeline System." *Water resources management*, 30(3), 1101-1115.

Kim, S. H. (2008). "Address-oriented impedance matrix method for generic calibration of heterogeneous pipe network systems." *Journal of Hydraulic Engineering*, 134(1), 66-75.

Kim, S. H., Zecchin, A., and Choi, L. (2014). "Diagnosis of a pipeline system for transient flow in low reynolds number with impedance method." *Journal of Hydraulic Engineering*, 140(12), 04014063.

Lai, C. (1988). "Comprehensive method of characteristics models for flow simulation." *Journal of Hydraulic Engineering*, 114(9), 1074-1097.

Lansey, K., El-Shorbagy, W., Ahmed, I., Araujo, J., and Haan, C. (2001). "Calibration assessment and data collection for water distribution networks." *Journal of Hydraulic Engineering*, 127(4), 270-279.

Lee, P., Tuck, J., Davidson, M., and May, R. (2017). "Piezoelectric wave generation system for condition assessment of field water pipelines." *Journal of Hydraulic Research*, 55(5), 721-730.

Lee, P. J., Duan, H.-F., Ghidaoui, M., and Karney, B. (2013). "Frequency domain analysis of pipe fluid transient behaviour." *Journal of hydraulic research*, 51(6), 609-622.

Lee, P. J., Lambert, M. F., Simpson, A. R., Vítkovský, J. P., and Liggett, J. (2006). "Experimental verification of the frequency response method for pipeline leak detection." *Journal of Hydraulic Research*, 44(5), 693-707.

Lee, P. J., Vítkovský, J. P., Lambert, M. F., Simpson, A. R., and Liggett, J. (2007). "Leak location in pipelines using the impulse response function." *Journal of Hydraulic Research*, 45(5), 643-652.

Lee, P. J., Vítkovský, J. P., Lambert, M. F., Simpson, A. R., and Liggett, J. A. (2005). "Leak location using the pattern of the frequency response diagram in pipelines: a numerical study." *Journal of Sound and Vibration*, 284(3), 1051-1073.

Liggett, J. A., and Chen, L.-C. (1994). "Inverse transient analysis in pipe networks." *Journal of Hydraulic Engineering*, 120(8), 934-955.

Liou, C. P. (1998). "Pipeline leak detection by impulse response extraction." *Journal of Fluids Engineering*, 120(4), 833-838.

Liu, Z., and Kleiner, Y. (2013). "State of the art review of inspection technologies for condition assessment of water pipes." *Measurement*, 46(1), 1-15.

Ljung, L. (1998). "System identification." *Signal analysis and prediction*, Springer, 163-173.

Lowe, M., and Cawley, P. (2006). "Long range guided wave inspection usage–current commercial capabilities and research directions."

Department of Mechanical Engineering, Imperial College London, 1-40.

McInnis, D., and Karney, B. W. (1995). "Transients in distribution networks: Field tests and demand models." *Journal of Hydraulic Engineering*, 121(3), 218-231.

Mcneiill, L. S., and Edwards, M. (2001). "Iron pipe corrosion in distribution systems." *Journal (American Water Works Association)*, 93(7), 88-100.

Meier, R. W., and Barkdoll, B. D. (2000). "Sampling design for network model calibration using genetic algorithms." *Journal of Water Resources Planning and Management*, 126(4), 245-250.

Meniconi, S., Brunone, B., Ferrante, M., Capponi, C., Carrettini, C., Chiesa, C., Segalini, D., and Lanfranchi, E. (2015). "Anomaly pre-localization in distribution–transmission mains by pump trip: preliminary field tests in the Milan pipe system." *Journal of Hydroinformatics*, 17(3), 377-389.

Meniconi, S., Brunone, B., Ferrante, M., and Massari, C. (2013). "Numerical and experimental investigation of leaks in viscoelastic pressurized pipe flow." *Drinking Water Engineering and Science*, 6(1), 11-16.

Meniconi, S., Duan, H., Lee, P., Brunone, B., Ghidaoui, M., and Ferrante, M. (2013). "Experimental Investigation of Coupled Frequency and Time-Domain Transient Test–Based Techniques for Partial Blockage Detection in Pipelines." *Journal of hydraulic engineering*, 139(10), 1033-1040.

Mergelas, B., and Kong, X. (2001). *Electromagnetic inspection of prestressed concrete pressure pipe*, American Water Works Association.

Mohapatra, P., Chaudhry, M., Kassem, A., and Moloo, J. (2006). "Detection of partial blockage in single pipelines." *Journal of Hydraulic Engineering*, 132(2), 200-206.

Mounce, S., Boxall, J., and Machell, J. (2009). "Development and verification of an online artificial intelligence system for detection of bursts and other abnormal flows." *Journal of Water Resources Planning and Management*, 136(3), 309-318.

Mounce, S. R., Mounce, R. B., and Boxall, J. B. (2011). "Novelty detection for time series data analysis in water distribution systems using support vector machines." *Journal of hydroinformatics*, 13(4), 672-686.

Mpesha, W., Gassman, S. L., and Chaudhry, M. H. (2001). "Leak detection in pipes by frequency response method." *Journal of Hydraulic Engineering*, 127(2), 134-147.

Mpesha, W., Hanif Chaudhry, M., and Gassman, S. L. (2002). "Leak detection in pipes by frequency response method using a step excitation." *Journal of hydraulic research*, 40(1), 55-62.

Mutikanga, H. E., Sharma, S. K., and Vairavamoorthy, K. (2012). "Methods and tools for managing losses in water distribution systems." *Journal of Water Resources Planning and Management*, 139(2), 166-174.

Nash, G. A., and Karney, B. W. (1999). "Efficient inverse transient analysis in series pipe systems." *Journal of Hydraulic Engineering*, 125(7), 761-764.

Nixon, W., Ghidaoui, M. S., and Kolyshkin, A. A. (2006). "Range of validity of the transient damping leakage detection method." *Journal of hydraulic engineering*, 132(9), 944-957.

Pezzinga, G. (2000). "Evaluation of unsteady flow resistances by quasi-2D or 1D models." *Journal of Hydraulic Engineering*, 126(10), 778-785.

Poli, R., Kennedy, J., and Blackwell, T. (2007). "Particle swarm optimization." *Swarm Intelligence*, 1(1), 33-57.

Prashanth Reddy, H., Silva-Araya, W. F., and Hanif Chaudhry, M. (2011). "Estimation of Decay Coefficients for Unsteady Friction for Instantaneous, Acceleration-Based Models." *Journal of Hydraulic Engineering*, 138(3), 260-271.

Puust, R., Kapelan, Z., Savic, D., and Koppel, T. (2010). "A review of methods for leakage management in pipe networks." *Urban Water Journal*, 7(1), 25-45.

Romano, M., Kapelan, Z., and Savić, D. A. (2012). "Automated detection of pipe bursts and other events in water distribution systems." *Journal of Water Resources Planning and Management*, 140(4), 457-467.

Rubio Scola, I., Besançon, G., and Georges, D. (2016). "Blockage and Leak Detection and Location in Pipelines Using Frequency Response Optimization." *Journal of Hydraulic Engineering*, 143(1), 04016074.

Sattar, A. M., Chaudhry, M. H., and Kassem, A. A. (2008). "Partial blockage detection in pipelines by frequency response method." *Journal of Hydraulic Engineering*, 134(1), 76-89.

Savic, D. A., Kapelan, Z. S., and Jonkergouw, P. M. (2009). "Quo vadis water distribution model calibration?" *Urban Water Journal*, 6(1), 3-22.

Shi, H., Gong, J., Zecchin, A. C., Lambert, M. F., and Simpson, A. R. (2017). "Hydraulic transient wave separation algorithm using a dual-sensor with applications to pipeline condition assessment." *Journal of Hydroinformatics*, 19(5), 752-765.

Soares, A. K., Covas, D. I., and Reis, L. F. R. (2011). "Leak detection by inverse transient analysis in an experimental PVC pipe system." *Journal of Hydroinformatics*, 13(2), 153-166.

St. Clair, A. M., and Sinha, S. (2012). "State-of-the-technology review on water pipe condition, deterioration and failure rate prediction models!" *Urban Water Journal*, 9(2), 85-112.

Stephens, M., Lambert, M., Simpson, A., Vítkovský, J., and Nixon, J. "Field tests for leakage, air pocket, and discrete blockage detection using inverse transient analysis in water distribution pipes." *Proc., 2004 World Water and Environmental Resources Congress*.

Stephens, M., Simpson, A., and Lambert, M. "Internal wall condition assessment for water pipelines using inverse transient analysis." *Proc., Proc., 10th Annual Symp. on Water Distribution Systems Analysis*, ASCE Reston, VA, 911-921.

Stephens, M. L. (2008). "Transient response analysis for fault detection and pipeline wall condition assessment in field water transmission and distribution pipelines and networks."

Stephens, M. L., Lambert, M. F., and Simpson, A. R. (2013). "Determining the internal wall condition of a water pipeline in the field using an inverse transient." *Journal of Hydraulic Engineering*, 139(3), 310-324.

Stephens, M. L., Lambert, M. F., Simpson, A. R., and Vitkovsky, J. (2011). "Calibrating the water-hammer response of a field pipe network by using a mechanical damping model." *Journal of Hydraulic Engineering*, 137(10), 1225-1237.

Suo, L., and Wylie, E. (1989). "Impulse response method for frequency-dependent pipeline transients." *Journal of fluids engineering*, 111(4), 478-483.

Taghvaei, M., Beck, S., and Boxall, J. (2010). "Leak detection in pipes using induced water hammer pulses and cepstrum analysis." *International Journal of COMADEM*, 13(1), 19.

Taghvaei, M., Beck, S., and Staszewski, W. (2006). "Leak detection in pipelines using cepstrum analysis." *Measurement Science and Technology*, 17(2), 367.

Tuck, J., and Lee, P. (2013). "Inverse Transient Analysis for Classification of Wall Thickness Variations in Pipelines." *Sensors*, 13(12), 17057-17066.

Vardy, A. E., and Brown, J. M. (1995). "Transient, turbulent, smooth pipe friction." *Journal of Hydraulic Research*, 33(4), 435-456.

Vitkovsky, J. P. (2001). "Inverse analysis and modelling of unsteady pipe flow: Theory, applications and experimental verification." Adelaide University, Department of Civil and Environmental Engineering.

Vítkovský, J. P., Lambert, M. F., Simpson, A. R., and Liggett, J. A. (2007). "Experimental observation and analysis of inverse transients for pipeline leak detection." *Journal of Water Resources Planning and Management*, 133(6), 519-530.

Vitkovsky, J. P., Lambert, M. F., Simpson, A. R., and Wang, X.-J. "An experimental verification of the inverse transient technique for leak detection." *Proc., 6th Conference on Hydraulics in Civil Engineering: The State of Hydraulics; Proceedings*, Institution of Engineers, Australia, 373.

Vítkovský, J. P., Lee, P. J., Stephens, M. L., Lambert, M. F., Simpson, A. R., and Liggett, J. A. (2003). "Leak and blockage detection in pipelines via an impulse response method." *Pumps, electromechanical devices and systems applied to urban water management*, 1, 423.

Vítkovský, J. P., Liggett, J. A., Simpson, A. R., and Lambert, M. F. (2003). "Optimal measurement site locations for inverse transient analysis in pipe networks." *Journal of Water Resources Planning and Management*, 129(6), 480-492.

Vítkovský, J. P., Simpson, A. R., and Lambert, M. F. (2000). "Leak detection and calibration using transients and genetic algorithms." *Journal of Water Resources Planning and Management*, 126(4), 262-265.

Volk, C., Dundore, E., Schiermann, J., and LeChevallier, M. (2000). "Practical evaluation of iron corrosion control in a drinking water distribution system." *Water research*, 34(6), 1967-1974.

Wang, X.-J., Lambert, M. F., and Simpson, A. R. (2005). "Detection and location of a partial blockage in a pipeline using damping of fluid

transients." *Journal of Water Resources Planning and Management*, 131(3), 244-249.

Wang, X.-J., Lambert, M. F., Simpson, A. R., Liggett, J. A., and V ı´ tkovský, J. P. (2002). "Leak detection in pipelines using the damping of fluid transients." *Journal of Hydraulic Engineering*, 128(7), 697-711.

Wylie, E. B., Streeter, V. L., and Suo, L. (1993). *Fluid transients in systems*, Prentice Hall Englewood Cliffs, NJ.

Yeh, W. W. G. (1986). "Review of parameter identification procedures in groundwater hydrology: The inverse problem." *Water Resources Research*, 22(2), 95-108.

Zecchin, A., Lambert, M., Simpson, A., and White, L. (2014). "Parameter identification in pipeline networks: transient-based expectation-maximization approach for systems containing unknown boundary conditions." *Journal of Hydraulic Engineering*, 140(6), 04014020.

Zecchin, A. C., Simpson, A. R., Lambert, M. F., White, L. B., and Vítkovský, J. P. (2009). "Transient modeling of arbitrary pipe networks by a Laplace-domain admittance matrix." *Journal of Engineering Mechanics*, 135(6), 538-547.

Zecchin, A. C., White, L. B., Lambert, M. F., and Simpson, A. R. (2013). "Parameter identification of fluid line networks by frequency-domain maximum likelihood estimation." *Mechanical Systems and Signal Processing*, 37(1), 370-387.

Zhang, C., Gong, J., Zecchin, A., Lambert, M., and Simpson, A. (2018a). "Faster Inverse Transient Analysis with a Head-Based Method of

Characteristics and a Flexible Computational Grid for Pipeline Condition Assessment." *Journal of Hydraulic Engineering*, 144(4), 04018007.

Zhang, C., Zecchin, A. C., Lambert, M. F., Gong, J., and Simpson, A. R. (2018b). "Multi-stage parameter-constraining inverse transient analysis for pipeline condition assessment." *Journal of Hydroinformatics*, jh2018154.

Zielke, W. (1968). "Frequency-dependent friction in transient pipe flow." *Journal of basic engineering*, 90(1), 109-115.